The Coordination of Signaling by 3' Phosphoinositide Concentration Thresholds during Phagocytosis

By

Youxin Zhang

A dissertation submitted in partial fulfillment
Of the requirements for the degree of
Doctor of Philosophy
(Biophysics)
In The University of Michigan
2009

Doctoral Committee:

Professor Joel A. Swanson, Chair
Professor Christin Carter-Su
Professor Jennifer J. Linderman
Associate Professor Nils G. Walter
Assistant Professor Jennifer P. Ogilvie

To My Mother and Father

Acknowledgments

First of all, I would like to thank Professor Joel Swanson for being a great advisor. He spent a lot of time helping me to finish my research projects as well as thesis writing. He also provided great support on my career development.

I would like to thank everyone in the Swanson Lab. I enjoyed working with them and learned a lot from them. Especially, Dr. Adam Hoppe and Dr. Pete Beemiller taught me how to do quantitative fluorescence imaging as well as other cell biology experiments.

The project described in chapter 3 was finished in collaboration with Dr. Pete Beemiller. The experiments described in chapter 4 were started by Dr. Lynn Kamen and were performed in collaboration with Dr. Heunjin Lee at Caltech. I would like to thank them for their contributions to my thesis.

Last but not least, I would like to thank my supportive family, especially my mother, my father and my wife.

Table of Contents

List of Figures

Figure

Chapter One

An Introduction to Signal Transduction during Phagocytosis

1.1 Phagocytosis in host defense

1.1.1 Overview of phagocytosis and host defense

Phagocytosis is classically defined as a mechanism for internalizing and destroying particles that are more than 1 μm in diameter (Cardelli, 2001). During phagocytosis, particles are first recognized by phagocytic receptors, internalized by an actin-driven process (Fig. 1.1A) and finally degraded by phagosome maturation. In some unicellular organisms, such as amoebae, phagocytosis serves as a method to acquire food. In multicellular organisms, phagocytosis plays important roles in embryonic organ remodeling, tissue repair after injury, clearance of apoptotic cells and host defense.

Host defense was defined as the mechanisms by which multicellular organisms protect themselves from infection by bacteria, viruses and unicellular eukaryotes such as fungi (Brown, 1995). There are two types of responses in host defense. Innate immune responses are activated rapidly, usually within minutes of pathogen recognition. However, innate immune responses often cannot eliminate pathogens completely and do not generate specific long-term immunity. In contrast, the adaptive immune response, which is induced by the innate immune response and appears later, can generate more powerful protection as well as long term immunity to pathogens.

Phagocytosis plays important roles in both innate and adaptive immune responses. Upon infection, macrophages and neutrophils, the major professional phagocytes, are recruited to the infection site by chemoattractants generated by the microbe-induced inflammatory responses of resident phagocytes. Some phagocytes internalize and destroy pathogens by generating reactive oxygen and nitrogen species. At the same time, macrophages can present the antigen to stimulate adaptive immune responses. During adaptive immune responses, activated Th1 T cells will activate macrophages, which exhibit increased killing of phagocytosed pathogens, antigen presentation and cytokine secretion. Activated B cells generate antibodies specific to the pathogen, which will also enhance receptor-mediated phagocytosis. In summary, phagocytosis is involved in many aspects of the highly integrated host defense system.

1.1.2 Types of phagocytes

Many mammalian cells can perform phagocytosis. For example, retinal pigmented epithelial cells have phagocytic activities to renew the sensory retina (Bosch et al., 1993). In addition, non-professional phagocytes contribute to the clearance of apoptotic cells, which is essential in tissue homeostasis (Birge and Ucker, 2008). Nevertheless, professional phagocytes, which include neutrophils, macrophages and dendritic cells (DCs), play a major role during host defense since they have the ability to recognize pathogens through immuno-receptors on their surfaces.

In mammals, neutrophils, macrophages and DCs derive from a common myeloid progenitor cell. Specific combinations of inductive events instruct differentiation of these common progenitors to different cell types (Stuart and Ezekowitz, 2005). Neutrophils in

peripheral blood have a short life span of 24 to 48 hours, and a high turnover rate (Dale et al., 2008). Neutrophils are recruited to the infection sites in tissues by chemotaxis in response to gradients of chemokines, proteins secreted by cells to induce directed movement in nearby responsive cells. The recruited neutrophils phagocytose pathogens and kill them by the fusion of neutrophil granule membranes with membranes of phagosomes (Cohn and Hirsch, 1960). NADPH oxidase plays an important role in the generation of superoxide, hydrogen peroxide and other reactive oxygen species to catalyze the microbicidal activities (Babior et al., 1976). In neutrophils, hydrogen peroxide interacts with myeloperoxidase, which is released from granules during phagocytosis, and chloride to generate hypochlorous acid, which has potent microbicidal activities, within the phagosome (Klebanoff, 2005). In addition to killing phagocytosed pathogens by fusion with phagosomes, granules can be secreted into the extracellular space to facilitate killing of extracellular pathogens.

The phagocytosis and chemotaxis of neutrophils are initiated by the activation of receptors on cell surfaces. Fc receptors interact with antibody-opsonized (coated) pathogens and facilitate phagocytosis through pathways affecting reorganization of the cytoskeleton (Kim et al., 2003). Complement receptors facilitate phagocytosis of complement-opsonized pathogens, though signaling pathways which are different from those of Fc receptor-mediated phagocytosis in many aspects (Groves et al., 2008). Complement receptors as well as several other chemotactic receptors, including receptors for N-formyl peptides, platelet activating factor and a variety of other chemokines, regulate the migration to infection sites after cells enter tissues from blood vessels (Gerard and Rollins, 2001).

Macrophages derive from monocytes, which share a common myeloid progenitor cell

with neutrophils. Monocytes are released from bone marrow and circulate in the blood stream. Although they share some physiological capacities with neutrophils, monocytes have a much longer life span and retain a proliferative capacity (Dale et al., 2008). When they migrate from blood vessels to different tissues, they can differentiate into resident macrophages such as Kupffer cells in the liver, alveolar macrophages in the lung and microglia in the central nervous system. When infection happens, monocytes can also migrate from blood vessels to the infection sites, like neutrophils, but their chemotactic responses and microbicidal activities are significantly different (Dale et al., 2008).

DCs may derive from common myeloid progenitors or from monocytes and plasmacytoid cells and thus are divided to different subsets (Ueno et al., 2007). DCs are primarily responsible for antigen presentation which induces adaptive immune responses when infection happens. Immature DCs have high phagocytic capacity and reside in both peripheral tissues and lymphoid organs. Pathogens are recognized by pathogen-associated molecular patterns through different families of pattern recognition receptors on DCs, including Toll-like receptors (Akira et al., 2006), cell surface C-type lectin receptors (Figdor et al., 2002) and intracytoplasmic nucleotide oligomerization domain-like receptors (Ting and Davis, 2005). Upon activation, mature DCs lose phagocytic capacity, due to the loss of phagocytic receptors, but enhance antigen presentation capacity through translocation of MHC class II molecules to cell surfaces (Pierre et al., 1997) and up-regulation of costimulatory molecules in cell membranes (Caux et al., 1994). Mature DCs migrate to secondary lymphoid organs such as lymph nodes to interact with and activate T-cells (Itano and Jenkins, 2003), as well as B-cells (Qi et al., 2006), thereby initiating adaptive immune responses.

1.1.3 Macrophages in innate immune responses

Upon infection, macrophages residing in tissues phagocytose microbes and initiate inflammatory responses. Various cytokines and chemokines are generated by tissue macrophages to recruit more macrophages and neutrophils from blood vessels to the infection sites in a process called leukocyte extravasation (Vestweber, 2007).

Leukocyte extravasation occurs in 4 steps (Petri and Bixel, 2006). The first step is rolling adhesion, during which leukocytes roll along vascular endothelial surfaces. Soon after the initiation of inflammatory responses, selectins are expressed on vascular endothelial cell surfaces. Selectins recognize carbohydrate moieties on leukocyte surfaces and mediate transient binding of leukocytes to endothelium, slowing leukocyte flow through the blood vessels (Ley et al., 1995). The second step is the formation of firm adhesions between integrins on leukocytes and intercellular adhesion molecules (ICAM) on the endothelial cells, a process greatly enhanced by chemokines generated during inflammatory responses. Then leukocytes migrate through the endothelial wall between endothelial cells, which also depends on integrins (Cooper et al., 1995). After exiting the blood vessels, leukocytes migrate up the gradient of chemokines to the infection sites, through intracellular signaling initiated by chemokine receptors.

After pathogens are internalized by macrophages, phagosomes begin a maturation process which can kill pathogens. During phagosome maturation, phagosomal pH decreases, creating an acidic environment which inhibits bacterial growth and enhances microbicidal chemistries. In addition, various proteins and lipids, which can also contribute to microbicidal activities, are delivered to phagosomes by fusion with late endosomes, lysosomes and probably also endoplasmic reticulum (ER) (Huynh et al., 2007). Reactive oxygen and nitrogen species also play important roles in microbicidal

activities. Macrophages can activate nitric oxide synthase (MacMicking et al., 1997) and NADPH oxidases, generating nitric oxide (Kaplan et al., 1996) and reactive oxygen species (Babior, 1999), respectively, which are toxic to many bacteria.

1.1.4 Macrophages in antigen presentation

Macrophages not only kill pathogens by themselves but also present antigens to induce adaptive immune responses, which generate stronger microbicidal activities and long term immunity. Two different pathways of antigen presentation exist. Major histocompatibility complex (MHC) class I molecules present peptides from intracellular pathogens, whose proteins are processed in cytoplasm by proteasomes, transported to ER via transporters associated with antigen processing (TAP) and loaded onto MHC class I in ER. The peptide-loaded MHC I are transported to the cell surface, where they may be recognized by T-cell receptors on CD8 T cells. MHC class II molecules present peptides from extracellular pathogens which have been taken up by endocytosis or phagocytosis. Phagosomal enzymes can degrade the proteins to peptides, which are then loaded onto MHC class II molecules. MHC class II molecules are synthesized in ER and routed through Golgi to endocytic compartments. Antigen loading onto MHC class II can happen in various endocytic pathway compartments from early endosomes to lysosomes (Hiltbold and Roche, 2002). Following transport to the cell surface, peptide-loaded MHC II may be recognized by T-cell receptors on CD4 T cells.

In contrast to these traditional MHC class I and class II pathways, antigens from phagocytosed pathogens can also be presented by MHC class I molecules, a process referred to as cross-presentation (Kaufmann and Schaible, 2005). It was claimed that ER fuses with phagosomes for antigen cross presentation (Guermonprez et al., 2003).

Consistant with this claim, proteomic analyses showed that proteins involved with each of the required steps of MHC class I antigen presentation are present on purified phagosomes (Houde et al., 2003). However, a fluorescence microscopy study challenged this claim by showing that most of phagosomal membrane is derived from plasma membrane and vesicles in endocytic pathways, instead of ER (Touret et al., 2005). Thus, the contribution of ER fusion to antigen cross-presentation during phagocytosis remains controversial.

1.2 Signaling during Fcγ receptor-mediated phagocytosis

1.2.1 Non-opsonic and opsonic phagocytic receptors

Opsonization is the process by which pathogens are coated with opsonic molecules, such as antibodies and complement fragments, to facilitate the ingestion by phagocytes. Receptors on macrophage surfaces can recognize pathogens either directly or through opsonic molecules. Non-opsonic receptors can recognize a number of characteristic molecular motifs on pathogen surfaces which are referred as pathogen-associated molecular patterns. For instance, the family of C type lectins, including macrophage mannose receptors, DC-Sign, L-Sign, Langerin and Dectin-1, can bind to the multiple carbohydrate binding domains on the surfaces of microorganisms (Stuart and Ezekowitz, 2005). Multiple types of receptors may contribute at the same time during phagocytosis, providing the ability to bind microorganisms even when carbohydrate-binding domains on their surfaces undergo changes (Cambi and Figdor, 2005).

In contrast to non-opsonic receptors, complement receptors and Fc receptors mediate phagocytosis of pathogens opsonized with complement fragments and antibodies,

respectively. The signaling for complement-mediated phagocytosis is different from that for Fc receptor-mediated phagocytosis. The following discussion focuses on the latter.

Antibody classes are defined by their heavy chains. Five classes of immunoglobulin antibodies exist: IgM, IgD, IgG, IgA and IgE. Their heavy chains are referred as μ,δ,γ,α and β, which have corresponding receptors on macrophage surfaces. The most extensively studied phagocytic receptor is Fcγ receptor (FcR). Three classes of Fcγ receptor have been identified: FcγI, FcγRII, FcγRIII, each of which consists of several isoforms (Ravetch and Bolland, 2001). FcγRI has high binding affinity to IgG while FcγRII and FcγRIII have low binding affinities. Most isoforms of FcR can mediate phagocytosis of IgG-opsonized particles through immunoreceptor tyrosine-based activation motifs (ITAMs) in the cytoplasmic domain of the receptor or in associated cytoplasmic proteins. Ligation of FcγRIIB generates signals inhibiting phagocytosis through immunoreceptor tyrosine-based inhibition motifs (ITIMs) in the cytoplasmic domain of the receptor (Barrow and Trowsdale, 2006).

1.2.2 Kinase activation and lipid modification during FcR-mediated phagocytosis

Phagocytosis of IgG-coated particles is initiated by the ligation of IgG with FcR on macrophage surfaces, which induces FcR clustering in the plasma membrane and subsequent phosphorylation of ITAMs by Src family tyrosine-kinases (Korade-Mirnics and Corey, 2000). Inactive Src family kinases are in a folded conformation and their catalytic sites are blocked (Erpel and Courtneidge, 1995). Some Src family kinases associate with ITAM domains on FcR and the clustering of FcR activate the Src family kinases (Strzelecka et al., 1997). Hck and Lyn of Src tyrosine-kinase family have been found associated with FcR in monocytes (Ghazizadeh et al., 1994). However, Hck-

deficient macrophages exhibit normal phagocytic capacities and Lyn-deficient macrophages exhibit only a mild decrease on phagocytic capacity (Fitzer-Attas et al., 2000), suggesting that functional redundancy exists among Src tyrosine-kinase family members.

Syk kinases are cytoplasmic proteins which bind phosphorylated ITAMs of FcR by their SH2 domains (Sada et al., 2001). Syk was found to be engaged in phagosomes at a later stage than Lyn but still as an early signal generated by ligated FcR (Strzelecka-Kiliszek et al., 2002). Syk is necessary for FcR-mediated phagocytosis since phagocytosis is inhibited in Syk-deficient macrophages (Crowley et al., 1997). Phosphorylated Syk interacts with the p85 subunit of phosphatidylinositol 3-kinase (PI3K) (Moon et al., 2005) and, through adaptor molecules, with phospholipase Cγ (PLCγ) (Sada et al., 2001), both of which are necessary for FcR-mediated phagocytosis.

Type I PI3K is composed of a p85 regulatory subunit and a p110 catalytic subunit. p85 is recruited to phagosomes during phagocytosis (Fig. 1.1B) by binding to phosphorylated ITAMs and Syk kinases (Moon et al., 2005). The conformation of p85 changes after binding, which activates the p110 catalytic subunit. Type I PI3K phosphorylates phosphatidylinositol (4,5)-bisphosphate ($PI(4,5)P_2$) and phosphatidylinositol (4)-phosphate, generating phosphatidylinositol (3,4,5)-trisphosphate (PIP_3) and phosphatidylinositol (3,4)-bisphosphate ($PI(3,4)P_2$), respectively (Hawkins et al., 1992). The recruitment of PI3K to FcR complexes is amplified by a scaffolding adaptor protein Gab2, which is recruited to phagosomes by binding to PIP_3 and then recruits more p85 (Gu et al., 2003).

PIP_3 serves as an important docking site for signaling proteins which contain pleckstrin

homology (PH) domains. In addition, PIP_3 regulates multiple GTPase activities as well as contractile activities by recruiting myosin X during phagocytosis (Swanson and Hoppe, 2004). Interestingly, the requirement of PIP_3 for phagocytosis is particle size-dependent. Phagocytosis of particles larger than 3 μm is inhibited in macrophages treated with PI3K inhibitors, such as LY294002 and wortmannin, while phagocytosis of particles smaller than 3 μm is less affected (Cox et al., 1999).

PIP_3 can also promote the phosphorylation and activation of PLCγ. PLCγ accumulates at phagosome membranes and is necessary for the pseudopod extension and actin accumulation during phagocytosis (Botelho et al., 2000). PLCγ hydrolyzes $PI(4,5)P_2$ to generate diacylglycerol (DAG) and inositol trisphosphate (IP_3). IP_3 can open Ca^{2+} channels on ER membranes and facilitate the release of Ca^{2+} from ER into cytosol. Phagocytosis induces an increase of cytosolic Ca^{2+} concentration, which was found, however, to be unnecessary for phagocytosis by macrophages (Myers and Swanson, 2002). In contrast, DAG can recruit protein kinase C (PKC), which is necessary for phagocytosis (Larsen et al., 2000).

PKCε localizes to phagosomes transiently, disappearing shortly after phagosome closure (Fig. 1.1B). In addition, overexpression of PKCε increases phagocytosis while overexpression of a fragment of PKCε that competes with endogenous PKCε decreases phagocytosis efficiency, confirming a role for PKCε in phagocytosis (Larsen et al., 2002). The binding of PKCε to DAG is necessary for its recruitment (Cheeseman et al., 2006) and $PI(3,4)P_2$ and PIP_3 can stimulate PKCε activity (Toker et al., 1994). However, how PKCε contributes to phagosome formation is still unknown.

1.2.3 GTPase activities during FcR-mediated phagocytosis

The Ras superfamily of GTPases is divided into 5 families, based on sequence and functional similarities: Ras, Ran, Rab, Rho and Arf (Wennerberg et al., 2005). They function as binary molecular switches, which are regulated by binding to GTP or GDP, in a variety of signaling pathways. The GTP-bound form is the ‘on’ state, since its conformation possesses high affinity for downstream effector molecules, while the GDP-bound form is the ‘off’ state (Takai et al., 2001). Cycling between GTP- and GDP-bound forms is regulated by guanine nucleotide exchange factors (GEFs), which catalyze GDP exchange to GTP to activate GTPases (Schmidt and Hall, 2002), and by GTPase-activating proteins (GAPs), which hydrolyze GTP to GDP to inactive GTPases (Bernards and Settleman, 2004). Most Ras superfamily GTPases are post-translationally modified with lipids and targeted to membranes to interact with downstream effector molecules (Wennerberg et al., 2005). In addition, Rho and Rab family GTPases are regulated by guanine nucleotide dissociation inhibitors (GDIs), which keep them in cytosol by interacting with the modified lipids (Seabra and Wasmeier, 2004).

The Ras family is mainly involved in signaling pathways controlling gene expression, cell proliferation, differentiation and survival (Cox and Der, 2002). The Ran family functions to transport both RNA and proteins through the nuclear envelope (Weis, 2003). Neither Ras nor Ran contributes to phagocytosis. The Rab family plays an important role in intracellular vesicle transportation of the endocytic and secretory pathways (Zerial and McBride, 2001). Rab5 is localized on early endosomes and is recruited to phagosomes during phagocytosis, regulating transient fusion between endosomes and phagosomes (Duclos et al., 2000). Rab7 is localized on late endosomes and lysosomes and is recruited to phagosomes after they are internalized (Henry et al., 2004), playing a role during phagosome maturation. Rho and Arf family GTPases play important roles during

phagosome internalization by regulating the cytoskeleton and membrane remodeling.

Rho family GTPases serve as key regulators for actin organization, cell cycle progession as well as gene expression (Etienne-Manneville and Hall, 2002). Cdc42, Rac1 and Rac2 regulate FcR-mediated phagocytosis while RhoA regulates complement receptor-mediated phagocytosis (Caron and Hall, 1998). Cdc42 is activated immediately after phagocytosis starts and the activated molecules persist at the leading edge of the phagocytic cup (Fig. 1.1B). Rac1 is also activated immediately after phagocytosis starts and remains activated throughout the whole process of internalization (Fig. 1.1B). In contrast, Rac2 is not activated until a later stage of internalization and activated molecules are mainly at the base of the phagocytic cup (Fig. 1.1B) (Hoppe and Swanson, 2004). Cdc42 and Rac1 are necessary for FcR-mediated phagocytosis since blocking either of them will affect formation of the actin cup (Groves et al., 2008). Rac2 is involved in phagosome maturation by facilitating electron transfer in the NADPH oxidase complex to generate superoxide (Diebold and Bokoch, 2001).

Arf6 and Arf1 are two of the best characterized Arf family GTPases and both of them are involved in phagocytosis (D'Souza-Schorey and Chavrier, 2006). Arf6 activates phosphatidylinositol 4-phosphate 5-kinase α (PIP5Kα) (Honda et al., 1999), generating $PI(4,5)P_2$, which facilitates actin polymerization during phagocytosis. Arf6 is also thought to facilitate membrane recycling and vesicle fusion to the phagosome since a dominant negative Arf6 mutant inhibits phagocytosis and recruitment of Vamp3, an indicator of fusion between recycling endosomes and phagosomes (Niedergang et al., 2003). Arf1 regulates membrane trafficking in the Golgi network (Boman et al., 2000). Like Cdc42 and Rac2, activated Arf6 and Arf1 are differentially distributed during phagocytosis (Beemiller et al., 2006). Arf6 is activated immediately after phagocytosis starts and the

activated molecules are maintained at the leading edge of the phagocytic cup (Fig. 1.1B). Arf1 is not activated until a later stage of internalization and activated molecules appear mainly at the base of the phagocytic cup (Fig. 1.1B). In addition, the transition from Arf6 activation to Arf1 activation during phagocytosis requires PI3K activity, probably through GEF and GAP activities which are regulated by PIP_3.

1.2.4 Actin polymerization during FcR-mediated phagocytosis

Successful FcR-mediated phagocytosis requires actin polymerization around phagosomes, generating force for pseudopod protrusion. Actin polymerizes at the leading edge of the phagocytic cup and depolymerizes at the base, even before the cup is closed (Hoppe and Swanson, 2004). Actin polymerization is not diminished by PI3K inhibitors (Diakonova et al., 2002), suggesting actin polymerization is at an earlier stage in the signal pathway than PIP_3 generation.

Both Cdc42 and Rac1 regulate actin polymerization by activating the Arp2/3 complex during phagocytosis. Cdc42 interacts with Wiskott- Aldrich Syndrome Protein (WASP) while Rac1 activates WASP family Verprolin-homologous (WAVE) (Swanson and Hoppe, 2004), both of which bind to Arp2/3 and stimulate its activation (Machesky and Insall, 1998). Arp2/3 colocalizes with actin in phagosomes, and promotes actin polymerization by stimulating the formation of new branching on actin filaments (Goley and Welch, 2006). In addition, active Cdc42 and Rac bind and activate p21-activated kinase 1 (PAK1), which phosphorylates and activates LIM kinase (LIMK) (Edwards et al., 1999). LIMK can phosphorylate and deactivate cofilin, which binds and deploymerizes actin filaments. Thus Cdc42 and Rac1 facilitate actin polymerization by both stimulating actin filament branching and blocking actin depolymerization.

However, Cdc42 is deactivated before actin polymerization reaches a peak and Rac1 is still in an active state even after actin depolymerizes completely around phagosomes (Hoppe and Swanson, 2004), suggesting that Cdc42 and Rac1 do not regulate actin polymerization on their own. In contrast, $PI(4,5)P_2$ is generated and hydrolyzed closely in parallel with actin polymerization and depolymerization temporally and spatially (Scott et al., 2005). In addition, increasing $PI(4,5)P_2$ generation or inhibiting $PI(4,5)P_2$ hydrolysis inhibits actin depolymerization and phagosome closure, indicating that $PI(4,5)P_2$ is an important regulator of actin remodeling during phagocytosis. In the presence of PI3K inhibitors, incomplete phagosomes persist as actin-rich phagocytic cups. This suggests that the 3' PIs generated by PI3K in phagosomal membranes are not required directly for actin polymerization but may serve as a signal that regulates actin depolymerization at later stages of phagocytosis.

1.2.5 The zipper model of FcR-mediated phagocytosis

The molecules mentioned above are only a small fraction of the molecules involved during phagocytosis. Proteomic analysis identified 617 proteins potentially associated with phagosomes in cells of Drosophila (Stuart et al., 2007). How so many molecules are organized to generate the complex phagocytosis process is still unknown. A zipper model (Griffin and Silverstein, 1974) states that FcR on the cell surface and IgG on the particle surface interact as a zipper, in an ordered progression as the phagocytic cup advances over the particle. The zipper model proposes that each ligated receptor generates intracellular signals locally and autonomously and governs the membrane and cytoskeleton activities in one small segment of the membrane (Fig. 1.2) (Swanson and Hoppe, 2004). In support of this model, particles half coated with IgG can only be half

phagocytosed (Griffin et al., 1976). In addition, the sequential activation of Cdc42, Rac1 and Rac2 seen in forming phagocytic cups (Fig. 1.1B) (Hoppe and Swanson, 2004) is consistent with zipper model.

If downstream signals are generated autonomously by each ligated FcR, we would expect that other properties of the target particle should not affect phagocytosis. However, recent studies indicate that signaling during phagocytosis may be modulated by physical features of particles such as particle stiffness or surface topology (Beningo and Wang, 2002; Champion and Mitragotri, 2006). In this thesis, I studied the autonomy of FcR signaling from different perspectives. I found that signaling during FcR-mediated phagocytosis is coordinated by integrating receptor signaling in a domain of the membrane, which prompts a revision of the zipper model.

1.3 Fluorescence microscopy to study phagocytosis

1.3.1 Measuring signal molecule recruitment to phagosomes

Although biochemical and genetic experiments revealed which molecules are involved in phagocytosis (Stuart et al., 2007), these methods only provide a static, snapshot view of cells (Stephens and Allan, 2003; Tsien, 2003). To understand phagocytosis at the molecular level, it is necessary to have information about how molecules are modified and relocated temporally and spatially during the process, which can be provided by fluorescence microscopy.

The immunofluorescence technique, which reveals the spatial distribution of proteins in fixed cells, has been used in almost all cell biology systems (Tsien, 2003). Although its

spatial resolution is classically limited to about 200 nm by the Rayleigh diffraction limit, which is an intrinsic property of optical imaging, it can probe multiple molecules with different colors at the same time. The localization of many signaling molecules to phagosomes during phagocytosis has been revealed by immunofluorescence techniques. However, the fixation necessary for immunofluorescence of intracellular molecules complicates analysis of dynamic processes during phagocytosis.

Fluorescent protein techniques allow one to study molecular behaviors in living cells (Lippincott-Schwartz and Patterson, 2003). The DNA sequences encoding green fluorescent protein (GFP) and its variants of other colors are linked with the DNA encoding proteins of interest and transfected into cells, leading to overexpression of fluorescent protein chimeras. Observing dynamic processes in living cells using fluorescence microscopy adds a vital extra dimension to our understanding of phagocytosis, as well as many other cellular processes.

The recruitment of signaling molecules to phagosomes can be tracked using wide field fluorescence microscopy by taking time-lapse images of macrophages transfected with fluorescent chimeras. However, recruitment cannot be quantified with single color widefield fluorescence microscopy because fluorescence intensities can vary simply with changes in cell thickness that accompany phagocytosis. In other words, it is difficult to tell whether the fluorescence change at phagosomes is due to fluorescent chimera recruitment or to increased cell thickness around phagosomes, especially when the recruitment is expected to be of low level.

Confocal fluorescence microscopy can partially solve the problem of out-of-focus light. Pinholes in front of the light source and light detector can partially eliminate out-of-focus

light. Confocal fluorescence microscopy has been applied to measure the recruitment of many molecules to phagosomes in living cells. However, the use of pinholes also reduced the fraction of the total fluorescence detected, thereby reducing the signal-to-noise ratio. To compensate for this effect, higher intensities of excitation light are usually used, which can increase photo-bleaching and photo-toxicity. This drawback limits the use of confocal microscopy for collecting time-lapse images at high temporal resolution or for long times during phagocytosis.

A ratiometric fluorescence microscopy technique was developed to solve the out-of-focus light problem (Henry et al., 2004; Kamen et al., 2007). Using widefield fluorescence microscopy, ratiometric imaging reduces photo-bleaching and photo-toxicity induced by the high intensity excitation light of confocal microscopy. Yellow fluorescent protein (YFP) chimeras and unlinked cyan fluorescent protein (CFP) are coexpressed in macrophages and time-lapse images of both YFP and CFP are taken during phagocytosis. Dividing YFP images by CFP images taken in rapid sequence (<1 sec) generates a ratio image, which corrects for most of the variation in cell thickness. If the YFP chimeras are distributed uniformly in resting cells and are not recruited to any specific locations during phagocytosis, the ratio image (YFP-chimera/CFP) will show a constant value for all pixels within the cell. But if the YFP chimeras are recruited to phagosomes, then the ratio will have a higher value in the phagosome region. Dividing the average ratio within the phagosome (Rp) by the average ratio within the whole cell (Rc) generates a value (Rp/Rc) representing the extent of YFP chimera recruitment to the phagosome. This method can measure the YFP chimera recruitment quantitatively with high time resolution. However, it requires an additional fluorescence channel for imaging the unlinked fluorophore, thus reducing the number of different fluorescent chimeras which can be monitored in the same cell.

1.3.2 Measuring GTPase activity around phagosomes

Fluorescence resonance energy transfer (FRET) has been extensively used to measure molecular interactions, since FRET signals largely depend on the distance between the donor and acceptor fluorophores (Truong and Ikura, 2001). CFP and YFP are a good FRET pair, since CFP emission and YFP excitation have a large spectral overlap necessary for FRET. To measure GTPase activity in living cells, CFP and YFP chimeras of GTPases and binding domains from their effectors are coexpressed in living cells (Hoppe and Swanson, 2004). When GTPases are activated, their GTP-bound forms bind to the binding domains, which bring the CFP and YFP close to each other and generate FRET signals.

FRET signals are measured by sensitized emission, exciting CFP and monitoring YFP emission signals, which avoids the single measurement limitations of FRET based on photobleaching approaches as well as the complicated experimental setup required to measure FRET with fluorescence polarization or fluorescence lifetime. However, the sensitized emission method has a problem caused by the broad excitation and emission spectra of CFP and YFP (Hoppe et al., 2002). When the cell is illuminated by CFP excitation light, a small fraction of YFP will be excited even in the absence of FRET, contributing to the signals collected at the YFP emission channel. Furthermore, a small fraction of CFP emission is transmitted through the YFP emission channel. Thus, the signals measured by filter sets for exciting CFP and monitoring YFP emission are composed of sensitized emission, which represents the FRET signal, plus directly activated of YFP and CFP bleed-through. FRET stoichiometry (Hoppe et al., 2002) was developed to separate FRET signals from those components and at the same time to

correct the out-of-focus light problem of widefield fluorescence microscopy. Three images are acquired by exciting CFP and imaging at the CFP channel, exciting YFP and imaging at the YFP channel as well as exciting CFP and imaging at the YFP channel. Then a series of calculations are performed to generate another three images: E_D whose intensity is proportional to the ratio of CFP molecules in complex with YFP chimeras, E_A whose intensity is proportional to the ratio of YFP molecules in complex with CFP chimeras and R_m, which represents the molar ratio of total YFP molecules to CFP molecules. When YFP and CFP are linked with GTPases and their binding domains, E_D and E_A are indicators of GTPase activity.

Using FRET stoichiometry, Cdc42, Rac1 and Rac2 activities were measured with p21-binding domain (PBD) from PAK1 (Hoppe and Swanson, 2004), and Arf6 and Arf1 activities were measured with the N-terminus of the GGA1 GAT domain (NGAT) (Beemiller et al., 2006) during phagocytosis. In addition, FRET stoichiometry has been adapted to three-dimensional imaging applications by combining the algorithms of FRET stoichiometry with three-dimensional image deconvolution algorithms (Hoppe et al., 2008). This reconstruction method can measure GTPase activities with detailed spatial information, but requires complex and time-consuming image processing.

In addition to FRET chimera pairs, FRET biosensors, which have both the donor and acceptor fluorophores on the same molecule, have also been applied to monitor GTPase activities in living cells (Itoh et al., 2002). CFP, a GTPase-binding domain and YFP are linked as one molecule, named raichu, and expressed in cells. When the GTPase is activated, it can bind to the binding domain of the chimera and cause a conformation change, which induces FRET signal changes. Since the molar ratio of donor and

acceptor is always 1 for FRET biosensors, the FRET signal can be measured by the ratio of acceptor emission to donor emission when the cell is excited at donor's excitation channel, which allows easier calculation than FRET stoichiometry. However, the signal from FRET biosensors is usually low (Nakamura et al., 2006).

1.3.3 Measuring lipid modification at phagosomes

Lipids, especially phosphoinositides, play important roles during phagocytosis (Yeung et al., 2006a). Since phosphoinositides serve as docking sites for multiple signaling molecules, fluorescent protein chimeras of lipid-binding domains, such as pleckstrin homology (PH) domains, from their downstream effectors, can probe the distribution of the lipids on membranes in living cells. Many of those probes have been used to study phagocytosis. For instance, GFP-labeled PLCδ-PH and C1δ were used to monitor the hydrolysis of $PI(4,5)P_2$ to DAG respectively (Botelho et al., 2000). YFP-labeled FYVE probes detected the patterns of PI3P generation on phagosomes (Henry et al., 2004). YFP-labeled BtkPH and Tapp1PH monitered PIP_3 and $PI(3,4)P_2$ generation and their relationship with PI3K recruitment (Kamen et al., 2007).

Although these probes have been widely used to monitor lipid modification in living cells, potential problems have been identified. First, the specificity of lipid recognition by those binding domains is sometimes affected by the lipid environment and by other molecules (Varnai and Balla, 2006). Second, overexpressed binding domains may inhibit intracellular signaling by competing with endogenous signaling molecules which bind to lipids. Binding domains from different molecules for the same phosphoinositides may even have different inhibitory effects in one single signaling event (Varnai et al., 2005). Thus, the application of these binding domains requires careful assessment of the

inhibitory effect in each specific situation.

1.3.4 Measuring membrane surface electric charges

The inner leaflet of the cell membrane has a negative surface charge contributed by phospholipids (Yeung and Grinstein, 2007). This negative surface charge contributes to interactions with proteins with positive-charged motifs, such as Rac1, Src and Ras (Yeung et al., 2008), which play important roles during phagocytosis. An electrostatic probe was constructed from C-terminal farnesylation and a neighboring positive-charged motif from K-Ras, the fluorescent chimera of which can detect surface charges both in vitro and inside living cells (Yeung et al., 2006b). It was found that phagosomes lost their strong negative charge at later stages during internalization, which probably contributes to the release of signaling molecules required for internalization.

1.4 Overview of this thesis

This thesis addresses the overall question of how signaling during phagocytosis is coordinated. It establishes that a 3'-phosphoinositide concentration threshold regulates commitment to phagocytosis by regulating late stage signal protein recruitment and GTPase activity transitions. In chapter 2, I address the question of whether signals are generated autonomously during FcR-mediated phagocytosis. With a newly developed recruitment measurement method, based on ratiometric fluorescence microscopy, I measure the magnitude of signal molecule recruitment as a function of ligand density and identified a role for 3'-phosphoinositide concentration thresholds in phagocytosis. In chapter 3, I address the question whether the 3'-phosphoinositide concentration threshold regulates Rho family GTPase activities. I also establish that the Rho GTPase

activity transition is required for FcR-mediated phagocytosis. In chapter 4, I demonstrate that the 3'-phosphoinositide concentration threshold correlates with the phenomenon that the shape of target particles affects phagocytosis. In summary, these three chapters study the role of 3'-phosphoinositide concentration thresholds in signal transduction during phagocytosis, from different perspectives and with various fluorescence microscopy techniques.

Figure 1.1 Signaling molecules display different spatial distributions during phagocytosis. (A) Different stages during the formation of a phagosome are shown. The grey line represents cell membranes. Grey dots under the grey line represent recruited actin molecules. The membranes of the half cup, marked with red color, are picked to show signaling molecule activation in Fig 1.1B. (B) The different patterns of GTPase activation, kinase activation and phospholipids generation are shown at different stages during phagosome formation. The locations of signal activation are shown in red lines.

Figure 1.1 (Adapted from Swanson, J.A. 2008 Shaping cups into phagosomes and macropinosomes *Nature Rev. Mol.Cell Biol*. 9:639-649.)

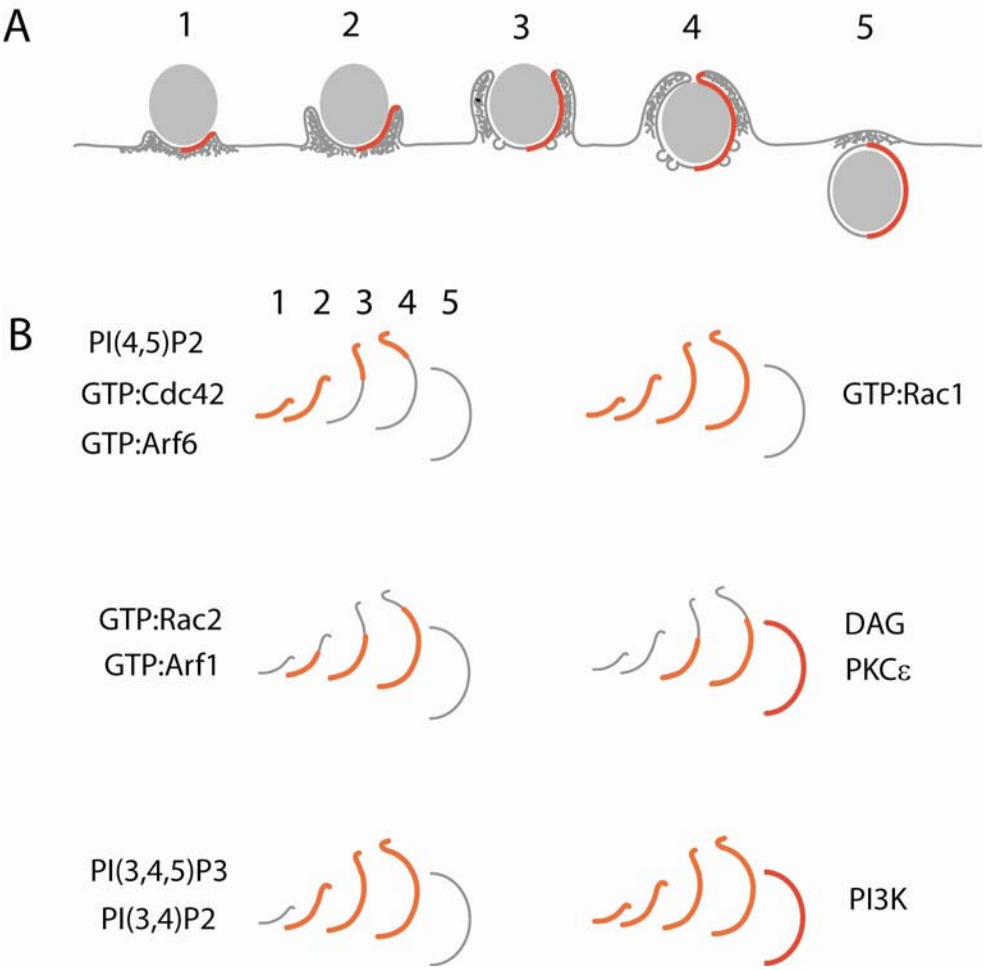

Figure 1.2 Signaling molecules are activated sequentially during phagocytosis in zipper model. The zipper model proposes that each ligated receptor generates intracellular signals locally and autonomously. Early stage signals (red) are generated at the beginning of phagocytosis. During the advance of the phagocytic cup, early stage signals are activated by newly ligated receptors at the leading edge of the phagocytic cup and deactivated at the base of the phagocytic cup. The signals at the base of phagocytic cup proceed to later stages (blue, green), causing a spatial gradient of signaling events.

Figure 1.2 (Adapted from Swanson, J.A. and Hoppe, A.D. 2004 The coordination of signaling during Fc receptor-mediated phagocytosis *J Leukoc Biol*. 76:1093-1103.)

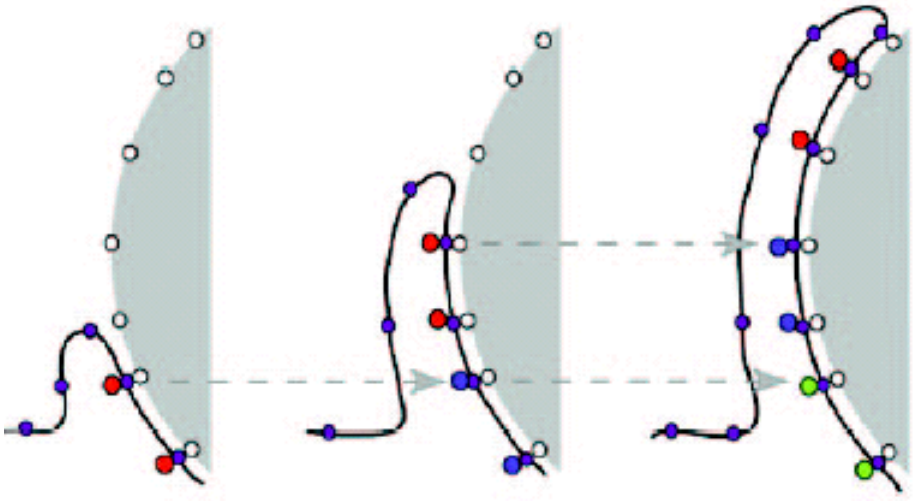

1.5 Bibliography

Akira, S., S. Uematsu, and O. Takeuchi. 2006. Pathogen recognition and innate immunity. *Cell*. 124:783-801.

Babior, B.M. 1999. NADPH oxidase: an update. *Blood*. 93:1464-76.

Babior, B.M., J.T. Curnutte, and B.J. McMurrich. 1976. The particulate superoxide-forming system from human neutrophils. Properties of the system and further evidence supporting its participation in the respiratory burst. *J Clin Invest*. 58:989-96.

Barrow, A.D., and J. Trowsdale. 2006. You say ITAM and I say ITIM, let's call the whole thing off: the ambiguity of immunoreceptor signalling. *Eur J Immunol*. 36:1646-53.

Beemiller, P., A.D. Hoppe, and J.A. Swanson. 2006. A phosphatidylinositol-3-kinase-dependent signal transition regulates ARF1 and ARF6 during Fcg receptor-mediated phagocytosis. *PLoS Biol*. 4:e162.

Beningo, K.A., and Y.-L. Wang. 2002. Fc-receptor-mediated phagocytosis is regulated by mechanical properties of the target. *J. Cell Sci.* 115:849-856.

Bernards, A., and J. Settleman. 2004. GAP control: regulating the regulators of small GTPases. *Trends Cell Biol*. 14:377-85.

Birge, R.B., and D.S. Ucker. 2008. Innate apoptotic immunity: the calming touch of death. *Cell Death Differ*. 15:1096-102.

Boman, A.L., C. Zhang, X. Zhu, and R.A. Kahn. 2000. A family of ADP-ribosylation factor effectors that can alter membrane transport through the trans-Golgi. *Mol Biol Cell*. 11:1241-55.

Bosch, E., J. Horwitz, and D. Bok. 1993. Phagocytosis of outer segments by retinal pigment epithelium: phagosome-lysosome interaction. *J Histochem Cytochem*. 41:253-63.

Botelho, R.J., M. Teruel, R. Dierckman, R. Anderson, A. Wells, J.D. York, T. Meyer, and S. Grinstein. 2000. Localized biphasic changes in phosphatidylinositol-4,5-bisphosphate at sites of phagocytosis. *J. Cell Biol.* 151:1353-1367.

Brown, E.J. 1995. Phagocytosis. *Bioessays*. 17:109-17.

Cambi, A., and C.G. Figdor. 2005. Levels of complexity in pathogen recognition by C-type lectins. *Curr Opin Immunol*. 17:345-51.

Cardelli, J. 2001. Phagocytosis and macropinocytosis in *Dictyostelium*: Phosphoinositide-based processes, biochemically distinct. *Traffic*. 2:311-320.

Caron, E., and A. Hall. 1998. Identification of two distinct mechanisms of phagocytosis controlled by different Rho GTPases. *Science*. 282:1717-1721.

Caux, C., C. Massacrier, B. Vanbervliet, B. Dubois, C. Van Kooten, I. Durand, and J. Banchereau. 1994. Activation of human dendritic cells through CD40 cross-linking. *J Exp Med*. 180:1263-72.

Champion, J.A., and S. Mitragotri. 2006. Role of target geometry in phagocytosis. *Proc Natl Acad Sci U S A*. 103:4930-4.

Cheeseman, K.L., T. Ueyama, T.M. Michaud, K. Kashiwagi, D. Wang, L.A. Flax, Y. Shirai, D.J. Loegering, N. Saito, and M.R. Lennartz. 2006. Targeting of protein kinase C-e during Fcg receptor-dependent phagocytosis requires the e-C1B domain and phospholipase C-g1. *Mol Biol Cell*. 17:799-813.

Cohn, Z.A., and J.G. Hirsch. 1960. The influence of phagocytosis on the intracellular distribution of granule-associated components of polymorphonuclear leucocytes. *J Exp Med*. 112:1015-22.

Cooper, D., F.P. Lindberg, J.R. Gamble, E.J. Brown, and M.A. Vadas. 1995. Transendothelial migration of neutrophils involves integrin-associated protein (CD47). *Proc Natl Acad Sci U S A*. 92:3978-82.

Cox, A.D., and C.J. Der. 2002. Ras family signaling: therapeutic targeting. *Cancer Biol Ther*. 1:599-606.

Cox, D., C.-C. Tseng, G. Bjekic, and S. Greenberg. 1999. A requirement for phosphatidylinositol 3-kinase in pseudopod extension. *J. Biol. Chem.* 274:1240-1247.

Crowley, M.T., P.S. Costello, C.J. Fitzer-Attas, M. Turner, F. Meng, C. Lowell, V.L.J. Tybulewicz, and A.L. DeFranco. 1997. A critical role for Syk in signal transduction and phagocytosis mediated by Fcg receptors on macrophages. *J. Exp. Med.* 186:1027-1039.

D'Souza-Schorey, C., and P. Chavrier. 2006. ARF proteins: roles in membrane traffic and beyond. *Nat Rev Mol Cell Biol*. 7:347-58.

Dale, D.C., L. Boxer, and W.C. Liles. 2008. The phagocytes: neutrophils and monocytes. *Blood*. 112:935-45.

Diakonova, M., G. Bokoch, and J.A. Swanson. 2002. Dynamics of cytoskeletal proteins during Fcg receptor-mediated phagocytosis in macrophages. *Mol. Biol. Cell*. 13:402-411.

Diebold, B.A., and G.M. Bokoch. 2001. Molecular basis for Rac2 regulation of phagocyte NADPH oxidase. *Nature Immunology*. 2:211-215.

Duclos, S., R. Diez, J. Garin, B. Papadopoulou, A. Descoteaux, H. Stenmark, and M. Desjardins. 2000. Rab5 regulates the kiss and run fusion between phagosomes and endosomes and the acquisition of phagosome leishmanicidal properties in RAW 264.7 macrophages. *J. Cell Sci.* 113:3531-3541.

Edwards, D.C., L.C. Sanders, G.M. Bokoch, and G.M. Gill. 1999. Activation of LIM-kinase by Pak1 couples Rac/Cdc42 GTPase signalling to actin cytoskeletal dynamics. *Nature Cell Biol.* 1:253-259.

Erpel, T., and S.A. Courtneidge. 1995. Src family protein tyrosine kinases and cellular signal transduction pathways. *Curr Opin Cell Biol*. 7:176-82.

Etienne-Manneville, S., and A. Hall. 2002. Rho GTPases in cell biology. *Nature*. 420:629-635.

Figdor, C.G., Y. van Kooyk, and G.J. Adema. 2002. C-type lectin receptors on dendritic cells and Langerhans cells. *Nat Rev Immunol*. 2:77-84.

Fitzer-Attas, C.J., M. Lowry, M.T. Crowley, A.J. Finn, F. Meng, A.L. DeFranco, and C.A. Lowell. 2000. Fcg receptor-mediated phagocytosis in macrophages lacking the Src family tyrosine kinases Hck, Fgr, and Lyn. *J. Exp. Med.* 191:669-681.

Gerard, C., and B.J. Rollins. 2001. Chemokines and disease. *Nat Immunol*. 2:108-15.

Ghazizadeh, S., J.B. Bolen, and H.B. Fleit. 1994. Physical and functional association of Src-related protein tyrosine kinases with Fc gamma RII in monocytic THP-1 cells. *J Biol Chem*. 269:8878-84.

Goley, E.D., and M.D. Welch. 2006. The ARP2/3 complex: an actin nucleator comes of age. *Nat Rev Mol Cell Biol*. 7:713-26.

Griffin, F.M., J.A. Griffin, and S.C. Silverstein. 1976. Studies on the mechanism of phagocytosis. II. The interaction of macrophages with anti-immunoglobulin IgG-coated bone marrow-derived lymphocytes. *J. Exp. Med.* 144:788-809.

Griffin, F.M., and S.C. Silverstein. 1974. Segmental response of the macrophage plasma membrane to a phagocytic stimulus. *J. Exp. Med.* 139:323-336.

Groves, E., A.E. Dart, V. Covarelli, and E. Caron. 2008. Molecular mechanisms of phagocytic uptake in mammalian cells. *Cell Mol Life Sci*. 65:1957-76.

Gu, H., R.J. Botelho, M. Yu, S. Grinstein, and B.G. Neel. 2003. Critical role for scaffolding adapter Gab2 in FcgR-mediated phagocytosis. *J. Cell Biol.* 161:1151-1161.

Guermonprez, P., L. Saveanu, M. Kleijmeer, J. Davoust, P. Van Endert, and S.

Amigorena. 2003. ER-phagosome fusion defines an MHC class I cross-presentation compartment in dendritic cells. *Nature*. 425:397-402.
Hawkins, P.T., T.R. Jackson, and L.R. Stephens. 1992. Platelet-derived growth factor stimulates synthesis of PtdIns(3,4,5)P3 by activating a PtdIns(4,5)P2 3-OH kinase. *Nature*. 358:157-9.
Henry, R.M., A.D. Hoppe, N. Joshi, and J.A. Swanson. 2004. The uniformity of phagosome maturation in macrophages. *J Cell Biol*. 164:185-94.
Hiltbold, E.M., and P.A. Roche. 2002. Trafficking of MHC class II molecules in the late secretory pathway. *Curr Opin Immunol*. 14:30-5.
Honda, A., M. Nogami, T. Yokozeki, M. Yamazaki, H. Nakamura, H. Watanabe, K. Kawamoto, K. Nakayama, A.J. Morris, M.A. Frohman, and Y. Kanaho. 1999. Phosphatidylinositol 4-phosphate 5-kinase a is a downstream effector of the small G protein ARF6 in membrane ruffle formation. *Cell*. 99:521-532.
Hoppe, A., K.A. Christensen, and J.A. Swanson. 2002. Fluorescence resonance energy transfer-based stoichiometry in living cells. *Biophys. J.* 83:3652-3664.
Hoppe, A.D., S.L. Shorte, J.A. Swanson, and R. Heintzmann. 2008. 3D-FRET Reconstruction Microscopy for Analysis of Dynamic Molecular Interactions in Live Cells. *Biophys J.* 95:400-418.
Hoppe, A.D., and J.A. Swanson. 2004. Cdc42, Rac1 and Rac2 display distinct patterns of activation during phagocytosis. *Mol. Biol. Cell*. 15:3509-3519.
Houde, M., S. Bertholet, E. Gagnon, S. Brunet, G. Goyette, A. Laplante, M.F. Princiotta, P. Thibault, D. Sacks, and M. Desjardins. 2003. Phagosomes are competent organelles for antigen cross-presentation. *Nature*. 425:402-406.
Huynh, K.K., J.G. Kay, J.L. Stow, and S. Grinstein. 2007. Fusion, fission, and secretion during phagocytosis. *Physiology (Bethesda)*. 22:366-72.
Itano, A.A., and M.K. Jenkins. 2003. Antigen presentation to naive CD4 T cells in the lymph node. *Nat Immunol*. 4:733-9.
Itoh, R.E., K. Kurokawa, Y. Ohba, H. Yoshizaki, N. Mochizuki, and M. Matsuda. 2002. Activation of Rac and Cdc42 video imaged by fluorescence resonance energy transfer-based single-molecule probes in the membrane of living cells. *Mol. Cell. Biol.* 22:6582-6591.
Kamen, L.A., J. Levinsohn, and J.A. Swanson. 2007. Differential Association of Phosphatidylinositol 3-Kinase, SHIP-1, and PTEN with Forming Phagosomes. *Mol Biol Cell*. 18:2463-2475.
Kaplan, S.S., J.R. Lancaster, Jr., R.E. Basford, and R.L. Simmons. 1996. Effect of nitric oxide on staphylococcal killing and interactive effect with superoxide. *Infect Immun*. 64:69-76.
Kaufmann, S.H., and U.E. Schaible. 2005. Antigen presentation and recognition in bacterial infections. *Curr Opin Immunol*. 17:79-87.
Kim, M.K., Z.Y. Huang, P.H. Hwang, B.A. Jones, N. Sato, S. Hunter, T.H. Kim-Han, R.G. Worth, Z.K. Indik, and A.D. Schreiber. 2003. Fcgamma receptor transmembrane domains: role in cell surface expression, gamma chain interaction, and phagocytosis. *Blood*. 101:4479-84.
Klebanoff, S.J. 2005. Myeloperoxidase: friend and foe. *J Leukoc Biol*. 77:598-625.
Korade-Mirnics, Z., and S.J. Corey. 2000. Src kinase-mediated signaling in leukocytes. *J. Leukoc. Biol.* 68:603-613.
Larsen, E.C., J.A. DiGennaro, N. Saito, S. Mehta, D.J. Loegering, J.E. Mazurkiewicz, and M.R. Lennartz. 2000. Differential requirement for classic and novel PKC isoforms in respiratory burst and phagocytosis in RAW 264.7 cells. *J. Immunol.* 165:2809-2817.
Larsen, E.C., T. Ueyama, P.M. Brannock, Y. Shirai, N. Saito, C. Larsson, D. Loegering,

P.B. Weber, and M.R. Lennartz. 2002. A role for PKC-e in FcgR-mediated phagocytosis by RAW 264.7 cells. *J. Cell Biol.* 159:939-944.

Ley, K., D.C. Bullard, M.L. Arbones, R. Bosse, D. Vestweber, T.F. Tedder, and A.L. Beaudet. 1995. Sequential contribution of L- and P-selectin to leukocyte rolling in vivo. *J Exp Med*. 181:669-75.

Lippincott-Schwartz, J., and G.H. Patterson. 2003. Development and use of fluorescent protein markers in living cells. *Science*. 300:87-91.

Machesky, L.M., and R.H. Insall. 1998. Scar1 and the related Wiskott-Aldrich syndrome protein, WASP, regulate the actin cytoskeleton through the Arp2/3 complex. *Curr Biol*. 8:1347-56.

MacMicking, J., Q.-w. Xie, and C. Nathan. 1997. Nitric oxide and macrophage function. *Annu. Rev. Immunol.* 15:323-350.

Moon, K.D., C.B. Post, D.L. Durden, Q. Zhou, P. De, M.L. Harrison, and R.L. Geahlen. 2005. Molecular basis for a direct interaction between the Syk protein-tyrosine kinase and phosphoinositide 3-kinase. *J Biol Chem*. 280:1543-51.

Myers, J.T., and J.A. Swanson. 2002. Calcium spikes in activated macrophages during Fcg receptor-mediated phagocytosis. *J. Leukoc. Biol.* 72:677-684.

Nakamura, T., K. Kurokawa, E. Kiyokawa, and M. Matsuda. 2006. Analysis of the spatiotemporal activation of rho GTPases using Raichu probes. *Methods Enzymol*. 406:315-32.

Niedergang, F., E. Colucci-Guyon, T. Dubois, G. Raposo, and P. Chavrier. 2003. ADP ribosylation factor 6 is activated and controls membrane delivery during phagocytosis in macrophages. *J. Cell Biol.* 161:1143-1150.

Petri, B., and M.G. Bixel. 2006. Molecular events during leukocyte diapedesis. *FEBS J*. 273:4399-407.

Pierre, P., S.J. Turley, E. Gatti, M. Hull, J. Meltzer, A. Mirza, K. Inaba, R.M. Steinman, and I. Mellman. 1997. Developmental regulation of MHC class II transport in mouse dendritic cells. *Nature*. 388:787-92.

Qi, H., J.G. Egen, A.Y. Huang, and R.N. Germain. 2006. Extrafollicular activation of lymph node B cells by antigen-bearing dendritic cells. *Science*. 312:1672-6.

Ravetch, J.V., and S. Bolland. 2001. IgG Fc receptors. *Annu Rev Immunol*. 19:275-90.

Sada, K., T. Takano, S. Yanagi, and H. Yamamura. 2001. Structure and function of Syk protein-tyrosine kinase. *J Biochem*. 130:177-86.

Schmidt, A., and A. Hall. 2002. Guanine nucleotide exchange factors for Rho GTPases: turning on the switch. *Genes Dev*. 16:1587-609.

Scott, C.C., W. Dobson, R.J. Botelho, N. Coady-Osberg, P. Chavrier, D.A. Knecht, C. Heath, P. Stahl, and S. Grinstein. 2005. Phosphatidylinositol-4,5-bisphosphate hydrolysis directs actin remodeling during phagocytosis. *J Cell Biol*. 169:139-49.

Seabra, M.C., and C. Wasmeier. 2004. Controlling the location and activation of Rab GTPases. *Curr Opin Cell Biol*. 16:451-7.

Stephens, D.J., and V.J. Allan. 2003. Light microscopy techniques for live cell imaging. *Science*. 300:82-6.

Strzelecka-Kiliszek, A., K. Kwiatkowska, and A. Sobota. 2002. Lyn and Syk kinases are sequentially engaged in phagocytosis mediated by Fc gamma R. *J Immunol*. 169:6787-94.

Strzelecka, A., K. Kwiatkowska, and A. Sobota. 1997. Tyrosine phosphorylation and Fcgamma receptor-mediated phagocytosis. *FEBS Lett*. 400:11-4.

Stuart, L.M., J. Boulais, G.M. Charriere, E.J. Hennessy, S. Brunet, I. Jutras, G. Goyette, C. Rondeau, S. Letarte, H. Huang, P. Ye, F. Morales, C. Kocks, J.S. Bader, M. Desjardins, and R.A. Ezekowitz. 2007. A systems biology analysis of the Drosophila phagosome. *Nature*. 445:95-101.

Stuart, L.M., and R.A. Ezekowitz. 2005. Phagocytosis: elegant complexity. *Immunity*. 22:539-50.

Swanson, J.A., and A.D. Hoppe. 2004. The coordination of signaling during Fc receptor-mediated phagocytosis. *J Leukoc Biol*. 76:1093-103.

Takai, Y., T. Sasaki, and T. Matozaki. 2001. Small GTP-binding proteins. *Physiol Rev*. 81:153-208.

Ting, J.P., and B.K. Davis. 2005. CATERPILLER: a novel gene family important in immunity, cell death, and diseases. *Annu Rev Immunol*. 23:387-414.

Toker, A., M. Meyer, K.K. Reddy, J.R. Falck, R. Aneja, S. Aneja, A. Parra, D.J. Burns, L.M. Ballas, and L.C. Cantley. 1994. Activation of protein kinase C family members by the novel polyphosphoinositides PtdIns-3,4-P2 and PtdIns-3,4,5-P3. *J Biol Chem*. 269:32358-67.

Touret, N., P. Paroutis, M. Terebiznik, R.E. Harrison, S. Trombetta, M. Pypaert, A. Chow, A. Jiang, J. Shaw, C. Yip, H.P. Moore, N. van der Wel, D. Houben, P.J. Peters, C. de Chastellier, I. Mellman, and S. Grinstein. 2005. Quantitative and dynamic assessment of the contribution of the ER to phagosome formation. *Cell*. 123:157-70.

Truong, K., and M. Ikura. 2001. The use of FRET imaging microscopy to detect protein-protein interactions and protein conformational changes *in vivo*. *Curr. Opin. Structural Biol.* 11:573-578.

Tsien, R.Y. 2003. Imagining imaging's future. *Nat Rev Mol Cell Biol*. Suppl:SS16-21.

Ueno, H., E. Klechevsky, R. Morita, C. Aspord, T. Cao, T. Matsui, T. Di Pucchio, J. Connolly, J.W. Fay, V. Pascual, A.K. Palucka, and J. Banchereau. 2007. Dendritic cell subsets in health and disease. *Immunol Rev*. 219:118-42.

Varnai, P., and T. Balla. 2006. Live cell imaging of phosphoinositide dynamics with fluorescent protein domains. *Biochim Biophys Acta*. 1761:957-67.

Varnai, P., T. Bondeva, P. Tamas, B. Toth, L. Buday, L. Hunyady, and T. Balla. 2005. Selective cellular effects of overexpressed pleckstrin-homology domains that recognize PtdIns(3,4,5)P3 suggest their interaction with protein binding partners. *J Cell Sci*. 118:4879-88.

Vestweber, D. 2007. Adhesion and signaling molecules controlling the transmigration of leukocytes through endothelium. *Immunol Rev*. 218:178-96.

Weis, K. 2003. Regulating access to the genome: nucleocytoplasmic transport throughout the cell cycle. *Cell*. 112:441-51.

Wennerberg, K., K.L. Rossman, and C.J. Der. 2005. The Ras superfamily at a glance. *J Cell Sci*. 118:843-6.

Yeung, T., G.E. Gilbert, J. Shi, J. Silvius, A. Kapus, and S. Grinstein. 2008. Membrane phosphatidylserine regulates surface charge and protein localization. *Science*. 319:210-3.

Yeung, T., and S. Grinstein. 2007. Lipid signaling and the modulation of surface charge during phagocytosis. *Immunol Rev*. 219:17-36.

Yeung, T., B. Ozdamar, P. Paroutis, and S. Grinstein. 2006a. Lipid metabolism and dynamics during phagocytosis. *Curr Opin Cell Biol*. 18:429-37.

Yeung, T., M. Terebiznik, L. Yu, J. Silvius, W.M. Abidi, M. Philips, T. Levine, A. Kapus, and S. Grinstein. 2006b. Receptor activation alters inner surface potential during phagocytosis. *Science*. 313:347-51.

Zerial, M., and H. McBride. 2001. Rab proteins as membrane organizers. *Nat Rev Mol Cell Biol*. 2:107-17.

Chapter Two

3' Phosphoinositide concentration thresholds regulate commitment to phagocytosis

2.1 Abstract

During Fcγ receptor (FcR)-mediated phagocytosis by macrophages, cytoplasm advances over immunoglobulin G (IgG)-coated particles by the sequential ligation of FcR in plasma membranes. If FcR signal autonomously, as suggested by the zipper model (Griffin et al., 1975), then signals generated in phagocytic cups should be proportional to the number of ligated receptors and independent of the outcome of the process. These properties were measured by quantifying the recruitment of yellow fluorescent protein (YFP)-labeled probes to phagosomes containing beads with different densities of surface IgG. Low IgG density on beads reduced the fraction of bound particles ingested but not the rate of phagosome formation, indicating regulation of cellular commitment to later stages of phagosome formation. Although early FcR-dependent signals correlated with IgG density on beads, later signals showed a threshold response which was regulated by the concentrations of phosphatidylinositol (3,4,5)-trisphosphate (PIP_3) in phagocytic cups. Thus, PIP_3 concentration thresholds regulate distinct cellular responses by integrating receptor signaling in a domain of membrane.

2.2 Introduction

In late stages of adaptive immune responses, particles or microbes coated with IgG are efficiently removed by FcR-mediated phagocytosis into neutrophils and macrophages. Ligated FcR on macrophage plasma membranes induce phosphorylation of tyrosines within the immunoreceptor tyrosine-based activation motif (ITAM) of FcR, which propagates intracellular signals required for phagocytosis (Swanson and Hoppe, 2004). Those signals include the recruitment of protein and lipid kinases, such as Syk (Nimmerjahn and Ravetch, 2006), phosphatidylinositol 3-kinase (PI3K) (Araki et al., 1996) and protein kinase C-ε (PKCε)(Larsen et al., 2002), the reorganization of the actin cytoskeleton (May and Machesky, 2001) and the increased synthesis of PIP_3, $PI(4,5)P_2$ and diacylglycerol (Araki et al., 1996; Botelho et al., 2000). The zipper model of FcR-mediated phagocytosis states that ligands (IgG) and receptors (FcR) interact in an ordered progression as the phagocytic cup advances over the particle, with each ligated receptor generating downstream signals locally and autonomously (Griffin et al., 1975). However, recent studies indicate that signaling during phagocytosis may be modulated by physical features of particles such as particle stiffness or surface topology (Beningo and Wang, 2002; Champion and Mitragotri, 2006). This indicates possible feedback regulation of FcR signaling cascades.

To determine whether receptors generate downstream signals independently of each other, we used ratiometric fluorescence microscopy to investigate the relationship between the number of ligated receptors and the magnitude of signaling molecule recruitment to phagosomes. We found the recruitment of early stage signals, including Syk, the p85 subunit of PI3K and actin, correlated with IgG density on beads. In contrast, PIP_3 generation was uniformly high when phagocytosis could be completed and low when phagocytosis stalled, indicating that PI3K amplification correlated with successful advance of the phagocytic cup. In addition, the recruitment of the late stage signal PKCε

showed an inverse relationship to IgG density on beads and was regulated by the concentrations of PIP_3 in phagocytic cups. Therefore, downstream signals are not generated autonomously by ligated receptors as predicted by zipper model. Instead, PIP_3 concentration thresholds regulate distinct cellular responses by integrating receptor signaling in a domain of membrane.

2.3 Results

2.3.1 Recruitment of YFP chimeras to phagocytosis of particles coated with different amounts of IgG can be measured by ratiometric fluorescence microscopy

To vary the numbers of ligated FcR in phagosomes, we prepared 5.6 μm polystyrene beads coated (opsonized) with different densities of Texas red-conjugated IgG (Fig. 2.1). The IgG on bead surfaces was measured by fluorescence microscopy and normalized to the lowest density which generated a phagocytic index higher than 0.5 (B1). Beads with 10-fold higher IgG density (B10) were ingested more readily (Fig. 2.2A), but the rates of phagosome formation were similar for both (Fig. 2.2B). This indicates that cellular commitment to phagocytosis triggers a uniform signaling cascade.

FcR-generated signals were measured by quantifying the recruitment of yellow fluorescent protein (YFP)-labeled probes to phagosomes containing beads with different densities of surface IgG. We developed a method to quantify the recruitment of YFP-chimeras to phagosomes as a function of IgG density on beads (Fig. 2.3). Ratiometric fluorescence imaging of macrophages expressing YFP chimeras and free cyan fluorescent protein (CFP) allowed correction for variations in cell thickness (Henry et al., 2004). Multiplying the CFP image by the average ratio of YFP to CFP fluorescence in the

cell ($\overline{\mathrm{Rc}}$) renormalized the CFP image to the YFP expression level. Subtraction of this YFP-pathlength image from the original YFP image created an image, Re, whose intensity quantified the specific recruitment of the YFP chimera to subregions of the cell. To correct for different sizes of phagocytic cups at different stages of phagosome formation, the average YFP-chimera recruitment per pixel was calculated from regions of phagosomes. Images were acquired from cells with similar YFP-chimera expression levels to ensure comparable contributions from endogenous signaling molecules. We then measured the recruitment of YFP chimeras of proteins essential to phagocytosis.

2.3.2 Early stages of signaling correlate with IgG density on beads

Syk kinases bind phosphorylated ITAMs of FcR by their SH2 domains (Sada et al., 2001) and Syk recruitment is an early signal generated by ligated FcR (Nimmerjahn and Ravetch, 2006). Syk-YFP was recruited to phagosomes containing B10 and remained on phagosomes during internalization (Fig. 2.4 A). Low IgG-density beads (B1) recruited less Syk-YFP than beads with higher IgG densities (Fig. 2.4 B, D). Recruitment correlated with ligand density, with some saturation at the highest IgG density (Fig. 2.4 E). The recruitment of Syk(R194A)-YFP, containing a point mutation in the SH2 domain which abrogates binding to FcR ITAMs (Mocsai et al., 2006), was low for both B10 and B1 (Fig. 2.4 C, E), indicating the specificity of the recruitment calculation method.

To investigate whether signals downstream of Syk are similarly recruited in proportion to IgG density, we examined the recruitment of YFP-p85, the regulatory domain of type I PI3K, and YFP-actin. p85 binds phosphorylated Syk (Moon et al., 2005) and is recruited to phagosomes early (Kamen et al., 2007). Actin is necessary for FcR-mediated

phagocytosis (May and Machesky, 2001) and is recruited at the first membrane movement (Hoppe and Swanson, 2004). If FcR signal autonomously, then the recruitment of YFP-p85 or YFP-actin to B10 and B1 should resemble that of Syk-YFP. However, although B10 recruited more YFP-p85 than did B1 (Fig. 2.4 F), the difference was only about 2-fold (Fig. 2.4 G) and B10 recruited only 30% more YFP-actin than B1 (Fig. 2.4 H, I). These non-linear signaling responses to 10-fold differences in IgG density suggested differential signal amplification, possibly through feedback amplification at low IgG densities, or signal suppression at higher IgG densities, which were inconsistent with a strictly autonomous signaling mechanism. Because more YFP-actin was recruited than Syk-YFP or YFP-p85, we could quantify YFP-actin in stalled phagocytic cups (covering about 1/6th of the bead surface). The YFP-actin recruited to stalled cups was only slightly lower than that recruited during successful phagocytic events (finished phagosomes; Fig. 2.4 I).

2.3.3 Later stages of signaling correlate inversely with IgG density on beads

Later stages of signaling showed a binary response related to successful particle ingestion. PI3K regulates contractile activities and membrane fusion necessary for completion of phagocytosis (Cox et al., 1999; Swanson et al., 1999) and has been implicated in a signal transition governing Arf GTPase activities during phagocytosis (Beemiller et al., 2006). YFP-AktPH, a YFP chimera of the pleckstrin homology (PH) domain of Akt, was used to localize PIP_3 and $PI(3,4)P_2$ (Hoppe and Swanson, 2004), the products of type I PI3K (Yeung and Grinstein, 2007). Notably, no difference of YFP-AktPH recruitment was observed during phagocytosis of B10 or B1 (Fig. 2.5 A, B, D, E). BtkPH-YFP, which binds PIP_3 specifically, and YFP-Tapp1PH, which binds $PI(3,4)P_2$ (Varnai et al., 2006), were also recruited to similar levels on B10 and B1 (Fig. 2.5 F-I). In

contrast, stalled phagocytic cups recruited significantly less YFP-AktPH than finished phagosomes, despite similar IgG densities on the beads (Fig. 2.5 C, E). Thus, PIP_3 concentrations were uniformly high when phagocytosis could be completed and low when phagocytosis stalled, indicating that PI3K amplification correlated with successful advance of the phagocytic cup.

PKCε-YFP showed a more pronounced threshold response. PKCε recruitment to phagosomes (Larsen et al., 2002) requires binding to diacylglycerol (Cheeseman et al., 2006). During phagocytosis, diacylglycerol is generated from $PI(4,5)P_2$ by PLCγ1, whose activation requires PIP_3 (Bae et al., 1998). Remarkably, PKCε-YFP recruitment during phagocytosis showed an inverse relationship to IgG density: more chimera was recruited to low-IgG beads than to high-IgG beads (Fig. 2.6 A-E). The strong signal on low-IgG bead phagosomes exaggerated the difference in signaling between stalled and successful phagocytic cups. PKCε-YFP recruitment was undetectable in stalled cups but was highly amplified on successfully formed phagosomes (Fig. 2.6 C, E), indicating that late signal amplification of PKCε-YFP correlated with commitment to phagosome formation.

These measurements indicated that early signaling from FcR was receptor-autonomous and proportional to the stimulus, but later signaling was responsive to positive and negative feedback regulation. The sequence of FcR signals, measured as the time from the beginning of phagocytic cup formation to the point when recruitment reached half maximal values, indicated a temporal recruitment sequence of Syk-YFP, YFP-p85, YFP-actin, YFP-AktPH then PKCε-YFP (Fig. 2.6 F). If FcR signaled autonomously and without feedback regulation, then the meganitude of all signals should be proportional to IgG density. However, the ratio of the average maximum recruitment of B1 to that of B10

increased for late signals to greater than one (Fig. 2.6 G), indicating inhibition of late-stage signals at high IgG density and aggregate behavior of FcR consistent with signal integration.

2.3.4 3' Phosphoinositide concentration thresholds regulate commitment to phagocytosis

The binary response to low IgG beads indicated that a concentration threshold regulated the transition to late signals. The role of PIP_3 in this transition was examined by modulating the cells' ability to generate PIP_3. Phagocytic indexes were measured for B0.3, B1 and B10 in the presence of inhibitors of PI3K or of phosphatase and tensin homologue (PTEN), which dephosphorylates PIP_3 to $PI(4,5)P_2$. The PTEN inhibitor bpv(pic) (Schmid et al., 2004) increased the phagocytic index of both B0.3 and B1, consistent with a positive role for PIP_3 in commitment to phagocytosis (Fig. 2.7 A, B). Conversely, the PI3K inhibitor LY294002 inhibited phagocytosis (Araki et al., 1996) (Fig. 2.7 B, C). TGX-221, an inhibitor specific for p110β isoform of type I PI3K (Chaussade et al., 2007), reduced the phagocytic index of B1, although to a lesser extent than LY294002 (Fig. 2.7 B).

These responses indicated that PIP_3 concentrations regulated the transition to late stages of signaling and cellular commitment to phagocytosis. To measure signals regulating commitment, signals on stalled cups were compared with signals in similarly shaped early cups of finished phagosomes, and with the unfinished cups formed after inhibition of PI3K with LY294002 (Araki et al., 1996). YFP-actin was recruited to similar levels on stalled cups and early finished cups, and was present in the unfinished cups of cells inhibited with LY294002 (Fig. 2.7 D), indicating that this early signal was

independent of PI3K activity. Although YFP-AktPH was detectable in stalled cups, its recruitment was significantly less than that in early cups (Fig. 2.7 E), indicative of a PIP_3 concentration threshold controlling the transition to late signals. PKCε-YFP was undetectable in stalled cups and cups of LY294002-treated cells (Fig. 2.7 F), indicating that its recruitment was responsive to suprathreshold concentration of PIP_3.

2.4 Discussion

The main contribution of this chapter is the identification of 3' phosphoinositide concentration thresholds correlated with FcR mediated phagocytosis. Although it has been established that PI3K is necessary for phagocytosis, 3' phosphoinositide concentration thresholds have not been defined or measured before. This chapter also shows that 3' phosphoinositide concentration thresholds regulate the initiation of late stage signaling events, which are required for commitment to phagocytosis.

Three lines of evidence indicated interdependence of FcR signaling controlling commitment to phagocytosis. First, low IgG density on beads reduced the fraction of bound particles ingested but not the rate of phagosome formation. Second, during phagocytosis of low IgG-density beads, stalled phagocytic cups accumulated low levels of PIP_3 and negligible levels of YFP-PKCε, but fully formed phagocytic cups recruited as much or more of those molecules than did phagosomes with high IgG-density beads. Third, phagocytosis was regulated by concentrations of PIP_3 in phagocytic cups, indicating that PIP_3 concentration thresholds control a transition from local, autonomous responses to the coordinated movements of phagosome formation (Fig. 2.8).

Two kinds of feedback inhibition identified here are inconsistent with strictly autonomous

signaling by FcR. First, PIP_3 concentrations in cup membranes controlled commitment to phagocytosis by regulating the transition to late stages of signaling, including recruitment of PKCε and likely also the deactivation of Arf6 and activation of Arf1 (Beemiller et al., 2006). Early signals and movements appeared independent of PIP_3, but late signals required suprathreshold concentrations of PIP_3. PIP_3 in phagocytic cup membranes may create thresholds for signal transitions via low affinity PIP_3-binding domains in regulatory enzymes (Falasca et al., 1998; Klarlund et al., 1998; Krugmann et al., 2006; Swanson, 2008). For example, suprathreshold concentrations of PIP_3 in phagocytic cups could be required to activate PLCγ1 for synthesis of diacylglycerol and recruitment of PKCε. A second feedback regulation is that IgG density modulates the magnitudes of later signals during successful phagosome formation. Late signal suppression at high IgG densities could buffer macrophage effector mechanisms.

Thus, although FcR activate small segments of plasma membrane, additional regulation organizes the movements that follow. The PIP_3 concentration threshold indicates cooperativity in FcR signaling and, more generally, that movements of cytoplasm which are regulated by receptor signaling can be coordinated over large domains of plasma membrane by local modifications of membrane phospholipids.

2.5 Materials and Methods

2.5.1 Materials and DNA constructs

Streptavidin-coated, 5.6 μm diameter polystyrene beads were purchased from Bangs Laboratories (Fishers, IN). Texas Red-conjugated rabbit antibodies (IgG) to streptavidin were purchased from Abcam (Cambridge, MA). Plasmids encoding monomeric cyan

fluorescent protein (CFP) and Citrine (YFP), an EYFP variant, were used for all constructs (Zacharias et al., 2002). Constructs of YFP chimeras of actin, AktPH, Tapp1PH and p85 were described previously (Hoppe and Swanson, 2004; Kamen et al., 2007). The construct for Syk was a gift from Robert Geahlen (Purdue University, West Lafayette, IN, United States) and was amplified by PCR and subcloned to mCitrine-N1 vector (Clontech, Mountain View, CA). The mutant construct Syk(R194A)-YFP was made from Syk-YFP with a QuikChange Site-Directed Mutagenesis Kit (Stratagene, La Jolla, CA). The plasmid of PKCε was a gift from Peter Lipp (Saarland University, Homburg, Germany) and was amplified by PCR and subcloned to mCitrine-N1 vector.

2.5.2 Microsphere opsonization and phagocytic index assay

10 µl beads were opsonized with different amounts of IgG in 200 µl PBS with 1% BSA and incubated at 37^{o} C for 30 minutes. The opsonized beads were washed 3 times with 500 µl PBS with 1% BSA to remove excess IgG before adding to cells for imaging. To measure the phagocytic index, RAW264.7 cells were plated on 13 mm coverslips at 5×10^{4} cells per coverslip 18 hours before inhibitor treatment. Thirty min after treatment with 50 µM LY294002, 100 nM TGX-221 or 200 nM bpv(pic) (EMD chemicals, Gibbstown, NJ), beads opsonized with Texas Red-IgG were added, and the macrophages were allowed to internalize the particles for 30 min at 37 C. Cells were then rinsed with PBS and fixed. Beads that were not completely internalized were marked with Alexa 488-conjugated goat anti-rabbit IgG (Invitrogen). Phagocytic indexes were counted for at least 50 macrophages per coverslip, measured as the percent of bound particles successfully internalized by macrophages.

2.5.3 Microscopy

Cell culture and transfection of RAW264.7, a macrophage-like cell line (American Type

Culture Collection), for fluorescence microscopy were described previously (Beemiller et al., 2006). Time-lapse images of phase-contrast, CFP and YFP, were acquired at 30-second intervals using a microscope described previously (Beemiller et al., 2006). YFP images were taken using 100 ms exposure or normalized to 100 ms if other exposure times were used. The ligand (IgG) densities on the internalized beads were measured from images in the TRITC channel (Exc. 555 ± 14 nm, Em. 605 ± 20 nm).

Because the results of the recruitment calculation and bead opsonization measurement were in units of YFP and TRITC intensities, respectively, it was necessary to calibrate the illumination intensity of the xenon lamp as the bulb aged. The calibration images of a mixture of green and red fluorescent beads (M7901 Component B, Invitrogen, Carlsbad, CA) were taken in YFP and TRITC channels. The average intensities of beads were calculated in both channels and divided by the values acquired at the time of bulb installation to generate a microscope intensity calibration factor (MICF). Both the recruitment calculation and the measurement of bead opsonization were divided by the MICF to normalize illumination intensities of the microscope.

2.5.4 Image analysis by recruitment calculation

The Recruitment calculation was performed by journals developed in Metamorph (Molecular Devices, Sunnyvale, CA). The bias and shading corrections of YFP and CFP images, described previously (Hoppe et al., 2002), generated YFPb and CFPb images, respectively. A ratio image (R) was calculated by dividing YFPb image by corresponding CFPb image and multiplying by 1000 to avoid truncation of significant digits in the integral math of Metamorph.

To quantify the recruitment of YFP chimeras to phagosomes, a 5.6 μm circular region

was created in the phase-contrast image and positioned over the internalized beads during phagocytosis by the tracking algorithm TRACOBJ in Metamorph (Henry et al., 2004). The average intensities in the bead regions transferred to YFPb and CFPb, excluding the non-cell portion, were recorded as YFPp and CFPp, respectively. For YFP-AktPH, which distributes similarly to free CFP in resting cells, the average values of cell regions in R images were recorded as $\overline{\mathrm{Rc}}$. For YFP chimeras of p85, Syk, actin and PKCε, which do not localize to nuclei as much as free CFP, the nuclear regions of cells were eliminated in YFPb, CFPb and R images by an additional mask created by a manual threshold in R images. The average value of the cell region excluding the nucleus in R images was recorded as $\overline{\mathrm{Rc}}$. The recruitment of YFP chimeras of signaling molecules to phagosomes (Re) were calculated by Equation 1. The product of CFPp and $\overline{\mathrm{Rc}}$ /1000 represents how that quantity of YFP would appear if there were no specific recruitment; and its difference from YFPp is proportional to the number of YFP chimeras recruited to phagosome.

$$\mathrm{Re} = \frac{(YFPp - CFPp \times \overline{Rc} / 1000)}{MICF} \qquad \text{Equation 1}$$

In control experiments, we measured YFP recruitment during ingestion of opsonized beads by RAW264.7 macrophages (RAWs) transfected with YFP and CFP and found that this method returned average values of recruitment per pixel of 6.4 ± 2.1 in phagosomal areas, which represents the systematic error of this imaging method, and was subtracted as baseline in subsequent recruitment measurements.

2.5.5 Statistical analysis

To compare means of data from different groups, Student's t-test was performed using data analysis tool in Excel (Microsoft, United States).

Figure 2.1 Streptavidin-coated silica beads opsonized with different amounts of Texas Red-conjugated anti-streptavidin (IgG). Different IgG amounts on bead surfaces were measured by widefield fluorescence microscopy and normalized. Texas Red fluorescence per bead was measured as a function of Texas Red-IgG concentration during opsonization.

Figure 2.1

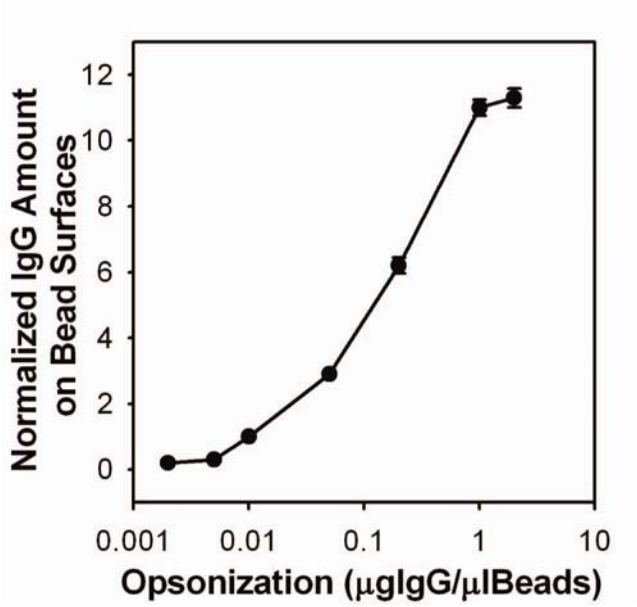
Normalized IgG Amount on Bead Surfaces
12
10
8
6
4
2
0
0.001
0.01
0.1
1
10
Opsonization (μgIgG/μlBeads)

Figure 2.2 IgG density on beads controls the frequency but not rate of phagocytosis. (**A**) Phagocytic indexes of B0.3, B1 and B10 were measured from 6 coverslips. Data represents mean ± s.e.m. The relationship between ligand density and phagocytic index was nonlinear. (**B**) The rates of phagosome formation, measured as the time from the first movement of cytoplasm to phagosome closure.

Figure 2.2

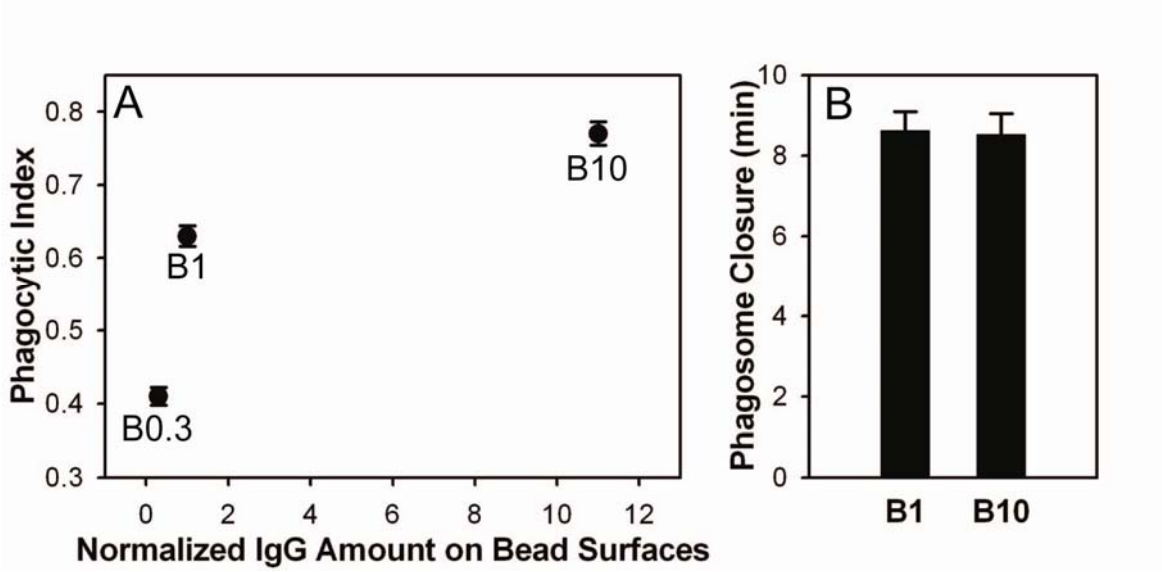
A
B
Phagocytic Index
0.8
0.7
0.6
0.5
0.4
0.3
B10
B1
B0.3
0
2
4
6
8
10
12
Normalized IgG Amount on Bead Surfaces
Phagosome Closure (min)
10
8
6
4
2
0
B1
B10

Figure 2.3 Quantitation of fluorescent chimera recruitment during phagocytosis. In cells expressing YFP chimeras and CFP, the ratio image was calculated by dividing corresponding pixels of the YFP and CFP images. The product of the CFP image and the average YFP/CFP ratio in cytosol, $\overline{Rc}$, generated a YFP pathlength image, representing how that quantity of YFP would appear without specific recruitment of YFP to the phagosome. Subtracting this image from the YFP image yielded the recruitment image, Re, which represented the specifically redistributed YFP fluorescence.

Figure 2.3

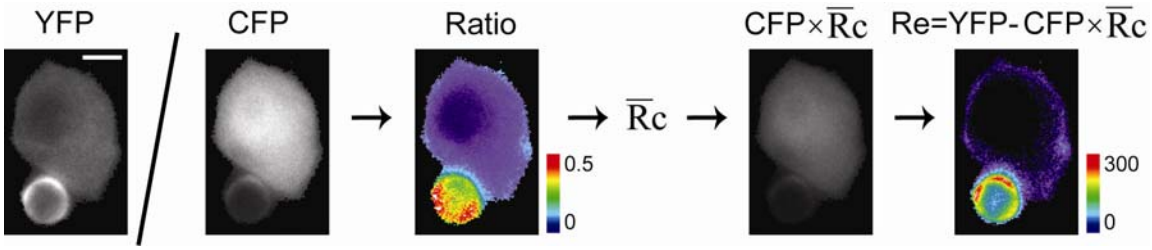
YFP
CFP
Ratio
0.5
0
$\overline{Rc}$
CFP×$\overline{Rc}$
Re=YFP-CFP×$\overline{Rc}$
300
0

Figure 2.4 Early signals correlate with IgG density. (**A-C**) Phase-contrast and Re images of Syk-YFP-expressing RAWs internalizing B10 (**A**) and B1 (**B**), and Syk(R194A)-YFP-expressing RAWs internalizing B10 (**C**). Arrowheads indicate regions with increased recruitment of Syk-YFP. Scale bar equals 5 μm. The average recruitment of Syk-YFP (**D**), YFP-p85 (**F**), YFP-actin (**H**), per pixel in phagosomes of B10 (red) and B1 (blue) were plotted as a function of time, aligned by the start of membrane movement for phagocytosis. (**E**) The maximum Syk-YFP recruitment, averaged from single phagocytic events for B10, B6, B3 and B1 (solid circles, n = 8), as well as Syk(R194A)-YFP recruitment for B10 and B1 (open triangles, n = 4). B10 phagosomes recruited more YFP-p85 (**G**, * P =0.024) and YFP-actin (**I**, * P =0.029) than B1 phagosomes. Stalled phagocytic cups recruited slightly less YFP-actin than did completed phagosomes (open circles, n = 5; ** P =0.129).

Figure 2.4

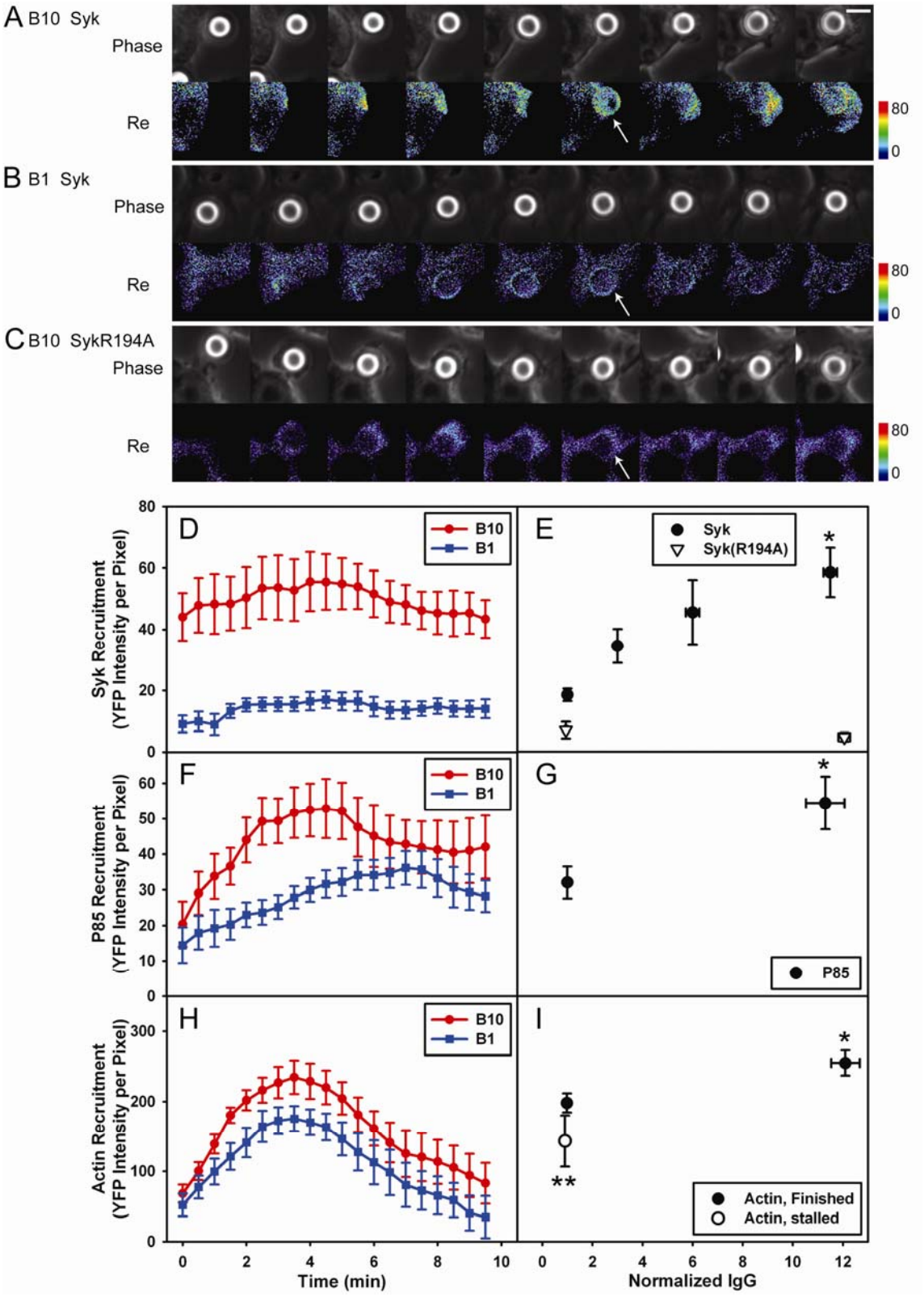
A B10 Syk
Phase
Re
80
0
B B1 Syk
Phase
Re
80
0
C B10 SykR194A
Phase
Re
80
0
D
B10
B1
Syk Recruitment (YFP Intensity per Pixel)
E
Syk
Syk(R194A)
*
F
B10
B1
P85 Recruitment (YFP Intensity per Pixel)
G
*
P85
H
B10
B1
Actin Recruitment (YFP Intensity per Pixel)
I
*
**
Actin, Finished
Actin, stalled
Time (min)
Normalized IgG

Figure 2.5 3' PIs were generated on complete phagosomes with similar magnitudes for B1 and B10. Time-lapse, phase-contrast and Re images of YFP-AktPH transfected RAWs internalizing B10 (**A**) and B1 (**B**) are shown at 2-minute intervals. The arrowheads show that B10 recruited similar amounts of YFP-AktPH with B1. Scale bar equals 5 μm. (**C**) Stalled phagocytic cups also recruited YFP-AktPH, but to a lower magnitude than finished phagosomes. The average recruitment of YFP-AktPH (mean ± s.e.m., n=8) (**D**), BtkPH-YFP (n=11) (**F**) and YFP-Tapp1PH (n=9) (**H**) per pixel in phagosomes of B10 (red) and B1 (blue) were plotted as a function of time, aligned by the start of membrane movement for phagocytosis. (**E**) The maximum YFP-AktPH recruitment during completed phagocytic events (solid circles, n=8) showed no difference between B10 and B1 (* P =0.223). In contrast, YFP-AktPH recruitment to stalled phagocytic cups (open circle, n = 5) increased slightly with ligand density, but remained significantly lower than in finished phagosomes (** P =0.001). The average maximum recruitment of BtkPH-YFP (**G**) and YFP-Tapp1PH (**I**) during completed phagocytic events showed no difference between B10 and B1.

Figure 2.5

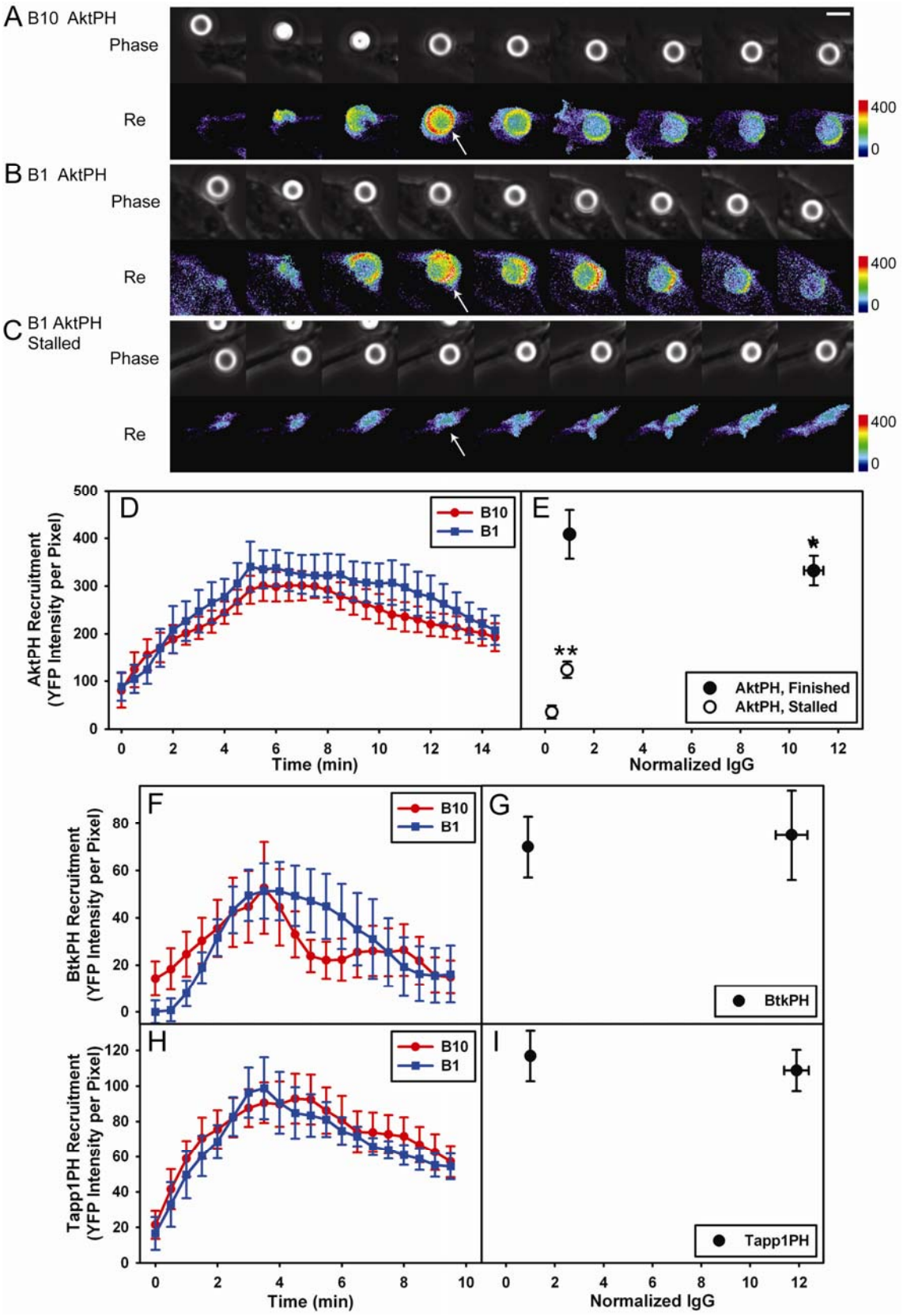
A B10 AktPH
Phase
Re
400
0
B B1 AktPH
Phase
Re
400
0
C B1 AktPH Stalled
Phase
Re
400
0
D
B10
B1
AktPH Recruitment (YFP Intensity per Pixel)
Time (min)
E
AktPH, Finished
AktPH, Stalled
Normalized IgG
F
B10
B1
BtkPH Recruitment (YFP Intensity per Pixel)
G
BtkPH
H
B10
B1
Tapp1PH Recruitment (YFP Intensity per Pixel)
Time (min)
I
Tapp1PH
Normalized IgG

Figure 2.6 Late signals correlate inversely with IgG density. (**A-C**) Beads coated with higher IgG density recruited less PKCε-YFP to phagosomes during phagocytosis. Time-lapse, phase-contrast and Re images of PKCε-YFP transfected RAWs internalizing B10 (**A**) and B1 (**B**) are shown at 2-minute intervals. The arrowheads show that B10 recruited less PKCε-YFP than B1. Scale bar is 5 μm. (**C**) Stalled phagocytic cups did not recruit PKCε-YFP. (**D**) The average recruitment of PKCε-YFP per pixel in phagosomes, aligned by the timing of phagosome closure (n = 8). (**E**) The maximum PKCε-YFP recruitment of completed phagocytic events (solid circles) showed B1 recruited more PKCε-YFP than did B10 (* P =0.034). In addition, PKCε-YFP recruitment to stalled phagocytic cups (open circles, n = 10) was significantly lower than in finished phagosomes (** $P < 0.0001$). (**F**) Times for half-maximal recruitment during phagosome formation. (**G**) Ratios of maximal YFP chimera recruitment to B1 vs. B10. All values show mean ± s.e.m.

Figure 2.6

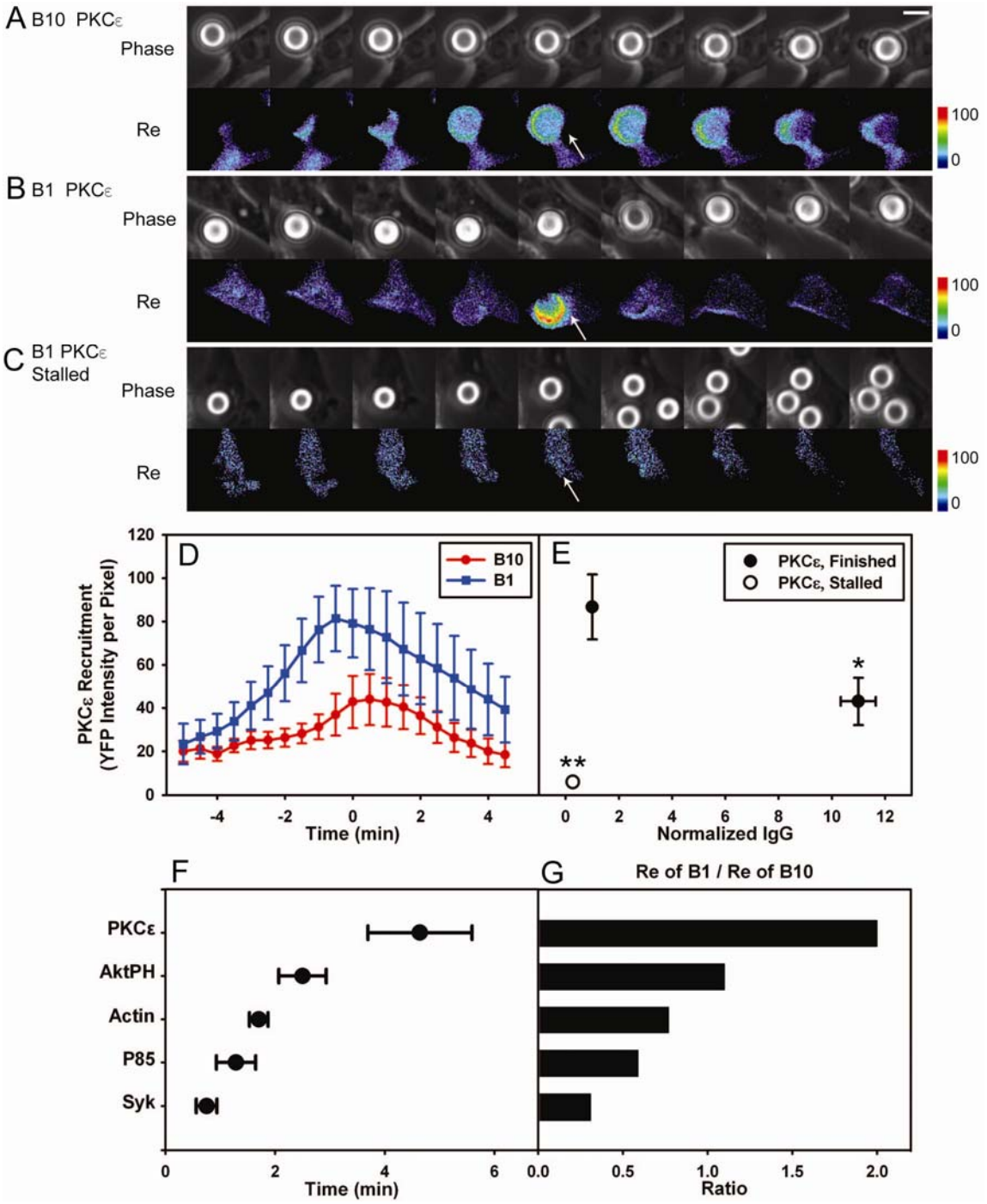
A B10 PKCε
Phase
Re
100
0
B B1 PKCε
Phase
Re
100
0
C B1 PKCε Stalled
Phase
Re
100
0
D
B10
B1
PKCε Recruitment (YFP Intensity per Pixel)
Time (min)
E
PKCε, Finished
PKCε, Stalled
**
*
Normalized IgG
F
PKCε
AktPH
Actin
P85
Syk
Time (min)
G
Re of B1 / Re of B10
Ratio

Figure 2.7 PIP_3 regulates commitment to phagocytosis with different effects on early and late signals. (**A**) Effect of Bpv(pic) on the phagocytic index of B0.3 (n = 6, * *P* < 0.0001). (**B**) Effects of inhibitors on the phagocytic indexes of B1. Bpv(pic) increased phagocytic index while LY294002 and TGX-221 decreased phagocytic indexes (n = 6, * *P* < 0.01, ** *P* < 0.001, *** *P* < 0.0001). (**C**) Effect of LY294002 on the phagocytic index of B10 (n = 6, * *P* < 0.0001). Percentages indicate actual phagocytic indexes. (**D-F**) Recruitment of YFP-actin (**D**), YFP-AktPH (**E**) and PKCε-YFP (**F**) to cups in LY294002-treated cells (LY cups), stalled cups and early (early cup) and maximal values (max) for successfully formed phagosomes. Early cups were similar in size and shape to stalled cups. YFP-AktPH recruitment to early cups was greater than recruitment to stalled cups (n = 5, * *P* =0.045). LY294002 did not inhibit the recruitment of YFP-actin (**D**) (n = 3), but inhibited the recruitment of YFP-AktPH (**E**) and PKCε-YFP (**F**) (n = 5).

Figure 2.7

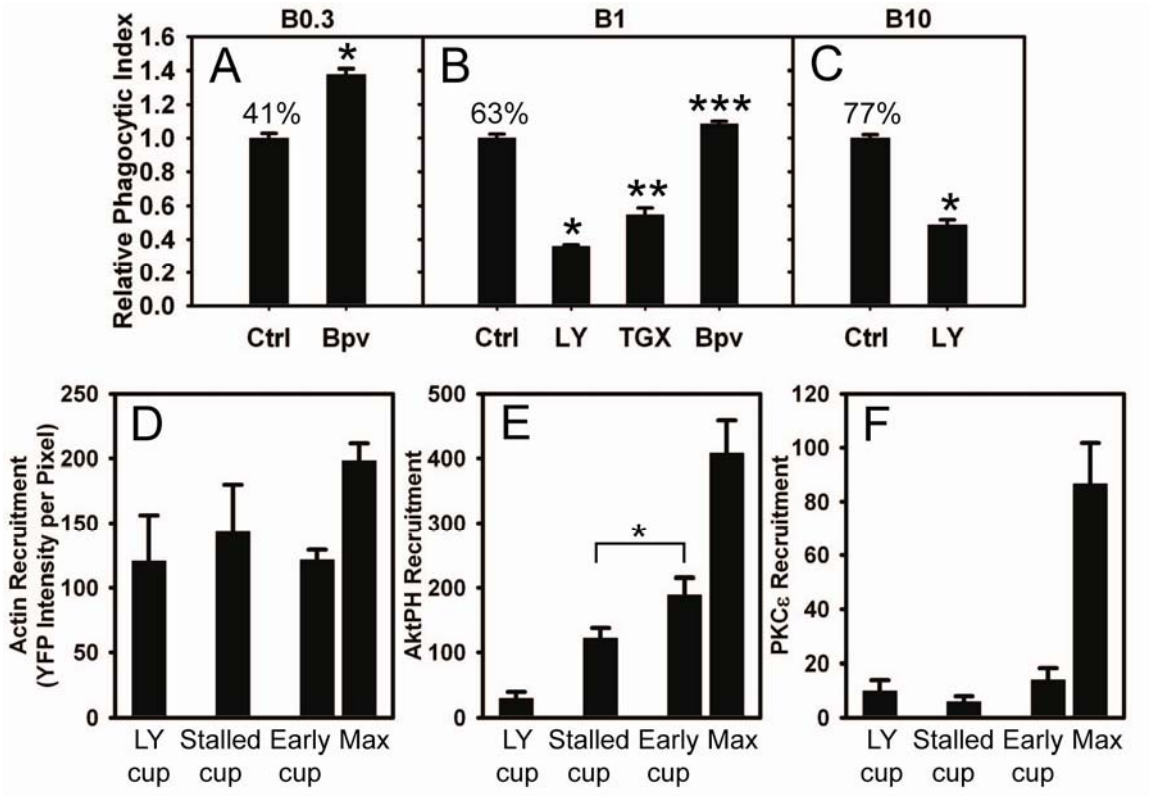
B0.3
B1
B10
A
B
C
Relative Phagocytic Index
1.6
1.4
1.2
1.0
0.8
0.6
0.4
0.2
0.0
41%
63%
77%
*
*
**
***
*
Ctrl
Bpv
Ctrl
LY
TGX
Bpv
Ctrl
LY
D
E
F
Actin Recruitment (YFP Intensity per Pixel)
AktPH Recruitment
PKCε Recruitment
250
200
150
100
50
0
500
400
300
200
100
0
120
100
80
60
40
20
0
*
LY cup
Stalled cup
Early cup
Max cup

Figure 2.8 A PIP_3 concentration threshold regulates commitment to late stages of signaling. Signaling during internalization by phagocytosis was divided into early and late stage signals depending on whether they appeared before or after PIP_3 generation. Recruitment of the late signal PKCε required PIP_3 to exceed a concentration threshold, whereas early stage signals, such as Syk, P85 and actin, did not. However, optimal recruitment of actin and p85 may require PIP_3 to exceed a threshold.

Figure 2.8

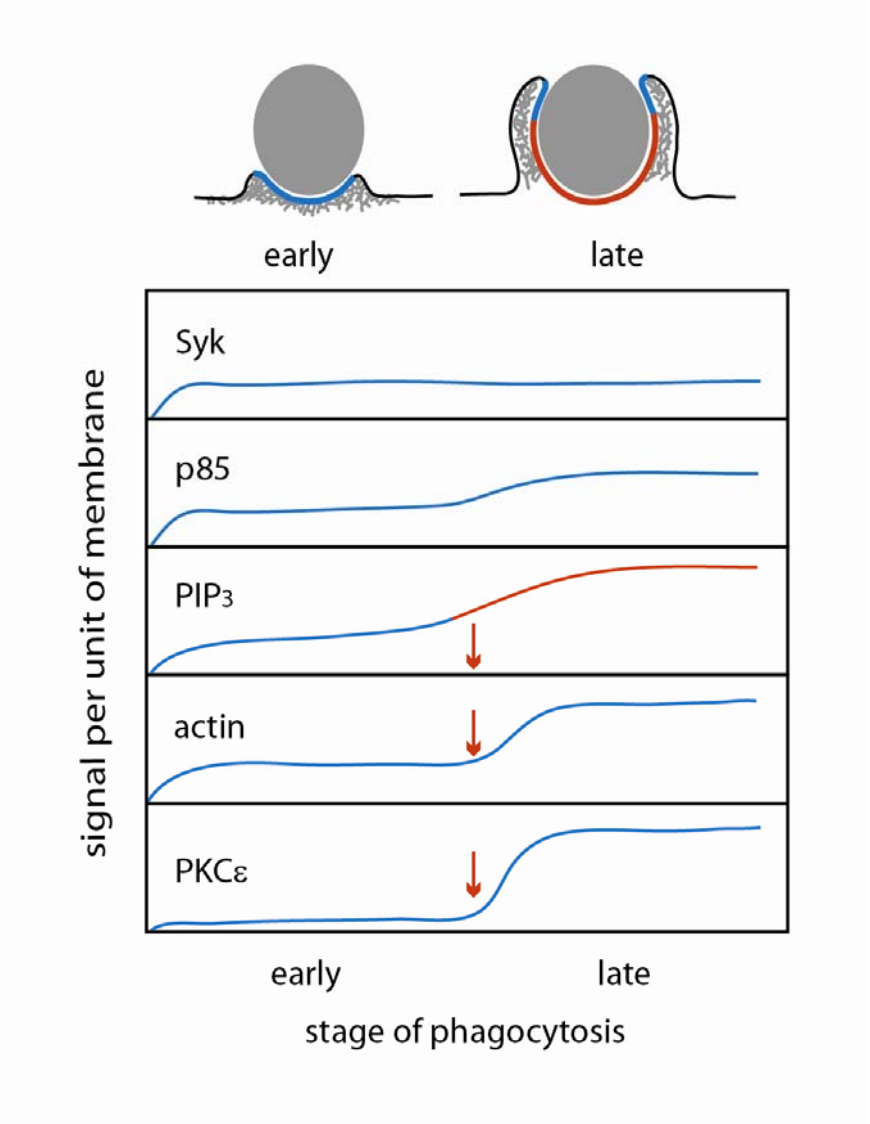
early
late
Syk
p85
PIP3
actin
PKCε
signal per unit of membrane
early
late
stage of phagocytosis

2.6 Bibliography

Araki, N., M.T. Johnson, and J.A. Swanson. 1996. A role for phosphoinositide 3-kinase in the completion of macropinocytosis and phagocytosis in macrophages. *J. Cell Biol.* 135:1249-1260.

Bae, Y.S., L.G. Cantley, C.S. Chen, S.R. Kim, K.S. Kwon, and S.G. Rhee. 1998. Activation of phospholipase C-gamma by phosphatidylinositol 3,4,5-trisphosphate. *J Biol Chem*. 273:4465-9.

Beemiller, P., A.D. Hoppe, and J.A. Swanson. 2006. A phosphatidylinositol-3-kinase-dependent signal transition regulates ARF1 and ARF6 during Fcγ receptor-mediated phagocytosis. *PLoS Biol*. 4:e162.

Beningo, K.A., and Y.-L. Wang. 2002. Fc-receptor-mediated phagocytosis is regulated by mechanical properties of the target. *J. Cell Sci.* 115:849-856.

Botelho, R.J., M. Teruel, R. Dierckman, R. Anderson, A. Wells, J.D. York, T. Meyer, and S. Grinstein. 2000. Localized biphasic changes in phosphatidylinositol-4,5-bisphosphate at sites of phagocytosis. *J. Cell Biol.* 151:1353-1367.

Champion, J.A., and S. Mitragotri. 2006. Role of target geometry in phagocytosis. *Proc Natl Acad Sci U S A*. 103:4930-4.

Chaussade, C., G.W. Rewcastle, J.D. Kendall, W.A. Denny, K. Cho, L.M. Gronning, M.L. Chong, S.H. Anagnostou, S.P. Jackson, N. Daniele, and P.R. Shepherd. 2007. Evidence for functional redundancy of class IA PI3K isoforms in insulin signalling. *Biochem J*. 404:449-58.

Cheeseman, K.L., T. Ueyama, T.M. Michaud, K. Kashiwagi, D. Wang, L.A. Flax, Y. Shirai, D.J. Loegering, N. Saito, and M.R. Lennartz. 2006. Targeting of protein kinase C-ε during Fcγ receptor-dependent phagocytosis requires the ε–C1B domain and phospholipase C-γ1. *Mol Biol Cell*. 17:799-813.

Cox, D., C.-C. Tseng, G. Bjekic, and S. Greenberg. 1999. A requirement for phosphatidylinositol 3-kinase in pseudopod extension. *J. Biol. Chem.* 274:1240-1247.

Falasca, M., S.K. Logan, V.P. Lehto, G. Baccante, M.A. Lemmon, and J. Schlessinger. 1998. Activation of phospholipase C γ by PI 3-kinase-induced PH domain-mediated membrane targeting. *EMBO J.* 17:414-22.

Griffin, F.M., J.A. Griffin, J.E. Leider, and S.C. Silverstein. 1975. Studies on the mechanism of phagocytosis. I. Requirements for circumferential attachment of particle-bound ligands to specific receptors on the macrophage plasma membrane. *J. Exp. Med.* 142:1263-1282.

Henry, R.M., A.D. Hoppe, N. Joshi, and J.A. Swanson. 2004. The uniformity of phagosome maturation in macrophages. *J Cell Biol*. 164:185-94.

Hoppe, A., K.A. Christensen, and J.A. Swanson. 2002. Fluorescence resonance energy transfer-based stoichiometry in living cells. *Biophys. J.* 83:3652-3664.

Hoppe, A.D., and J.A. Swanson. 2004. Cdc42, Rac1 and Rac2 display distinct patterns of activation during phagocytosis. *Mol. Biol. Cell*. 15:3509-3519.

Kamen, L.A., J. Levinsohn, and J.A. Swanson. 2007. Differential Association of Phosphatidylinositol 3-Kinase, SHIP-1, and PTEN with Forming Phagosomes. *Mol Biol Cell*. 18:2463-2475.

Klarlund, J.K., L.E. Rameh, L.C. Cantley, J.M. Buxton, J.J. Holik, C. Sakelis, V. Patki, S. Corvera, and M.P. Czech. 1998. Regulation of GRP1-catalyzed ADP ribosylation factor guanine nucleotide exchange by phosphatidylinositol 3,4,5-trisphosphate.

J. Biol. Chem. 273:1859-1862.
Krugmann, S., S. Andrews, L. Stephens, and P.T. Hawkins. 2006. ARAP3 is essential for formation of lamellipodia after growth factor stimulation. *J Cell Sci*. 119:425-32.
Larsen, E.C., T. Ueyama, P.M. Brannock, Y. Shirai, N. Saito, C. Larsson, D. Loegering, P.B. Weber, and M.R. Lennartz. 2002. A role for PKC-ε in FcγR-mediated phagocytosis by RAW 264.7 cells. *J. Cell Biol.* 159:939-944.
May, R.C., and L.M. Machesky. 2001. Phagocytosis and the actin cytoskeleton. *J. Cell Sci.* 114:1061-1077.
Mocsai, A., C.L. Abram, Z. Jakus, Y. Hu, L.L. Lanier, and C.A. Lowell. 2006. Integrin signaling in neutrophils and macrophages uses adaptors containing immunoreceptor tyrosine-based activation motifs. *Nat Immunol*. 7:1326-33.
Moon, K.D., C.B. Post, D.L. Durden, Q. Zhou, P. De, M.L. Harrison, and R.L. Geahlen. 2005. Molecular basis for a direct interaction between the Syk protein-tyrosine kinase and phosphoinositide 3-kinase. *J Biol Chem*. 280:1543-51.
Nimmerjahn, F., and J.V. Ravetch. 2006. Fcγ receptors: old friends and new family members. *Immunity*. 24:19-28.
Sada, K., T. Takano, S. Yanagi, and H. Yamamura. 2001. Structure and function of Syk protein-tyrosine kinase. *J Biochem*. 130:177-86.
Schmid, A.C., R.D. Byrne, R. Vilar, and R. Woscholski. 2004. Bisperoxovanadium compounds are potent PTEN inhibitors. *FEBS Lett*. 566:35-8.
Swanson, J.A. 2008. Shaping cups into phagosomes and macropinosomes. *Nat Rev Mol Cell Biol*. 9:639-649.
Swanson, J.A., and A.D. Hoppe. 2004. The coordination of signaling during Fc receptor-mediated phagocytosis. *J Leukoc Biol*. 76:1093-103.
Swanson, J.A., M.T. Johnson, K. Beningo, P. Post, M. Mooseker, and N. Araki. 1999. A contractile activity that closes phagosomes in macrophages. *J. Cell Sci.* 112:307-316.
Varnai, P., B. Thyagarajan, T. Rohacs, and T. Balla. 2006. Rapidly inducible changes in phosphatidylinositol 4,5-bisphosphate levels influence multiple regulatory functions of the lipid in intact living cells. *J Cell Biol*. 175:377-82.
Yeung, T., and S. Grinstein. 2007. Lipid signaling and the modulation of surface charge during phagocytosis. *Immunol Rev*. 219:17-36.
Zacharias, D.A., J.D. Violin, A.C. Newton, and R.Y. Tsien. 2002. Partitioning of lipid-modified monomeric GFPs into membrane microdomains of live cells. *Science*. 296:913-916.

Chapter Three

A Cdc42 Activation Cycle Coordinated by PI 3-kinase during Fc Receptor-mediated Phagocytosis

(Experiments in this chapter were completed together with Peter Beemiller. He did experiments for figure 3.1, 3.4 and 3.5. I did experiments for figure 3.2, 3.3, 3.6, 3.7 and 3.8.)

3.1 Abstract

Fcγ Receptor (FcR)-mediated phagocytosis in macrophages requires PI 3-kinase (PI3K) and activation of the Rho-family GTPases Cdc42 and Rac1. Rac1 is active throughout phagosome formation, Cdc42 activity is restricted to the advancing edge of the phagocytic cup and Rac2 activity increases at the base of the cup during phagosome closure (Hoppe and Swanson, 2004). Cdc42 deactivation coincides with the increase in 3' phosphoinositide (3'PI) concentrations in cup membranes, which suggests a role for 3' PIs in Cdc42 deactivation. We therefore examined the relationships between PI3K and Rho-family GTPase activities during phagocytosis. Inhibition of PI3K resulted in persistently active Cdc42 and Rac1, but not Rac2, in stalled phagocytic cups. Patterns of 3' PIs and Rho-family GTPase activities were similar during phagocytosis of 5 μm and 2 μm diameter microspheres, indicating similar underlying mechanisms despite particle size-dependent sensitivities to PI3K inhibition. Expression of constitutively active Cdc42 (Cdc42(G12V)) inhibited phagocytosis of larger particles at the stalled cup stage by a

mechanism that was additive with PI3K inhibition. Moreover, expression of Cdc42(G12V) increased 3'PI concentrations in plasma membranes and small phagosomes, indicating a role for Cdc42 in activation of PI3K. Together, these studies demonstrate a requirement for a Cdc42 activation cycle during phagocytosis, in which Fc receptor-activated Cdc42 stimulates PI3K and the resulting increase of 3' PIs in cup membranes inactivates Cdc42 to allow completion of phagosome formation.

3.2 Introduction

Fcγ receptor (FcR)-mediated phagocytosis occurs through a series of morphological stages, beginning when FcRs on the surface of the phagocyte bind to IgG-class immunoglobulins that have coated (opsonized) particles. In conjunction with membrane remodeling at sites of phagocytosis, transient assembly of actin filaments pushes the macrophage plasma membrane over target particles (Greenberg et al., 1991). This is followed by fusion of intracellular membranous compartments with the phagosome (Bajno et al., 2000; Niedergang et al., 2003) and myosin-dependent contractile activities that constrict the distal margins of the cup, closing the phagosome (Swanson et al., 1999). During phagocytosis, actin depolymerization can occur at the base of the cup even as actin filaments continue to extend at the distal margin. A central question regarding phagocytosis is how the ligation of a single kind of receptor, FcR, can generate this spatially organized sequence of distinct activities.

Type 1 PI3K generates PIP_3 and $PI(3,4)P_2$, and fluorescent reporters of 3' phosphoinositide (3'PI) distributions in living cells indicate that 3' PIs are generated on the inner membranes of forming phagocytic cups (Botelho et al., 2000; Marshall et al., 2001; Vieira et al., 2001). The PI3K inhibitors wortmannin and LY294002 block the

activities required to complete phagocytosis of particles larger than 3 μm diameter (Araki et al., 1996; Cox et al., 1999). In the presence of PI3K inhibitors, incomplete phagosomes persist as actin-rich phagocytic cups. This suggests that the 3' PIs generated by PI3K in phagosomal membranes serve as a signal that organizes later stages of phagocytosis.

FcR-mediated phagocytosis requires the Rho-family GTPases Cdc42 and Rac1 (Caron and Hall, 1998; Cox et al., 1997), which regulate actin filament assembly and disassembly, and the Arf-family GTPases Arf1 and Arf6 (Beemiller et al., 2006; Zhang et al., 1998), which regulate membrane trafficking (Balch et al., 1992; Dittie et al., 1996; Donaldson et al., 1992) and remodeling (Ge et al., 2001; Honda et al., 1999; Melendez et al., 2001; O'Luanaigh et al., 2002). The GTPases alternate between inactive, GDP-bound states and active, GTP-bound states. GTP binding and activation are stimulated by guanine nucleotide exchange factors (GEFs), while inactivation by GTP hydrolysis is accelerated by GTPase-activating proteins (GAPs). The active GTPases regulate distinct combinations of effector kinases and downstream activities, including actin polymerization and depolymerization, myosin contractility and vesicle fusion with plasma membranes.

Studies of phagocytosis in macrophages expressing fluorescent chimeras of GTPases indicate three patterns of GTPase activity during FcR-mediated phagocytosis (Beemiller et al., 2006; Hoppe and Swanson, 2004). Cdc42, Rac1 and Arf6 are active at the advancing edge of phagocytic cups. Cdc42 and Arf6 become inactive a short distance from the distal margin of the phagocytic cup, but Rac1 remains active throughout phagosome formation, and is inactivated only after phagosome closure. Rac2 and Arf1 activation are delayed and localized to the base of the phagocytic cup, where they

remain activated until after phagosome closure.

Some of the GEFs and GAPs that control GTPase activities during phagocytosis may be regulated by 3'PIs. Many GEFs and GAPs contain pleckstrin-homology (PH) domains, which tether the proteins to 3'PIs in membranes and are necessary for their activities. Consistent with this model, Arf1 and Arf6 are coordinately regulated by PI3K in response to FcR ligation. Inhibition of PI3K with LY294002 blocked the activation of Arf1 and deactivation of Arf6, such that unclosed phagocytic cups contained persistently activated Arf6 and basal levels of activated Arf1 (Beemiller et al., 2006). This indicated that PI3K mediates a signal transition in which the generation of 3' PI s on phagocytic membranes activates the GAPs that deactivate Arf6 and the GEFs that activate Arf1. Conversely, Rac and Cdc42 have been shown to stimulate PI3K (Srinivasan et al., 2003; Zheng et al., 1994).

If a localized increase in 3' PIs is a general mechanism coordinating the movements of phagocytosis, then the Rho-family GTPases should also exhibit a signal transition. Accordingly, in the phagocytic cups of LY294002-inhibited macrophages, Cdc42 should be persistently activated and Rac2 should remain inactive. As the patterns of Rac1 activity in phagocytosis differ from Arf1 and Arf6, it is not clear how its activation would respond to PI3K inhibition.

This study examined signaling by PI3K and Rho-family GTPases during FcR-mediated phagocytosis. We show that Cdc42 and Rac1 are activated independent of PI3K. Phagocytosis in the presence of PI3K inhibitors implicated PI3K activity directly in the deactivation of Cdc42 and the activation of Rac2. Similar profiles of PIP_3 generation and Rho-family GTPase activities were identified during phagocytosis of large and small

particles. Moreover, constitutively active Cdc42 inhibited phagocytosis but stimulated PI3K. Double inhibition experiments using constitutively active Cdc42 and LY294002-treated macrophages showed that PI3K and Cdc42 deactivation both contribute to phagocytosis of smaller particles. These studies indicate therefore that the stages of signaling in phagocytosis are organized by linked cycles of Cdc42 and PI3K activation. FcR-activated Cdc42 stimulates PI3K, which increases concentrations of PIP_3 in phagocytic cups, allowing PIP_3-dependent deactivation of Cdc42 which is necessary for completion of phagocytosis.

3.3 Results

3.3.1 Rho-family GTPases are coordinately regulated by PI3K during phagocytosis

Prompted by the similarities between the activation profiles of Arf- and Rho-family GTPases (Beemiller et al., 2006; Hoppe and Swanson, 2004), we used FRET microscopy to determine which Rho-family GTPases were activated in phagocytic cups of macrophages in LY294002. GTPase activities at sites of phagocytosis were measured by applying fluorescence resonance energy transfer (FRET) stoichiometry (Hoppe et al., 2002) to images of cells expressing CFP-p21-binding domain (CFP-PBD) and either YFP-Cdc42, YFP-Rac1 or YFP-Rac2. PBD is the Cdc42/Rac-binding domain from p21-activated kinase-1 (PAK1), which binds specifically to Cdc42 or Rac GTPases in their GTP-bound conformations (Manser et al., 1993). Component fluorescence images of macrophages performing phagocytosis of IgG-opsonized sheep erythrocytes were collected at 30-sec intervals and E_A images, which indicate the fraction of YFP-GTPase bound to CFP-PBD, were calculated as described previously (Beemiller et al., 2006; Hoppe et al., 2002). RAW264.7 macrophages expressing YFP-Cdc42 and CFP-PBD,

pretreated with LY294002, showed activated Cdc42 immediately after particle binding (Fig. 3.1A). However, in contrast to control phagosomes, Cdc42 remained activated in the persistent, unclosed cups (observation period ~20 min). The magnitude of activation, measured as the fraction of YFP-Cdc42 in the GTP-bound state (G*; see (Hoppe and Swanson, 2004)) was similar to the peak level of activation in control macrophages (Fig. 3.1D).

This analysis was repeated using YFP-Rac1, which can be activated by PI3K in some cells (Srinivasan et al., 2003). Macrophages in LY294002 showed rapid activation of Rac1 in response to bound opsonized erythrocytes (Fig. 3.1B). Like Cdc42 and Arf6 (Beemiller et al., 2006), Rac1 activation persisted in the unclosed phagocytic cups. LY294002 treatment did not delay Rac1 activation or decrease the magnitude of Rac1 activation (Fig. 3.1E), indicating that Rac1 activation was PI3K-independent.

In contrast, the FRET reporters YFP-Rac2 and CFP-PBD indicated little activation of Rac2 in the unclosed phagocytic cups (Fig. 3.1C). Unlike control phagocytic events, which displayed intermediate levels of active Rac2 during pseudopod extension around erythrocytes and a prominent spike in activation during phagosome closure, the persistent, unclosed cups of LY294002-treated macrophages showed basal levels of activated Rac2 (Fig. 3.1F). Thus, Cdc42, Rac1 and Rac2 showed strikingly different activation properties after inhibition of PI3K: Cdc42 and Rac1 were persistently active in cups whereas Rac2 remained inactive.

3.3.2 Deactivation of endogenous Cdc42 is regulated by PI3K during phagocytosis

To confirm that activities of endogenous Cdc42 are also regulated by PI3K, the

recruitment of YFP-Cdc42-binding domain (CBD), which binds to GTP-Cdc42 (Cannon et al., 2001; Tskvitaria-Fuller et al., 2006), was measured by ratiometric fluorescence microscopy during phagocytosis. The recruitment index, a cell volume- and transfection efficiency-normalized indicator of YFP-chimera recruitment to phagosomes, was measured during phagocytosis of sheep erythrocytes. Consistent with the YFP-Cdc42 FRET microscopy, YFP-CBD was recruited early during phagocytosis (Fig. 3.2A). The recruitment was highest at the leading edge of phagocytic cups, confirming that Cdc42 is activated there (Hoppe and Swanson, 2004). The recruitment of YFP-CBD to the base of the cups decreased less than the decrease observed by FRET microscopy (Hoppe and Swanson, 2004), possibly due to different Cdc42-binding properties of CBD and PBD. Since the YFP-CBD recruitment produced a low Ri signal (Fig. 3.2C), YFP recruitment was measured during similar phagocytosis events as a negative control to ensure the reliability of the YFP-CBD recruitment data (Fig. 3.2C). At the beginning of phagocytosis, when the erythrocytes were still at the edge of the cell, Ri of YFP/CFP was slightly lower than the expected value of one but gradually increased as the particle was internalized (Fig. 3.2C). Thus, the difference between the Ri of YFP-CBD and YFP represented the magnitude of YFP-CBD recruitment during phagocytosis; YFP-CBD was recruited to phagosomes immediately after phagocytosis began and continued until internalization was completed (Fig. 3.2C), confirming that the activities of endogenous Cdc42 during phagocytosis were similar to the activities of overexpressed Cdc42 measured by FRET stoichiometry.

YFP-CBD was also recruited to stalled phagocytic cups formed in LY294002-treated macrophages and remained in the cups, indicating persistent activation of endogenous Cdc42 (Fig. 3.2D). Since LY294002 inhibits both type I and type III PI3K, we also measured endogenous Cdc42 activities using another PI3K inhibitor, TGX-221, which is

specific for the β-isoform of type I PI3K (Chaussade et al., 2007). YFP-CBD was also recruited to incomplete phagocytic cups formed in TGX-221-treated macrophages (Fig. 3.2B, D) and persisted in those cups, suggesting that Cdc42 deactivation was required by the products of type I PI3K: PIP_3 and $PI(3,4)P_2$.

3.3.3 Large and small particles stimulate similar patterns of signaling during phagocytosis

PI3K inhibitors have less effect on phagocytosis of 2 μm diameter particles than 5 μm particles (Cox et al., 1999). The differential sensitivity of small and large particle phagocytosis to PI3K inhibition suggests that different signals regulate phagocytosis of small and large particles. We therefore examined whether differences in 3' PI synthesis or GTPase activation patterns during phagocytosis of different sizes of particles could explain the size-dependence of inhibition by PI3K inhibitors. Streptavidin-coated silica microspheres of 2 μm and 5 μm diameter were opsonized with equivalent levels of IgG-labeling per unit surface area (see Materials and Methods and Fig. 3.3). To compare the 3' PI responses during phagocytosis, macrophages expressing CFP and a YFP fusion to the PH domain of Akt (YFP-AktPH) were presented opsonized 2 μm and 5 μm microspheres and observed by ratiometric fluorescence imaging. AktPH binds to PIP_3 and $PI(3,4)P_2$ (Kavran et al., 1998); and sub-cellular localization of fluorescent AktPH chimeras has been used previously to localize activity of PI3K (Hoppe and Swanson, 2004; Vieira et al., 2001). Quantitative measures of multiple phagocytic events showed that for both 2 μm and 5 μm phagosomes the maximum 3'PI accumulation appeared ~2–3 min after the initiation of pseudopod extension (Fig. 3.4A). The average peak level of 3' PIs during phagocytosis of the large microspheres was 12% greater than the peak for

smaller microspheres. After peak levels were reached, 3' PI levels declined much more rapidly on 2 μm phagosomes. Elevated 3' PI levels were observed on 5 μm phagosomes until 10–15 min after the initiation of phagocytosis (~2–5 minutes after closure), consistent with increased total receptor ligation. Thus, phagocytosis of both small and large particles generated robust, localized 3'PI responses of similar magnitudes.

We then measured the activation dynamics of the Rho-family GTPases during phagocytosis of 2 μm and 5 μm microspheres. Cdc42 was activated during phagocytosis of both small and large target microspheres, with peak activation of Cdc42 occurring within the first few minutes of pseudopod extension (Fig. 3.4B - E). Average levels of activated Cdc42 decreased more slowly on 5 μm phagosomes than on erythrocyte phagosomes or 2 μm phagosomes, consistent with the increased time required to engulf larger particles. Cdc42 activation per unit area in the distal margins of phagosomes was essentially identical on 2 μm and 5 μm phagosomes (compare initial time points in Figs. 3.4B and 3.4C). Rac1 was activated with peaks at 0.5–2 min and 6.5–8 min after the onset of phagocytosis of 5 μm microspheres (Fig. 3.4B, F) while a single, sharp peak in Rac1 activation was observed at 0.5–2 min during 2 μm particle phagocytosis (Fig. 3.4C, G). Rac1 activity was slightly delayed relative to Cdc42 on 2 μm phagosomes (Fig. 3.4C). YFP-Rac2 was activated gradually during formation of 5 μm phagosomes, peaking 5–9 minutes after phagocytosis commenced (Fig. 3.4B and 3.4H). These peak levels were reached later than the peaks in YFP-AktPH recruitment (compare Fig. 3.4A and 3.4B). When macrophages expressing YFP-Rac2 and CFP-PBD were presented with opsonized 2 μm microspheres, Rac2 activated approximately 2–4 min after the onset of pseudopod extension (Fig. 3.4C). Peak Rac2 activation levels were ~20% lower than those observed at 5 μm microsphere phagosomes (Fig. 3.4B, C). Although a fraction of

particles failed to activate Rac2, the average activation profile of Rac2 during phagocytosis of 2 μm microspheres was similar to the activation observed during phagocytosis of erythrocytes or 5 μm microspheres. Therefore, the signal transition occurred during phagocytosis of both large and small beads: the peak of Cdc42 activation preceded the peak of PIP_3 accumulation, which preceded the peak of Rac2 activation. Rac1 activation spanned the signal transition.

Similar activation dynamics of Cdc42, Rac1 and Rac2 were also observed during complete phagocytosis of 2 μm microspheres by macrophages pretreated with LY294002. Cdc42 was not deactivated after phagosome closure, but remained active on phagosomes for at least 20 minutes (Fig. 3.5). In contrast, Rac1 deactivation followed closure of phagosomes (Fig. 3.5). Rac1 deactivation was slower in LY294002-treated cells, indicating a partial dependence on PI3K activity. Rac2 was not activated on 2 μm microsphere phagosomes (Fig. 3.5), indicating that its activation was regulated by PI3K-generated 3' PIs, rather than by closure. Thus, the deactivation of Cdc42 and the activation of Rac2 correlated directly with 3' PI generation on phagosomal membranes.

3.3.4 Deactivation of Cdc42 is required to complete phagocytosis

We next investigated whether deactivation of Cdc42, Rac1 or Rac2 was required for phagosome closure around large and small particles. As macrophages likely express many potential GAPs for Cdc42 and Rac, and the identities of the GAPs required for phagocytosis are not known, we mimicked the loss of GAP activity by over-expressing constitutively active GTPase mutants. Phagocytic indexes were measured in macrophages over-expressing wild-type or constitutively active YFP-chimeras of Cdc42,

Rac1 or Rac2. Constitutively active YFP-Rac1(Q61L) or YFP-Rac2(G12V) did not inhibit phagocytosis of 2 μm or 5 μm particles, suggesting that deactivation of Rac1 or Rac2 were not required for phagocytosis (Fig. 3.6A). However, cells expressing YFP-Cdc42(G12V) showed a small reduction in the phagocytosis of 2 μm microspheres (~20% reduction relative to cells expressing YFP), and a significantly reduced uptake of 5 μm microspheres (two-tailed t-test, $p<0.001$). This indicated that deactivation of Cdc42 was necessary for closure of phagosomes, especially over large particles.

To examine whether phagocytosis of 2 μm microspheres is independent of the signal transition, phagocytic indexes of 2 μm or 5 μm particles were measured in cells expressing Cdc42(G12V) and exposed to LY294002. The double inhibition reduced the phagocytic index of 2 μm or 5 μm particle to about half of that seen under single inhibition (Fig. 3.6B), indicating that phagocytosis of 2 μm microspheres also requires the signal transition. This further suggests that phagocytosis of 2 μm microspheres employs the same signals as phagocytosis of 5 μm microspheres, but that the PI3K-dependent late activities are not sufficiently inhibited to arrest phagocytosis. The fact that double inhibition by Cdc42(G12V) overexpression and LY294002 treatment leads to lower phagocytic index than either inhibition alone indicated that Cdc42 deactivation and PI3K activation are parallel and additive activities.

3.3.5 Multiple feedback responses stimulate PI3K

We next asked if Cdc42 regulates PI3K during phagocytosis. Previous biochemical studies found that Cdc42-GTP binds and activates PI3K (Zheng et al., 1994), but its role in regulating PI3K during FcR-mediated phagocytosis has not been examined. To study

the effect of Cdc42 activation on PI3K, we monitored PIP_3 generation by ratiometric imaging of macrophages coexpressing CFP-AktPH, mCherry and mCit-Cdc42(G12V) and control cells expressing YFP-AktPH and CFP. In control cells, YFP-AktPH was uniformly distributed within the cell (Fig. 3.7A, C), indicating low PIP_3 on cell membranes. In contrast, cells overexpressing YFP-Cdc42(G12V) showed CFP-AktPH recruitment to the membranes of resting cells, even before phagocytosis started (Fig. 3.7B, C), indicating that Cdc42(G12V) increased overall PI3K activity in resting macrophages.

To ask if active Cdc42 enhanced PI3K activity during phagocytosis, we measured CFP-AktPH recruitment during ingestion of 2 μm microspheres by macrophages expressing YFP-Cdc42(G12V). As expected, CFP-AktPH was recruited to a higher level and for a longer duration in macrophages overexpressing YFP-Cdc42(G12V) than in control cells (Fig. 3.7D, F-I), indicating that YFP-Cdc42(G12V) promoted PI3K activity to generate more PIP_3 during successful phagocytosis. YFP-Cdc42(G12V) overexpression inhibited the closure of 5 μm phagosomes but not cup formation (Fig. 3.7L, M), allowing the measurement of CFP-AktPH recruitment to the stalled phagocytic cups. CFP-AktPH was recruited to those stalled phagocytic cups, with a value significantly higher than baseline value (acquired from cells expressing free YFP and CFP; Fig. 3.7E). However, CFP-AktPH recruitment was less than that observed during complete phagocytosis in macrophages without Cdc42(G12V) overexpression (Fig. 3.7E, H, I). This indicated that although PI3K was stimulated by active Cdc42, a feedback from some late-stage signal was required for maximum PI3K activation.

Thus, feedback responses promoted PI3K activity and the Cdc42 activation cycle during phagocytosis. At the beginning of phagocytosis, PI3K and Cdc42 were activated

following FcR ligation. Activated Cdc42 further increased PI3K activity and the accumulated 3' PIs provided a negative feedback response to deactivate Cdc42 (Fig. 3.9).

To examine the mechanism by which Cdc42 deactivation contributes to phagocytosis, we measured and compared the dynamics of actin in phagosomes of cells expressing mCherry-actin, mCFP with or without YFP-Cdc42(G12V). Cells only expressing mCherry-actin and mCFP showed a strong and transient recruitment of mCherry-actin to forming phagosomes (Fig. 3.8). In cells expressing YFP-Cdc42(G12V), less mCherry-actin was recruited to phagocytic cups (Fig. 3.8). mCherry-actin persisted on cups that failed to close but was lost from those cups that did close. These results indicated YFP-Cdc42(G12V) prevented maximal actin recruitment into the cups. Furthermore, this suggested that the activation of Cdc42 and its PI3K-dependent inactivation organize actin filament turnover in forming phagosomes.

3.4 Discussion

This work examined the contributions of PI3K to the coordination of signaling by Rho-family GTPases during phagocytosis. Previous studies of FcR-mediated phagocytosis identified a coordinated sequence of early and late signals in forming phagocytic cups (Beemiller et al., 2006; Hoppe and Swanson, 2004). Early signals appear at the advancing edge of the cup; some disappear a short distance from the edge (Cdc42:GTP and Arf6:GTP) and others persist throughout phagocytosis (Rac1:GTP). Late signals, which include Rac2:GTP, Arf1:GTP and PKCε (Larsen et al., 2000) are delayed relative to the advancing edge of the phagosome and localize to the base of the forming cup or the fully closed phagosome. After inhibition of PI3K by LY294002, the unclosed

phagocytic cups containing IgG-opsonized erythrocytes display persistently active Arf6 without activation of Arf1 (Beemiller et al., 2006), which indicates that PI3K is necessary for the transition from early to late signals. The results presented here are consistent with previous studies, in that PI3K inhibition allowed sustained activation of early (Cdc42, Rac1) but not late (Rac2) signals in unclosed cups. Ratiometric imaging of YFP-CBD recruitment to phagosomes indicated that endogenous Cdc42 activities were similar to those indicated by FRET microscopy. Thus, the signal transition of Rho-family GTPase activities is also PI3K-dependent. Since TGX-221, a PI3K inhibitor specific for the β-isoform of type I PI3K, generated effects similar to LY294002, we propose that PIP_3 or $PI(3,4)P_2$ generated by type I PI3K in phagocytic cups coordinately activate the GAPs for Cdc42 and Arf6 and the GEFs for Rac2 and Arf1. It is likely that not all of these transitions are directly responsive to 3'PIs. A single 3'PI-dependent activity could regulate other changes at the signal transition. However, the increased inhibition seen in Cdc42(G12V)-expressing cells treated with LY294002 suggests that at least two PI3K-dependent activities regulate the transition.

Phagocytosis of 1-3 μm diameter particles is relatively unaffected by PI3K inhibitors (Cox et al., 1999). Three possible underlying mechanisms could explain the differential effects of PI3K inhibitors on phagocytosis of large and small particles. First, cells may employ distinct signaling pathways for phagocytosis of large and small particles. Earlier studies indicated that uptake of very small particles (immune complexes and IgG-coated microspheres < 1 μm diameter) occurs by clathrin-dependent mechanisms (Tse et al., 2003). However, the maximal size of particle for this endocytosis was smaller than the maximal size of particle in which uptake is insensitive to PI3K inhibitors. Secondly, PI3K-dependent activities may be present for all phagocytic activities, but only necessary to organize the construction of large phagosomes. Finally, PI3K-dependent activities may

be present for all phagocytic activities but required to different extents for the construction of large and small phagosomes. We therefore studied whether phagocytosis of large and small particles utilize different signaling pathways and found that PIP_3 generation and Rho-family GTPase activities exhibited similar patterns of activation during phagocytosis of both 2 μm and 5 μm microspheres. In addition, the deactivation of Cdc42 and activation of Rac2 also require PI3K activity during phagocytosis of 2 μm microspheres. We mimicked the inhibition of GTPase deactivation by overexpressing constitutively active mutants of GTPase and found that the deactivation of Cdc42 was necessary for phagocytosis of 5 μm microspheres but less so for 2 μm microspheres. Together, our research demonstrates that PI3K-dependent activities are present for all phagocytic activities but required to different extents for the construction of large and small phagosomes. Closure of smaller phagosomes in the presence of PI3K inhibitors may be achieved by the persisting activities of Rac1 and Cdc42, actin polymerization and PI3K-independent contractile activities (Araki et al., 2003).

The fact that double inhibition by Cdc42(G12V) overexpression and LY294002 treatment further reduced phagocytosis for both 2 μm and 5 μm microspheres also indicated that the Cdc42 activation cycle and PI3K activation are parallel signaling pathways (Fig. 3.9). Consistent with an earlier study (Zheng et al., 1994), we found that constitutively active Cdc42 increased PIP_3 in membranes of resting cells and during phagocytosis of 2 μm microspheres, probably by promoting PI3K activity. However, the incomplete phagocytic cups formed on 5 μm microspheres in cells expressing YFP-Cdc42(G12V) showed less PIP_3 generation than complete phagocytosis of 5 μm microspheres, indicating that maximum PIP_3 generation during phagocytosis requires feedback amplification from

later signals (Fig. 3.9), which could include PI3K activation by FcR-associated Syk and Gab2 (Gu et al., 2003). An essential feature of the signal transition was the deactivation of Cdc42, which was required to a larger extent to complete phagocytosis of larger particles. Cdc42 deactivation may lead to the termination of actin polymerization so that exocytic membrane insertion can proceed without interference from a cytoskeletal network (Scott et al., 2005). Indeed, studies of neutrophils indicated that constitutively active Cdc42 inhibits phagosome-lysosome fusion by inhibiting the depletion of actin from phagosomes (Lerm et al., 2007). We propose that 3' PI-dependent deactivation of Cdc42 in the inner membrane of the phagocytic cup facilitates actin filament turnover in the forming phagosome which allows other essential late activities.

3.5 Materials and Methods

3.5.1 Tissue Culture, Transfection and PI3K inhibition

RAW264.7 cells from the American Type Culture Collection (Manassas, Virginia) were cultured in Advanced DMEM supplemented with 2% heat-inactivated FBS, 4 mM L-glutamine, 20 U/mL penicillin and 20 µg/mL streptomycin. All cell culture products were purchased from Invitrogen (Carlsbad, CA). To prepare cells for time-lapse fluorescence microscopy, ~2.5×10^5 cells were plated onto acid-washed 25 mm coverslips 18–24 hr prior to imaging. For phagocytosis assays, ~5×10^4 cells were plated onto 12 mm coverslips.

Cells were transfected using FuGene-6 or Fugene-HD (Roche Diagnostics, Indianapolis, IN). Constructs for YFP-AktPH domain, YFP-Cdc42/Rac and CFP-PBD constructs were described previously (Hoppe and Swanson, 2004). YFP-CBD was constructed by

inserting the Cdc42-binding domain from WASP (Cannon et al., 2001; Tskvitaria-Fuller et al., 2006) into the YFP vector at XhoI/EcoRI sites (gift from Max Krummel, UCSF). For time-lapse FRET imaging, approximately 1 μg of plasmid DNA for YFP-Cdc42, YFP-Rac or PBD-CFP was used for each coverslip. 1.2 μg YFP-CBD and 0.8 μg CFP or 0.8 μg YFP-Cdc42(G12V), 1 μg mCFP-AktPH and 0.4 μg mCherry was used for each coverslip for time-lapse ratiometric imaging. Transfection for phagocytosis assays was accomplished using ~300 ng of DNA for YFP or YFP-Cdc42/Rac. All plasmids described here are available through Addgene (www.addgene.com/Joel_Swanson). To test for PI3K inhibition, macrophages were pre-treated with 50 μM LY294002 or 100 nM TGX-221 for 30 min in complete medium. Opsonized microspheres were then added, and phagocytosis efficiency assessed.

3.5.2 Microsphere Opsonization

2 μm and 5 μm streptavidin-coated, silica microspheres were purchased from Corpuscular (Cold Spring Harbor, NY) and Bangs Labs (Fisher, IN), respectively. To prepare beads with equivalent surface concentrations of IgG, aliquots of 2 μm and 5 μm beads representing an equal surface area (corresponding to 50–100 μg of 5 μm microspheres) were resuspended in PBS plus 1% BSA and incubated at room temperature with various concentrations of anti-streptavidin polyclonal IgG (Abcam, Cambridge, MA). Following opsonization, beads were rinsed 3× with PBS-BSA to remove unbound IgG. Beads were resuspended in SDS-PAGE loading buffer and heated to 95 C for 5 min to elute the bound IgG. The eluted IgG was Western blotted to estimate the amount of IgG on the particles (Supplemental Fig. 3.3). Each lot of microspheres was tested to ensure equivalent opsonization.

3.5.3 Phagocytosis Efficiency Assays

RAW264.7 cells were transfected with YFP, YFP fusions to wildtype Cdc42 or Rac, or YFP fusions to constitutively-active mutants of Cdc42 or Rac. After ~18 hours, opsonized 2 μm and 5 μm microspheres were added, and the macrophages were allowed to internalize the particles for 30 min at 37 C. Cells were then rinsed with PBS, fixed in 4% paraformaldehyde for 30 min at room temperature, rinsed again and the nonspecific binding sites were blocked with PBS plus 2% goat serum. After rinsing with PBS, beads that were not completely internalized were marked with Alexa 595-conjugated goat anti-rabbit IgG (Invitrogen). Phagocytic efficiencies (the percent of bound particles successfully internalized by macrophages) were counted for at least 25 macrophages per coverslip. Phagocytic efficiencies in cells expressing fusion proteins were divided by the phagocytic efficiencies in macrophages expressing YFP (typically ~60–75%). Statistical analysis was performed on data from at least two experiments in Prism 3 (GraphPad Software, San Diego, CA).

3.5.4 FRET Microscopy, Ratiometric Microscopy and Image processing

Component FRET images (I_A, I_D and I_F representing YFP acceptor, CFP donor and FRET images, respectively), ratiometric images (I_A and I_D) and phase-contrast images were acquired on an inverted Nikon Eclipse TE-300 microscope through a 60×, 1.4 NA, oil-immersion objective (Nikon USA, Melville, NY). Epifluorescence illumination was provided by a Lambda LS Xenon arc lamp (Sutter Instrument Company, Novato, CA). Transmitted light illumination was controlled by a Uniblitz VMM-D1 shutter driver (Vincent Associates, Rochester, NY). A JP4v2 CFP/YFP filter set (Chroma Technology,

Rockingham, VT) controlled by a Lambda 10–2 filter wheel controller (Sutter Instrument Company) was used to select wavelengths for CFP, YFP, FRET and mCherry image acquisition. Images were recorded on a CoolSnap HQ cooled-CCD (Roper Scientific, Tucson, AZ). All hardware was controlled using Metamorph 6.1 or 6.2 (Universal Imaging, Melville, PA). Calculation of the FRET stoichiometry images E_A, the fraction of *acceptor* molecules in complex with donor molecules times the efficiency of energy transfer, E_D, the fraction of *donor* molecules in complex with acceptor molecules times the efficiency of energy transfer, and R_M, the molar ratio of acceptors to donors, corrected for suppression of donor fluorescence by energy transfer, were performed in Metamorph using the shade/bias corrected images as described previously (Beemiller et al., 2006; Hoppe et al., 2002). To convert E_A values to G* values, which represent the fraction of YFP-GTPases in the GTP-bound state, the mean cellular ratio of acceptors to donors and the characteristic FRET efficiency of the YFP-GTPase:CFP-PBD complexes were used as described previously (Hoppe and Swanson, 2004).

Recruitment indexes (R_i), which represent the cell volume- and transfection efficiency-normalized translocation of probes to the phagosome region, were calculated as described previously (Hoppe and Swanson, 2004). In cells expressing constitutively active Cdc42, Ri was obtained from the ratio image between the CFP and RFP (mCherry) channels. In control cells, Ri was obtained from the ratio images of the YFP and CFP channels.

To measure FRET or Ri as a function of time during phagocytosis, the TRACKOBJ particle-tracking algorithm of Metamorph was used to identify and track erythrocytes or microspheres bound by macrophages and to automate the measurement of average gray values in a predefined measurement circle centered around the target particle, as

described previously (Henry et al., 2004; Hoppe and Swanson, 2004). A 2.2 μm diameter circle was used for 2 μm microspheres and a 5.4 μm circle was used for erythrocytes and 5 μm microspheres. Particle traces for independent phagocytic events were aligned using the frame of each YFP image series in which a phagocytic cup was first detectable.

To measure relative recruitment of CFP-AktPH to membranes in resting cells, line scans were performed in two lines perpendicular to each other in ratio images. Three pixels with non-zero values on each end of the line were picked as the membrane region and pixels between them were defined as the cytosol region. Average values from the membrane region were divided by average values from the cytosol region on the two perpendicular lines to generate relative recruitment to membrane (Rm/Rc). As Ri, this relative recruitment to membrane was normalized for cell volume- and transfection efficiency.

Figure 3.1 Activation of Rho GTPases in phagocytic cups after LY294002 inhibition. Activation of YFP-Cdc42 (A), YFP-Rac1 (B) and YFP-Rac2 (C) was measured by FRET microscopy in LY294002-treated macrophages during phagocytic cup formation around IgG-opsonized erythrocytes. (A–C) Presented in the image series are phase-contrast (PC), YFP-Cdc42/Rac (I_A) and pseudocolored E_A images indicating GTPase activation. White and red arrows indicate phagocytic cups. Scale bars at the lower-right of the E_A image series are 3 μm. Numbers in the lower-right of the PC images indicate the time in minutes after binding of the first erythrocyte. E_A values of pseudocolor images in A–C correspond to G* values of 0.74, 0.68 and 0.97, respectively. (D–F) GTPase activation in LY294002-treated macrophages (black triangles) was quantified and compared to activation by control macrophages (circles). Results were averaged from 10 events with and without LY294002 for Cdc42 (D), 13 events with and without LY294002 for Rac1 (E), and 10 events with LY294002 and 13 events without LY294002 for Rac2 (F). Error bars in D–F correspond to plus/minus the standard error of the mean (SEM).

Figure 3.1

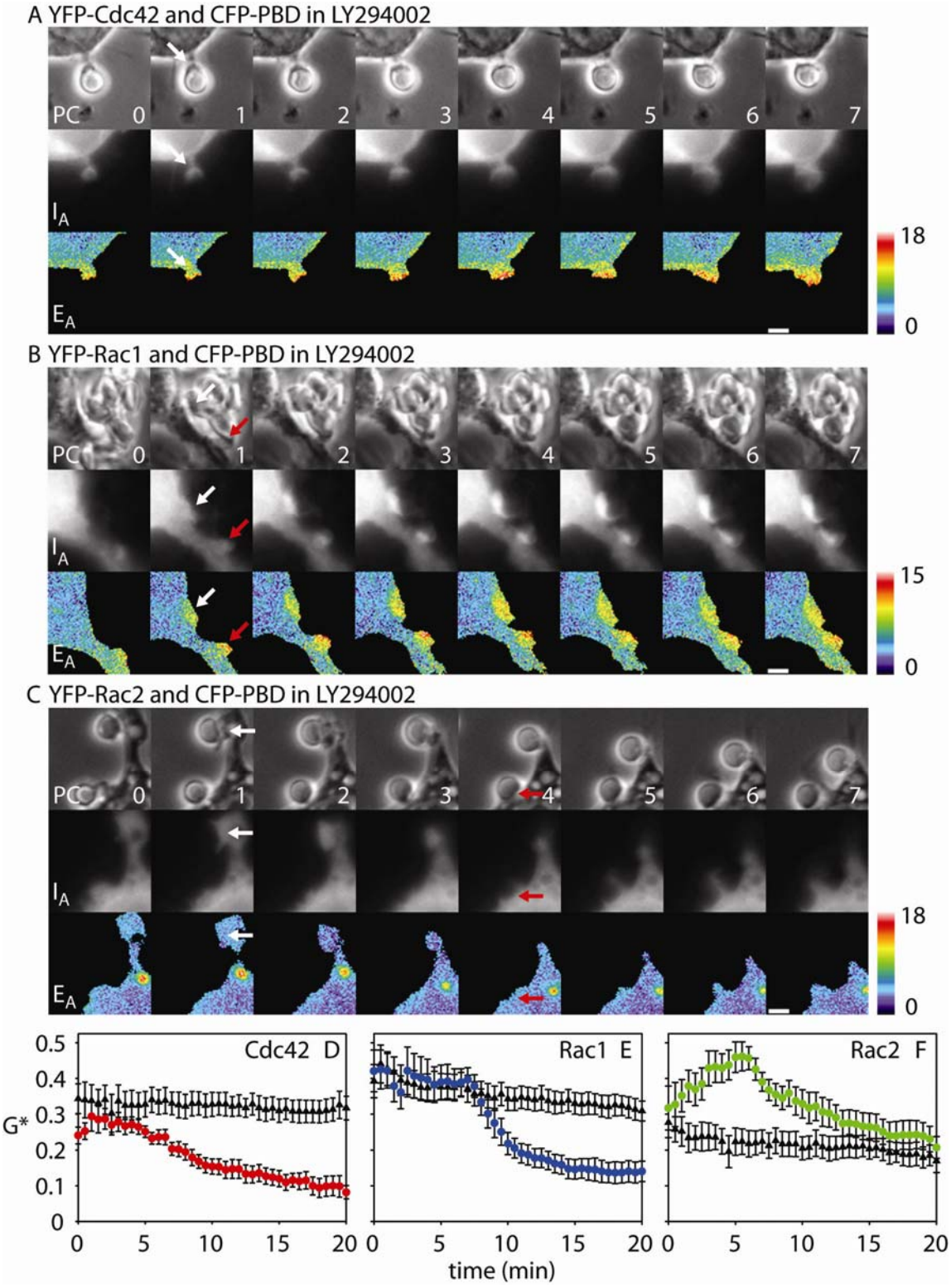
A YFP-Cdc42 and CFP-PBD in LY294002
PC
0
1
2
3
4
5
6
7
I_A
E_A
18
0
B YFP-Rac1 and CFP-PBD in LY294002
15
C YFP-Rac2 and CFP-PBD in LY294002
Cdc42 D
Rac1 E
Rac2 F
G*
0.5
0.4
0.3
0.2
0.1
0
5
10
15
20
time (min)

Figure 3.2 Activation of endogenous Cdc42 during phagocytosis. (A, B) Phase (top) and ratio images (bottom) of RAW264.7 macrophages expressing YFP-CBD and CFP show that endogenous Cdc42 was activated at the leading edge of phagocytic cups during complete phagocytosis (A) and remained activated on incomplete cups formed by TGX-221-treated macrophages (B). Scale bar is 5 μm. (C) Recruitment indexes of YFP-CBD (solid circle) and free YFP (open triangle), as a negative control, show that endogenous Cdc42 was activated on phagosomes early during phagocytosis and deactivated after internalization was complete. (n=11). (F) Recruitment indexes of YFP-CBD on incomplete phagocytic cups formed by TGX-221-treated (solid circle) and LY294002-treated (open triangle) macrophages were higher than that of free YFP on incomplete phagocytic cups formed by LY294002-treated macrophages (solid square), indicating that PIP_3 regulates the deactivation of endogenous Cdc42. n=8. Error bars in E and F represent plus/minus the SEM.

Figure 3.2

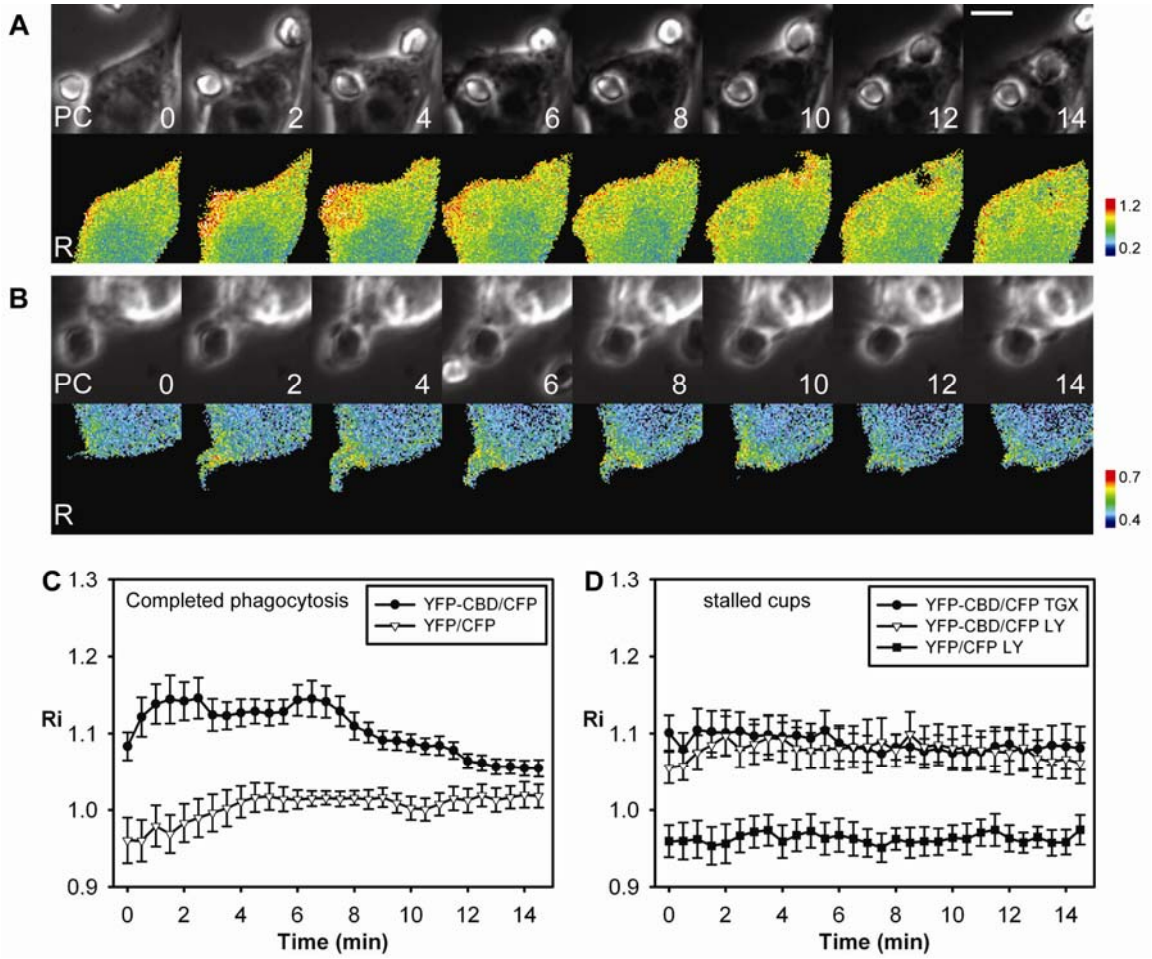
A
PC
0
2
4
6
8
10
12
14
R
1.2
0.2
B
PC
0
2
4
6
8
10
12
14
R
0.7
0.4
C
Completed phagocytosis
YFP-CBD/CFP
YFP/CFP
Ri
1.3
1.2
1.1
1.0
0.9
0
2
4
6
8
10
12
14
Time (min)
D
stalled cups
YFP-CBD/CFP TGX
YFP-CBD/CFP LY
YFP/CFP LY
Ri
1.3
1.2
1.1
1.0
0.9
0
2
4
6
8
10
12
14
Time (min)

Figure 3.3 Uniform labeling of microspheres. 50 μg of 5 μm microspheres or 20 μg of 2 μm microspheres were incubated with the indicated amounts of anti-streptavidin IgG for 30 min, then beads were extracted and Western blotted to determine the relative amount of IgG bound by each sample of beads. Opsonization for phagocytosis assays and time-lapse fluorescence microscopy were then performed using microsphere-to-immunoglobulin ratios that gave equivalent binding per unit surface area of particles.

Figure 3.3

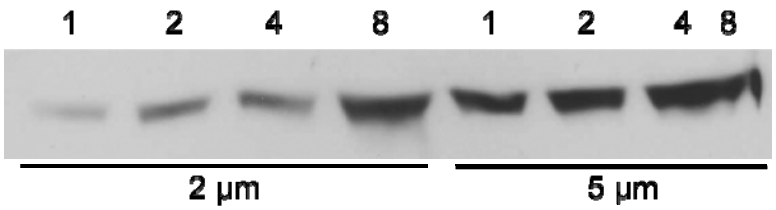

Figure 3.4 The signal transition is present during phagocytosis of small and large particles. (A) 3'PI dynamics on phagosomes were measured using ratiometric imaging of YFP-AktPH; 2 μm phagosomes (grey triangles): *n*=7; 5 μm phagosomes (black circles): *n*=5. (B and C) G* indicates the fraction of YFP-Cdc42, YFP-Rac1 or YFP-Rac2 activated in each pixel during phagocytosis of 2 μm and 5 μm diameter microspheres. (B) Cdc42, Rac1 and Rac2 activation during phagocytosis of 5 μm microspheres; n = 9, 9 and 8 phagocytic events for Cdc42, Rac1 and Rac2, respectively. (C) Activation of Cdc42, Rac1 and Rac2 during phagocytosis of 2 μm microspheres; n=12, 11, and 13 phagocytic events for Cdc42, Rac1 and Rac2, respectively. (D, F, H) I_A and E_A image series are presented for uptake of 5 μm microspheres by macrophages expressing CFP-PBD and either YFP-Cdc42 (D), YFP-Rac1 (F) or YFP-Rac2 (H). (E, G, I) I_A and E_A image series showing activation of Cdc42 (E), Rac1 (G), or Rac2 (I) during phagocytosis of 2 μm particles. White arrows indicate microspheres undergoing phagocytosis. Numbers at the lower-right of I_A images represent the time (min) after the first appearance of the phagocytic cup. Scale bars in D–I are 3 μm.

Figure 3.4

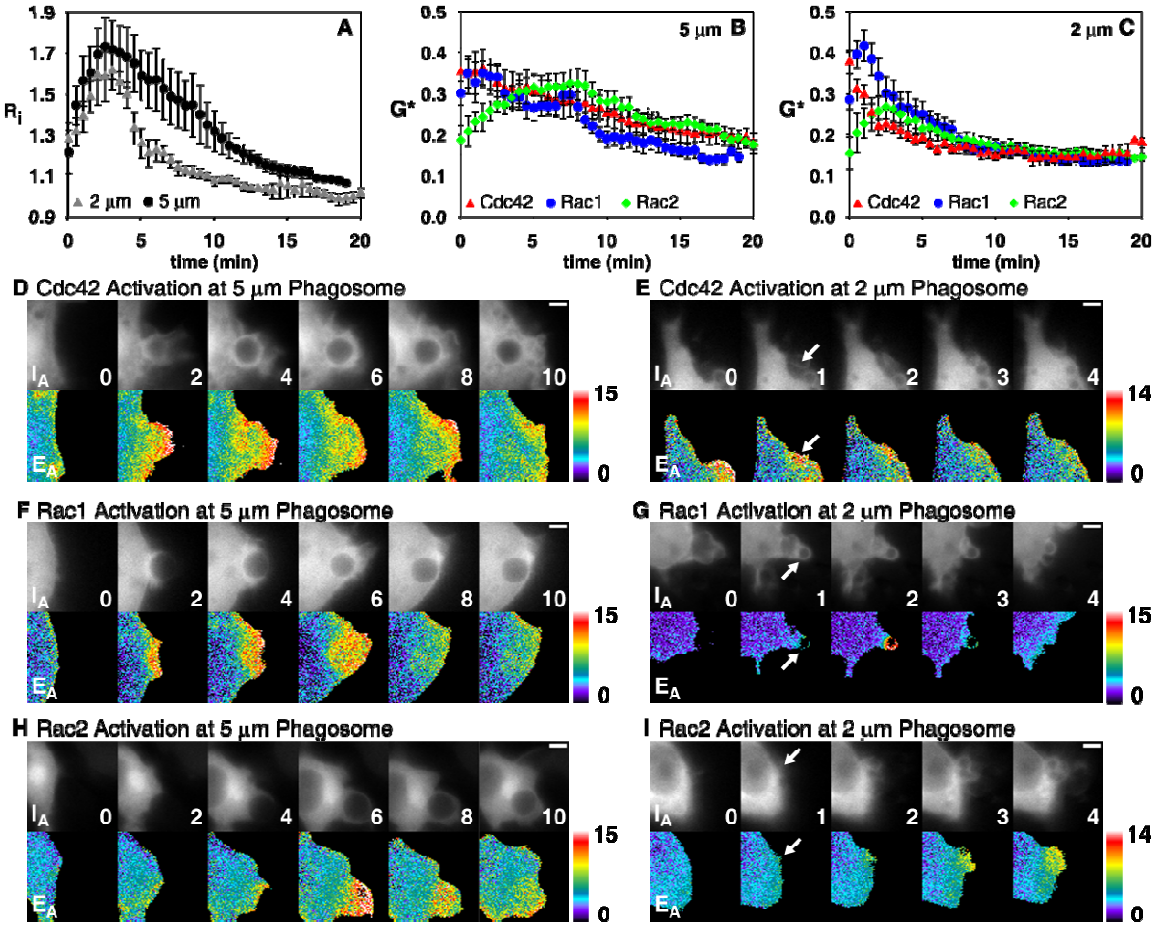
A
R_i
2 µm
5 µm
time (min)
5 µm B
G*
Cdc42
Rac1
Rac2
time (min)
2 µm C
G*
Cdc42
Rac1
Rac2
time (min)
D Cdc42 Activation at 5 µm Phagosome
I_A
E_A
E Cdc42 Activation at 2 µm Phagosome
I_A
E_A
F Rac1 Activation at 5 µm Phagosome
I_A
E_A
G Rac1 Activation at 2 µm Phagosome
I_A
E_A
H Rac2 Activation at 5 µm Phagosome
I_A
E_A
I Rac2 Activation at 2 µm Phagosome
I_A
E_A

Figure 3.5 The signal transition for Cdc42 and Rac2, but not Rac1, is inhibited by LY294002 despite competed phagocytosis of small particles. Cdc42 and Rac activation during phagocytosis of IgG-opsonized 2 μm microspheres in the absence (A) and presence (B) of LY294002 was quantified using FRET stoichiometry and particle-tracking analysis of image series. Cdc42 (red triangles) was activated immediately upon particle binding; *n*=12 phagocytic events. Maximum activation of Rac1 (blue circles) occurred 1 min after binding (*n*=11), while Rac2 activation (green diamonds) peaked at 2.5 min (*n*=13). Error bars represent plus/minus the SEM.

Figure 3.5

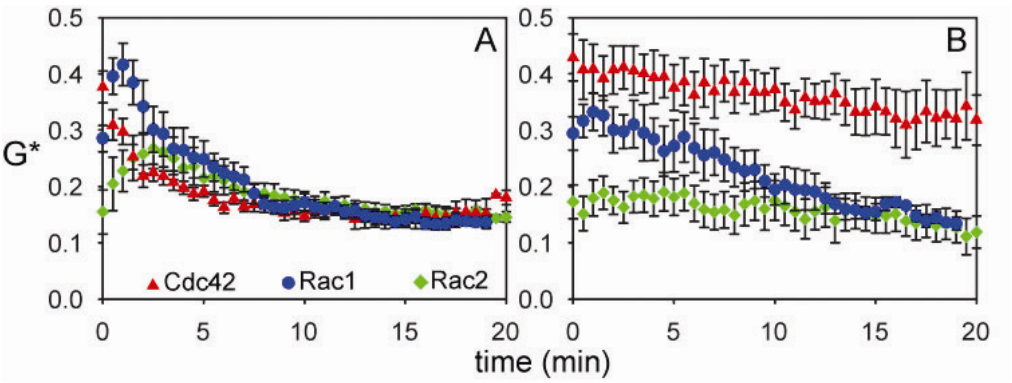

Figure 3.6 PI3K inhibition and constitutively active Cdc42 reduce phagocytosis additively. (A) Relative Phagocytic indexes (the phagocytic efficiency of GTPase-transfected cells relative to control cells expressing YFP) of macrophages over-expressing YFP-Cdc42 (grey bars) or YFP-Cdc42(G12V) (red), YFP-Rac1(Q61L) (blue) and YFP-Rac2(G12V) (green) were measured for opsonized 2 μm and 5 μm microspheres. Cdc42(G12V) produced a particle size-dependent inhibition of phagocytosis. Active Rac mutants were not inhibitory. Error bars represent SEM. (B) Phagocytic index of untransfected RAW 264.7 macrophages not treated (light grey) or treated (dark grey) with LY294002 and macrophages expressing YFP-Cdc42(G12V) not treated (red) or treated (dark red) with LY294002 were measured for 2 μm and 5 μm microspheres. All values were normalized to the phagocytic index of untransfected, untreated macrophages. Error bars represent plus/minus the SEM.

Figure 3.6

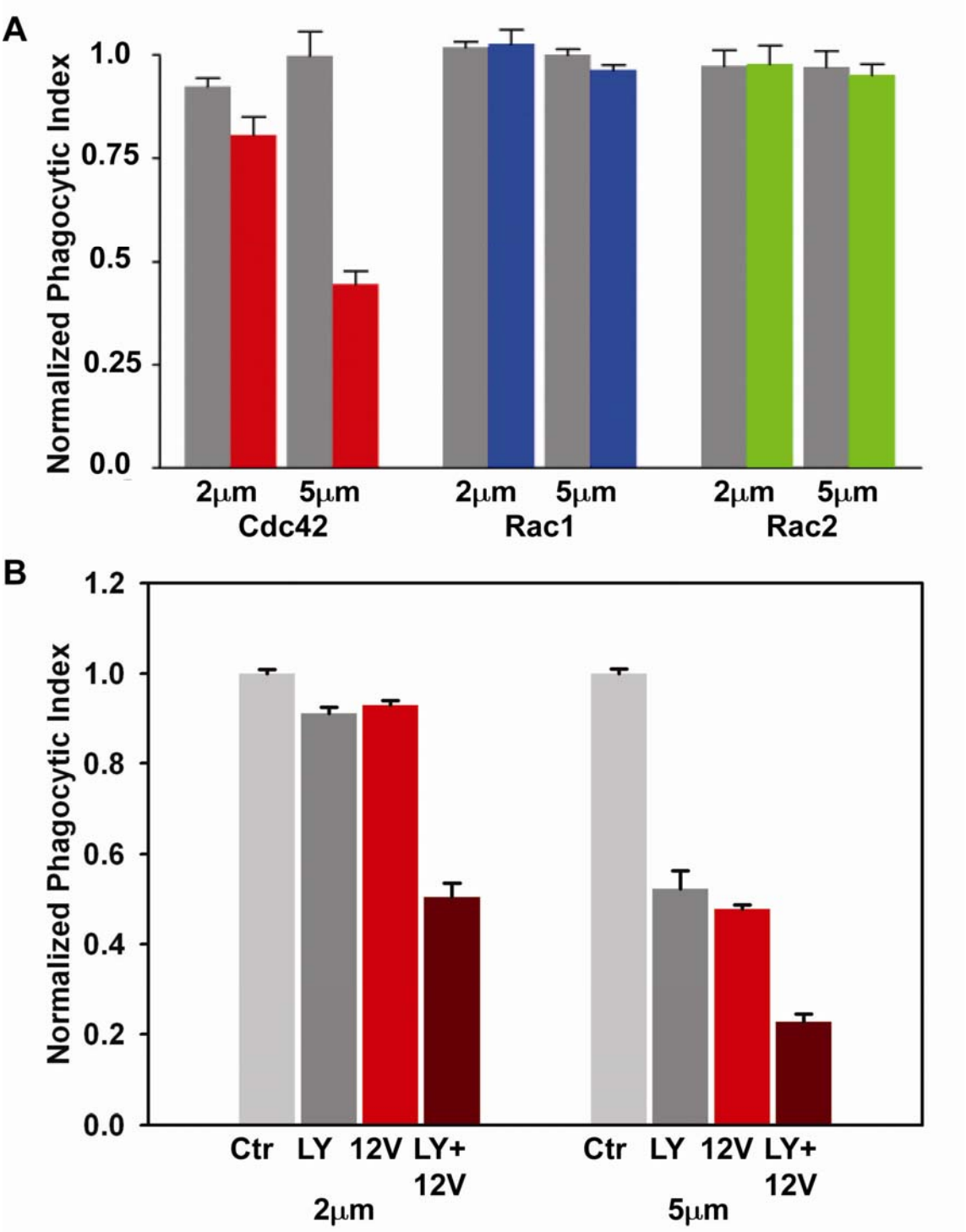
A
Normalized Phagocytic Index
1.0
0.75
0.5
0.25
0.0
2μm
5μm
Cdc42
2μm
5μm
Rac1
2μm
5μm
Rac2
B
Normalized Phagocytic Index
1.2
1.0
0.8
0.6
0.4
0.2
0.0
Ctr
LY
12V
LY+ 12V
2μm
Ctr
LY
12V
LY+ 12V
5μm

Figure 3.7 Cdc42(G12V) stimulates PI3K activity during phagocytosis. (A) Phase-contrast (PC) and ratio images (R) of RAW264.7 macrophage expressing YFP-AktPH and CFP. PIP_3 was not evident on membranes of resting cells. (B) Phase-contrast and ratio images of RAW264.7 macrophages expressing CFP-AktPH, YFP-Cdc42(G12V) and mCherry. PIP_3 was generated on membranes of resting cells overexpressing Cdc42(G12V). (C) Relative CFP-AktPH recruitment to membranes (Rm/Rc) was measured in control cells and in cells expressing YFP-Cdc42(G12V); n=6. (D, E) YFP recruitment (control) and CFP-AktPH recruitment to 2 μm (D) and 5 μm (E) phagosomes were measured by ratiometric imaging, n=7. Error bars represent plus/minus the SEM. Phase-contrast and ratio images of macrophages without (F, H) or with Cdc42(G12V) (G, I) during phagocytosis of 2 μm (F, G) and 5 μm (H, I) microspheres. Scale bars are 5 μm

Figure 3.7

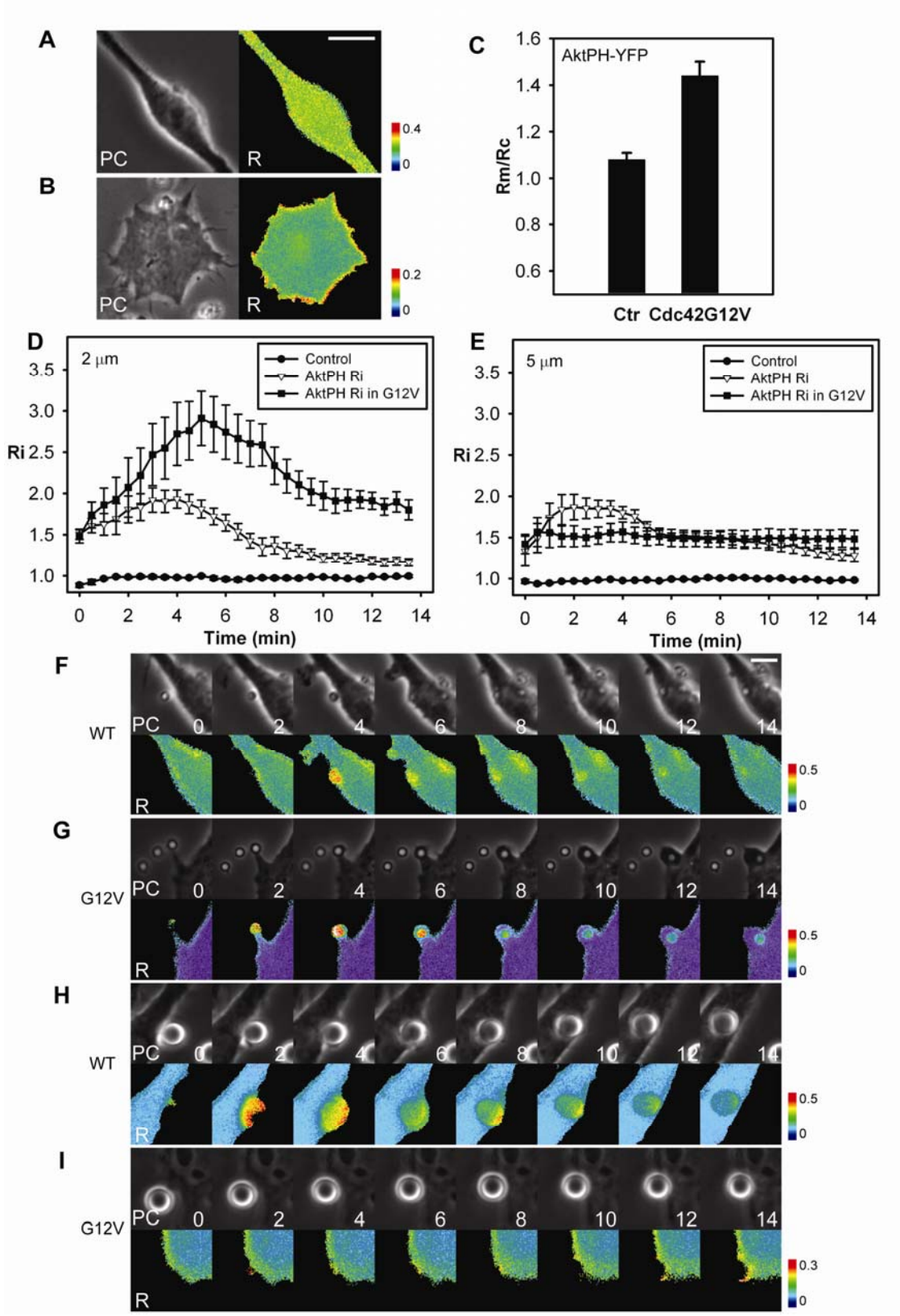
A
PC
R
0.4
0
B
PC
R
0.2
0
C
AktPH-YFP
Rm/Rc
1.6
1.4
1.2
1.0
0.8
0.6
Ctr Cdc42G12V
D
2 μm
Control
AktPH Ri
AktPH Ri in G12V
Ri
3.5
3.0
2.5
2.0
1.5
1.0
0 2 4 6 8 10 12 14
Time (min)
E
5 μm
Control
AktPH Ri
AktPH Ri in G12V
Ri
3.5
3.0
2.5
2.0
1.5
1.0
0 2 4 6 8 10 12 14
Time (min)
F
WT
PC
0 2 4 6 8 10 12 14
R
0.5
0
G
G12V
PC
0 2 4 6 8 10 12 14
R
0.5
0
H
WT
PC
0 2 4 6 8 10 12 14
R
0.5
0
I
G12V
PC
0 2 4 6 8 10 12 14
R
0.3
0

Figure 3.8 Actin recruitment was reduced by overexpression of Cdc42(G12V) during phagocytosis. Macrophages expressing mCherry-actin, CFP without (black) (n=5) or with (Green and red) YFP-Cdc42(G12V) (n=9) were imaged during phagocytosis of red blood cells and the recruitment of mCherry-actin to phagosomes was quantified as Ri. Constitutively-active Cdc42 reduced the recruitment of mCherry-actin to phagosomes. mCherry-actin persisted on cups that failed to close (Red) but was lost from those cups that did close (Green). Error bars represent plus/minus the SEM

Figure 3.8

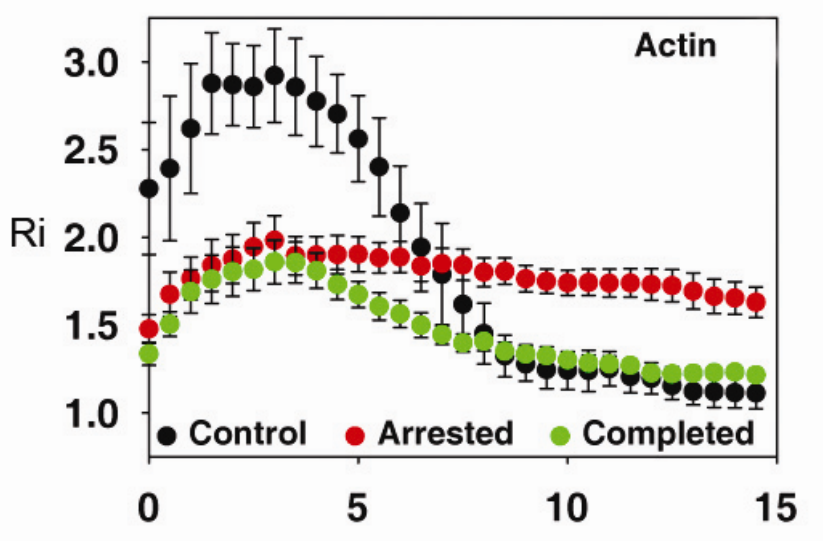

Figure 3.9 Summary of interactions between PI3K and Rho-family GTPases. (A) At the early stage of phagocytosis, ligated FcR mediate the activation of Cdc42, Rac1 and PI3K. Rac1:GTP and Cdc42:GTP promote the activation of PI4P5K and PI3K respectively, which in turn generate $PI(4,5)P_2$ and PIP_3 at phagosomes. $PI(4,5)P_2$, Rac1:GTP and Cdc42:GTP have been found to stimulate actin polymerization, which generates force for phagocytic cup protrusion. Molecules labeled red represent high recruitment or generation around phagosomes while molecules labeled grey represent low levels of activity. PI3K and PIP_3 are shown in blue since they are activated at intermediate levels during early stages of phagocytosis. (B) At the late stage of phagocytosis or the rear of the forming phagocytic cup, PIP_3 is generated to high levels, regulating the deactivation of Cdc42, which is necessary for the closure of phagosomes. We hypothesize that the deactivation of Cdc42 regulates the depolymerization of actin and the vesicle fusion at the base of phagocytic cups.

Figure 3.9

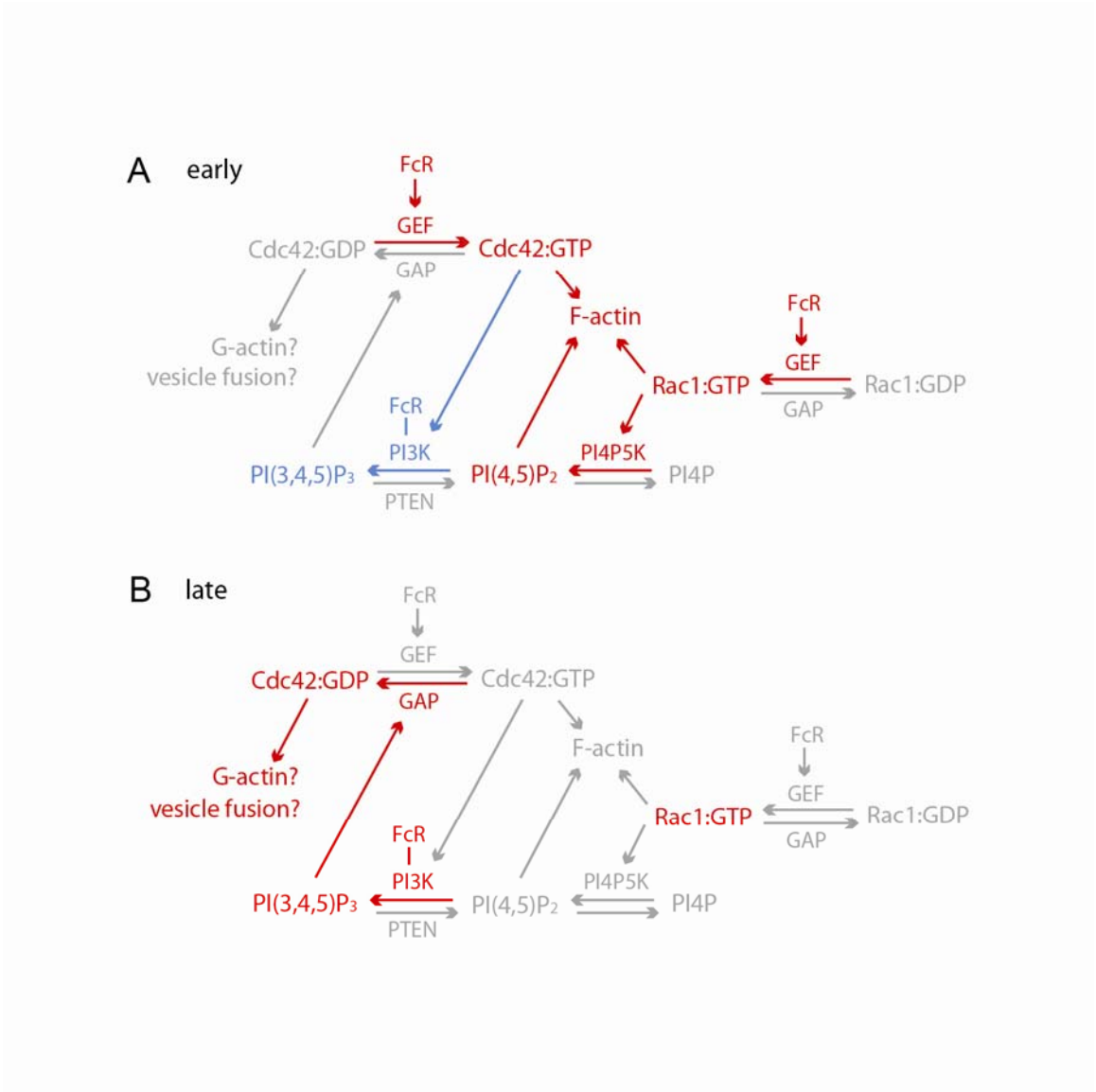
A
early
FcR
GEF
Cdc42:GDP
GAP
Cdc42:GTP
F-actin
FcR
G-actin?
vesicle fusion?
GEF
Rac1:GTP
Rac1:GDP
GAP
FcR
PI3K
PI4P5K
PI(3,4,5)P3
PI(4,5)P2
PI4P
PTEN
B
late
FcR
GEF
Cdc42:GDP
GAP
Cdc42:GTP
F-actin
FcR
G-actin?
vesicle fusion?
GEF
Rac1:GTP
Rac1:GDP
GAP
FcR
PI3K
PI4P5K
PI(3,4,5)P3
PI(4,5)P2
PI4P
PTEN

3.6 Bibliography

Araki, N., T. Hatae, A. Furukawa, and J.A. Swanson. 2003. Phosphoinositide-3-kinase-independent contractile activities associated with Fcγ-receptor-mediated phagocytosis and macropinocytosis in macrophages. *J. Cell Sci.* 116:247-257.

Araki, N., M.T. Johnson, and J.A. Swanson. 1996. A role for phosphoinositide 3-kinase in the completion of macropinocytosis and phagocytosis in macrophages. *J. Cell Biol.* 135:1249-1260.

Bajno, L., X.-R. Peng, A.D. Schreiber, H.-P. Moore, W.S. Trimble, and S. Grinstein. 2000. Focal Exocytosis of VAMP3-containing Vesicles at Sites of Phagosome Formation. *J. Cell Biol.* 149:697-706.

Balch, W.E., R.A. Kahn, and R. Schwaninger. 1992. ADP-ribosylation factor is required for vesicular trafficking between the endoplasmic reticulum and the cis-Golgi compartment. *J. Biol. Chem.* 267:13053-13061.

Beemiller, P., A.D. Hoppe, and J.A. Swanson. 2006. A Phosphatidylinositol-3-Kinase-Dependent Signal Transition Regulates ARF1 and ARF6 during Fcγ Receptor-Mediated Phagocytosis. *PLoS Biology*. 4.

Botelho, R.J., M. Teruel, R. Dierckman, R. Anderson, A. Wells, J.D. York, T. Meyer, and S. Grinstein. 2000. Localized biphasic changes in phosphatidylinositol-4,5-bisphosphate at sites of phagocytosis. *The Journal of cell biology*. 151:1353-1368.

Cannon, J.L., C.M. Labno, G. Bosco, A. Seth, M.H. McGavin, K.A. Siminovitch, M.K. Rosen, and J.K. Burkhardt. 2001. Wasp recruitment to the T cell:APC contact site occurs independently of Cdc42 activation. *Immunity*. 15:249-59.

Caron, E., and A. Hall. 1998. Identification of Two Distinct Mechanisms of Phagocytosis Controlled by Different Rho GTPases. *Science*. 282:1717-1721.

Chaussade, C., G.W. Rewcastle, J.D. Kendall, W.A. Denny, K. Cho, L.M. Gronning, M.L. Chong, S.H. Anagnostou, S.P. Jackson, N. Daniele, and P.R. Shepherd. 2007. Evidence for functional redundancy of class IA PI3K isoforms in insulin signalling. *Biochem J*. 404:449-58.

Cox, D., P. Chang, Q. Zhang, P.G. Reddy, G.M. Bokoch, and S. Greenberg. 1997. Requirements for Both Rac1 and Cdc42 in Membrane Ruffling and Phagocytosis in Leukocytes. *J. Exp. Med.* 186:1487-1494.

Cox, D., C.-C. Tseng, G. Bjekic, and S. Greenberg. 1999. A requirement for phosphatidylinositol 3-kinase in pseudopod extension. *J. Biol. Chem.* 274:1240-1247.

Dittie, A.S., N. Hajibagheri, and S.A. Tooze. 1996. The AP-1 adaptor complex binds to immature secretory granules from PC12 cells, and is regulated by ADP-ribosylation factor. *J. Cell Biol.* 132:523-536.

Donaldson, J.G., D. Cassel, R.A. Kahn, and R.D. Klausner. 1992. ADP-ribosylation factor, a small GTP-binding protein, is required for binding of the coatomer protein beta-COP to Golgi membranes. *Proceedings of the National Academy of Sciences of the United States of America*. 89:6408-6412.

Ge, M., J.S. Cohen, H.A. Brown, and J.H. Freed. 2001. ADP Ribosylation Factor 6 Binding to Phosphatidylinositol 4,5-Bisphosphate-Containing Vesicles Creates Defects in the Bilayer Structure: An Electron Spin Resonance Study. *Biophys. J.* 81:994-1005.

Greenberg, S., J. el Khoury, F. di Virgilio, E.M. Kaplan, and S.C. Silverstein. 1991. Ca(2+)-independent F-actin assembly and disassembly during Fc receptor-mediated phagocytosis in mouse macrophages. *J. Cell Biol.* 113:757-767.

Gu, H., R.J. Botelho, M. Yu, S. Grinstein, and B.G. Neel. 2003. Critical role for scaffolding adapter Gab2 in FcγR-mediated phagocytosis. *J. Cell Biol.* 161:1151-1161.

Henry, R.M., A.D. Hoppe, N. Joshi, and J.A. Swanson. 2004. The uniformity of phagosome maturation in macrophages. *The Journal of cell biology*. 164:185-194.

Honda, A., M. Nogami, T. Yokozeki, M. Yamazaki, H. Nakamura, H. Watanabe, K. Kawamoto, K. Nakayama, A.J. Morris, M.A. Frohman, and Y. Kanaho. 1999. Phosphatidylinositol 4-phosphate 5-kinase alpha is a downstream effector of the small G protein ARF6 in membrane ruffle formation. *Cell*. 99:521-532.

Hoppe, A., K. Christensen, and J.A. Swanson. 2002. Fluorescence resonance energy transfer-based stoichiometry in living cells. *Biophysical journal*. 83:3652-3664.

Hoppe, A.D., and J.A. Swanson. 2004. Cdc42, Rac1, and Rac2 Display Distinct Patterns of Activation during Phagocytosis. *Mol. Biol. Cell*. 15:3509-3519.

Kavran, J.M., D.E. Klein, A. Lee, M. Falasca, S.J. Isakoff, E.Y. Skolnik, and M.A. Lemmon. 1998. Specificity and Promiscuity in Phosphoinositide Binding by Pleckstrin Homology Domains. *J. Biol. Chem.* 273:30497-30508.

Larsen, E.C., J.A. DiGennaro, N. Saito, S. Mehta, D.J. Loegering, J.E. Mazurkiewicz, and M.R. Lennartz. 2000. Differential requirement for classic and novel PKC isoforms in respiratory burst and phagocytosis in RAW 264.7 cells. *J. Immunol.* 165:2809-2817.

Lerm, M., V.P. Brodin, I. Ruishalme, O. Stendahl, and E. Sarndahl. 2007. Inactivation of Cdc42 Is Necessary for Depolymerization of Phagosomal F-Actin and Subsequent Phagosomal Maturation. *J Immunol*. 178:7357-7365.

Manser, E., T. Leung, H. Salihuddin, L. Tan, and L. Lim. 1993. A non-receptor tyrosine kinase that inhibits the GTPase activity of p21cdc42. *Nature*. 363:364-367.

Marshall, J.G., J.W. Booth, V. Stambolic, T. Mak, T. Balla, A.D. Schreiber, T. Meyer, and S. Grinstein. 2001. Restricted accumulation of phosphatidylinositol 3-kinase products in a plasmalemmal subdomain during Fc gamma receptor-mediated phagocytosis. *The Journal of cell biology*. 153:1369-1380.

Melendez, A.J., M.M. Harnett, and J.M. Allen. 2001. Crosstalk between ARF6 and

protein kinase Calpha in Fc(gamma)RI-mediated activation of phospholipase D1. *Current biology : CB*. 11:869-874.

Niedergang, F., E. Colucci-Guyon, T. Dubois, G. Raposo, and P. Chavrier. 2003. ADP ribosylation factor 6 is activated and controls membrane delivery during phagocytosis in macrophages. *The Journal of cell biology*. 161:1143-1150.

O'Luanaigh, N., R. Pardo, A. Fensome, V. Allen-Baume, D. Jones, M.R. Holt, and S. Cockcroft. 2002. Continual production of phosphatidic acid by phospholipase D is essential for antigen-stimulated membrane ruffling in cultured mast cells. *Molecular biology of the cell*. 13:3730-3746.

Scott, C.C., W. Dobson, R.J. Botelho, N. Coady-Osberg, P. Chavrier, D.A. Knecht, C. Heath, P. Stahl, and S. Grinstein. 2005. Phosphatidylinositol-4,5-bisphosphate hydrolysis directs actin remodeling during phagocytosis. *J. Cell Biol.* 169:139-149.

Srinivasan, S., F. Wang, S. Glavas, A. Ott, F. Hofmann, K. Aktories, D. Kalman, and H.R. Bourne. 2003. Rac and Cdc42 play distinct roles in regulating $PI(3,4,5)P_3$ and polarity during neutrophil chemotaxis. *J. Cell Biol.* 160:375-385.

Swanson, J.A., M.T. Johnson, K. Beningo, P. Post, M. Mooseker, and N. Araki. 1999. A contractile activity that closes phagosomes in macrophages. *J Cell Sci*. 112:307-316.

Tse, S.M.L., W. Furuya, E. Gold, A.D. Schreiber, K. Sandvig, R.D. Inman, and S. Grinstein. 2003. Differential role of actin, clathrin, and dynamin in Fcγ receptor-mediated endocytosis and phagocytosis. *J. Biol. Chem.* 278:3331-3338.

Tskvitaria-Fuller, I., A. Seth, N. Mistry, H. Gu, M.K. Rosen, and C. Wulfing. 2006. Specific patterns of Cdc42 activity are related to distinct elements of T cell polarization. *J Immunol*. 177:1708-20.

Vieira, O.V., R.J. Botelho, L. Rameh, S.M. Brachmann, T. Matsuo, H.W. Davidson, A. Schreiber, J.M. Backer, L.C. Cantley, and S. Grinstein. 2001. Distinct roles of class I and class III phosphatidylinositol 3-kinases in phagosome formation and maturation. *J. Cell Biol.* 155:19-25.

Zhang, Q., D. Cox, C.-C. Tseng, J.G. Donaldson, and S. Greenberg. 1998. A Requirement for ARF6 in Fcgamma Receptor-mediated Phagocytosis in Macrophages. *J. Biol. Chem.* 273:19977-19981.

Zheng, Y., S. Bagrodia, and R.A. Cerione. 1994. Activation of phosphoinositide 3-kinase activity by Cdc42Hs binding to p85. *J Biol Chem*. 269:18727-30.

Chapter Four

Target geometry affects intracellular signaling during phagocytosis

(Heunjin Lee at Caltech built the optical tweezers system. Lynn Kamen optimized the rod opsonization procedure. I collected data in collaboration with Heunjin Lee and processed data.)

4.1 Abstract

The interactions between ligands on particles and FcR on macrophage membranes play vital roles in initiating phagocytosis. However, other factors have been found to affect the outcome of phagocytosis. Local particle shape at the initial contact point between the particles and macrophages can determine whether phagocytosis can be finished (Champion and Mitragotri, 2006), but the molecular mechanism of this phenomenon is still unknown. In this chapter, the recruitment of YFP-AktPH, YFP-actin and PKCε-YFP was studied during successful phagocytosis from the end of rod-shaped particles and during frustrated phagocytosis from the side of rod-shaped particles. YFP-AktPH was highly recruited during successful phagocytosis but was only moderately recruited to

cups during frustrated phagocytosis, suggesting that the 3' phosphoinositide concentration thresholds correlate with the outcome of phagocytosis. Both YFP-actin and PKCε-YFP, which are, respectively, early and late signaling molecules during phagocytosis of spheres, were also recruited to successfully formed phagosomes initiated from rod ends. However, PKCε-YFP was not detected on cups during frustrated phagocytosis, indicating that late stage signals were not activated. These results suggest that target geometry can modulate the generation of intracellular 3' phosphoinositides, whose concentrations can affect the late stage signals and the outcome of phagocytosis.

4.2 Introduction

The hypothesis of autonomous signaling proposed in zipper model (Griffin et al., 1976) is challenged by several other experiments in addition to the research described in chapter 2. Based on the zipper model, the outcome of phagocytosis should only depend on the interaction between the ligands and receptors. However, physical properties of target particles, such as rigidity and shape, have been found to affect the outcome of phagocytosis. Among particles with identical chemical properties, bone marrow-derived macrophages showed much higher phagocytosis capacity for rigid particles than for soft particles (Beningo and Wang, 2002). In addition, their research showed that constitutively active Rac1 could stimulate the phagocytosis of soft particles (Beningo and Wang, 2002), indicating that the rigidity of target particle is involved in regulating

intracellular signaling pathways. Target geometry also affects the outcome of phagocytosis. Champion and Mitragotri (2006) found the local particle shape at the initial contact point between the particles and macrophages affects whether phagocytosis can be finished. For a rod-shaped particle uniformly coated with IgG, phagocytosis that starts from the rod end can be finished, but phagocytosis that starts from the flat rod side cannot. Membranes spread over such particles but phagocytosis is not completed. These results suggest that phagocytosis is a coordinated process which can be affected by factors other than Fc receptor activation.

Whether the target geometry can affect intracellular signaling is still unknown. In this chapter, we report that 3' phosphoinositide concentration thresholds correlated with the outcome of rod-shaped particle phagocytosis. Also, the local particle shape at the initial contact point between the particles and macrophages limited the generation of the late stage signal, PKCε, but not early stage signal, actin. These results lead to the hypothesis that target geometry can affect the 3' phosphoinositide concentration thresholds which are necessary for the generation of late stage signals and the closure of phagosomes.

4.3 Results

4.3.1 Complete phagocytosis of rod-shaped particles correlates with 3' phosphoinositide concentrations

To examine whether the 3' phosphoinositide concentration thresholds identified in chapter 2 affect phagocytosis of rod-shaped particles, we measured the recruitment index of YFP-AktPH (Hoppe and Swanson, 2004) during successful and frustrated phagocytosis of rod-shaped particles. Rods were placed around RAW 264.7 macrophages using optical tweezers. When phagocytosis started from the rod end and proceeded to closure, YFP-AktPH was recruited to the forming phagocytic cups (Fig. 4.1 A, B), indicating that high concentrations of 3' phosphoinositide were generated during successful phagocytosis. When phagocytosis started from the rod side, phagocytosis could not be finished, as reported previously (Champion and Mitragotri, 2006). YFP-AktPH was also recruited to the incomplete cups formed during frustrated phagocytosis, but to a much lower level (Fig. 4.1 C, D). Measurement of Ri at the 1/4 cup-, 1/2 cup- or the whole phagosome stages was significantly higher than the maximum Ri measured during frustrated phagocytosis (Fig. 4.1 E). This indicated that successful phagocytosis from rod ends correlated with the generation of suprathreshold concentrations of 3' PIs.

4.3.2 Early but not late stage signals are recruited to incomplete cups of frustrated phagocytosis

Based on the result of chapter 2, we expected that early stage signals, such as actin filament assembly (Diakonova et al., 2002), should appear in incomplete cups even

when the 3’ phosphoinositide concentration thresholds cannot be reached, and that late stage signals, such as PKCε recruitment (Larsen et al., 2002), should not appear. We first compared the recruitment of YFP-actin during successful and frustrated phagocytosis of rod-shaped particles. YFP-actin was recruited during successful phagocytosis from rod ends and was concentrated at the leading edges of phagocytic cups (Fig. 4.2 A, B). Interestingly, in a few cases YFP-actin persisted at the back of the rod after it was fully internalized (Fig. 4.2 A, B). YFP-actin was also recruited to incomplete cups of frustrated phagocytosis starting from the rod side (Fig. 4.2 C, D), although the recruitment was less than that observed during successful phagcytosis (Fig. 4.2 E). This phenomenon is reminiscent of actin dynamics on beads with low IgG densities; YFP-actin was recruited moderately to stalled phagocytic cups

.

Although YFP-actin recruitment during frustrated phagocytosis indicated that the signaling cascade was initiated by ligated receptors (Fig. 4.3 I), PKCε-YFP was not recruited to those incomplete cups (Fig. 4.3 G, H). This suggested that the 3’ phosphoinositide concentration thresholds were required for later stage signals to complete phagocytosis. During successful phagocytosis from rod ends, PKCε-YFP was recruited to phagocytic cups later than CFP-actin (Fig. 4.3 A-F). Two patterns of PKCε-YFP recruitment were identified. In some events, PKCε-YFP was recruited to the whole phagocytic cup at a late stage of internalization and remained until after phagosome closure (Fig. 4.3 A, B). In other events, PKCε-YFP was recruited early but disappeared

before phagosome closure (Fig. 4.3 D, E). The explanation for this difference is still under study but these two patterns of PKCε-YFP recruitment correlated with different patterns of actin recruitment. In the former situations, CFP-actin was recruited as a belt-shaped band which was restricted to the leading edge of the cup until the internalization was finished (Fig. 4.3 C). In the latter situations, the bands disappeared before internalization finished, leaving irregular membrane ruffling to complete the ingestion process (Fig. 4.3 F). Although PKCε-YFP showed different recruitment patterns, it was recruited during all the successful phagocytosis events. In summary, both early and late signals appeared when 3' phosphoinositide concentration thresholds were reached during success phagocytosis starting from rod ends, but only early stage signals were present during frustrated phagocytosis when 3' phosphoinositide concentration thresholds could not be reached. These results suggest that cell membrane curvature does not affect early stage signals generated by ligation of receptors but affects the magnitude of PIP_3 accumulation, which is necessary for late stage signals and commitment to phagocytosis.

4.4 Discussion

In this chapter, we found that 3' phosphoinositide concentration thresholds correlate with the outcome of phagocytosis of rod-shaped particles. This phenomenon is similar in many respects to what we observed during phagocytosis of spherical particles coated

with different ligand densities. 3’ phosphoinositides in phagocytic cups reached high concentrations when phagocytosis of rod-shaped particles started from the rod end or when spherical particles were coated with enough IgG. Phagocytosis could be finished in both situations. If 3’ phosphoinositides cannot reach significantly high concentrations, due to first contact at flat side of rod, very low IgG densities on spherical particles or treatment of PI3K inhibitor, then phagocytosis will not finish. Thus, we hypothesized that 3’ phosphoinositide concentrations are key factors determining the outcome of phagocytosis. In addition, early stage signals, such as actin recruitment, but not late stage signals, such as PKCε recruitment, are present on incomplete cups when phagocytosis cannot be finished, indicating that 3’ phosphoinositide concentration thresholds regulate the transition to late stage signals. Thus downstream signals are not generated automatically by Fc receptor ligation. Instead, PIP_3 concentration thresholds regulate distinct cellular responses by integrating receptor signaling in a domain of membrane.

The different outcome during phagocytosis of spherical particles coated with different ligand densities can be explained by feedback responses (Brandman and Meyer, 2008). The scaffolding adaptor protein, Grb-associated binder 2 (Gab2) is recruited to phagosomes by PIP_3 through its PH domain. Gab2 also interacts with the p85 subunit of PI3K and this interaction is important for optimal PI3K activation (Gu et al., 2003). Thus, a Gab2-dependent positive feedback response may serve as a PIP_3 amplifier during

phagocytosis, which generates suprathreshold 3' phosphoinositide concentrations to complete phagocytosis. However, the effect of target geometry on the result of phagocytosis may not be simply explained by feedback responses in signaling pathways since the IgG density on those particles is uniform and should generate similar signaling outcomes regardless of the geometry.

There are several possible explanations to explain the effect of target geometry on phagocytosis. Macrophages may be able to sense the target geometry by molecules such as Amphiphysin (Gold et al., 2000), whose BAR domain may sense membrane curvature (Zimmerberg and McLaughlin, 2004). Amphiphysin II is recruited to phagosomes in a PI3K-dependent manner (Gold et al., 2000). Another possibility is that the target geometry affects the properties or the assembly of the cup domain, a subregion of plasma membrane in which PIP_3 can reach suprathreshold concentrations required for late stages of signaling (Swanson, 2008). In both phagocytosis and macropinocytosis, a cup domain with lipid and protein composition different from the rest of the plasma membrane integrates and amplifies intracellular signals (Swanson, 2008). The diffusion of lipids is slower in the phagocytic cup than in other parts of the membrane (Corbett-Nelson et al., 2006). The properties of molecular diffusion and the distinct signaling patterns within the cup suggest a diffusion barrier exists at the rim of the cup, although the nature of such a barrier is not known. Target geometry may affect whether a complete barrier can be formed at the cup rim, which can affect the diffusion

and concentration of PIP_3 within the cup domain, consequently affecting the outcome of phagocytosis. It is also possible that the PIP_3 diffusion is simply affected by the curvature of membrane (Yoshigaki, 2007), a pure physical effect independent of biological molecules.

Although understanding how target shape can affect the outcome of phagocytosis requires more examination, this phenomenon leads to the question on whether different shapes of bacteria provide a mechanism for bacteria to avoid being phagocytosed by macrophages. No research has been done about this hypothesis, but studying the signaling during phagocytosis of rod-shaped bacteria should contribute to our understanding of pathogen invasion and to the development of novel treatments for infectious diseases.

4.5 Materials and methods

Materials, DNA constructs and ratiometric image were described in chapters 2 and 3. Rod-shaped particles are a gift from Julie Champion (University of California, Santa Barbara). To opsonize particles, rods were incubated with 0.25 mg/ml IgG from rabbit serum (Sigma-Aldrich) for 30 minutes and washed twice with PBS. For time-lapse ratiometric imaging, plasmid DNA encoding YFP-AktPH (1.5 μg) and mCherry (0.5 μg), YFP-actin (1.5 μg) and mCherry (0.5 μg) or YFP-PKCε (0.8 μg), mCFP-actin (0.8 μg)

and mCherry (0.4 μg) was used for each coverslip. The optical tweezers and fluorescence imaging system was described previously (Lee et al., 2008). A 1064 nm laser was used to manipulate the rods and to position them near RAW264.7 macrophages expressing fluorescent probes. The rods were released from optical trap by blocking the laser after they became attached to macrophages. A mercury lamp was used as illumination for time-lapse fluorescence imaging of overexpressed chimeras during phagocytosis. The calculation of ratio images and Ri were described in chapter 3.

Figure 4.1 Complete phagocytosis of rod-shaped particles generate high concentrations of 3' phosphoinositides. Time-lapse, phase-contrast (A, C) and Ratio images (B, D) of RAWs transfected with YFP-AktPH and mCherry during internalization of rod-shaped particles from the end (A, B) or the side (C, D), shown at 80 second intervals. Scale bar is 3 μm. (E) The maximum YFP-AktPH recruitment index on the incomplete cup of frustrated phagocytosis from rod side was significantly lower than YFP-AktPH recruitment index of complete phagocytosis from rod end when 1/4, 1/2 or whole cup formed. n=4.

Figure 4.1

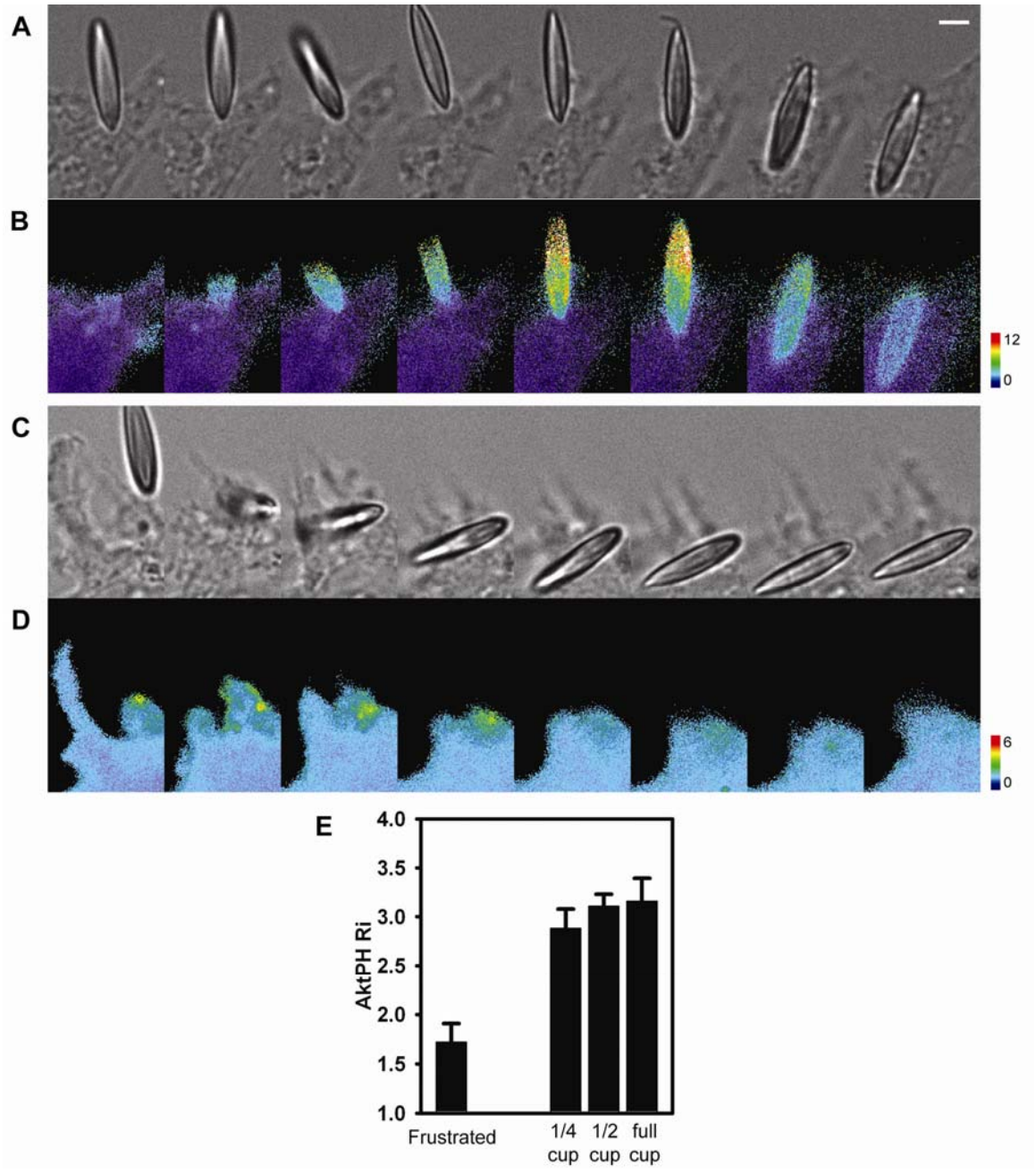
A
B
12
0
C
D
6
0
E
AktPH Ri
4.0
3.5
3.0
2.5
2.0
1.5
1.0
Frustrated
1/4 cup
1/2 cup
full cup

Figure 4.2 YFP-actin is recruited to phagocytic cups during both successful and frustrated phagocytosis of rods. Time-lapse, phase-contrast (A, C) and Ratio images (B, D) of YFP-actin- and mCherry- transfected RAWs engaging rod-shaped particles from the end (A, B) or the side (C, D) are shown at 80-second intervals. Scale bar is 3 μm. (E) YFP-actin was significantly recruited to incomplete cups of frustrated phagocytosis from the rod side, although the maximum YFP-actin recruitment index on incomplete cups was lower than the YFP-actin recruitment index of complete phagocytosis from rod end when 1/4, 1/2 or whole cup is formed. n=9.

Figure 4.2

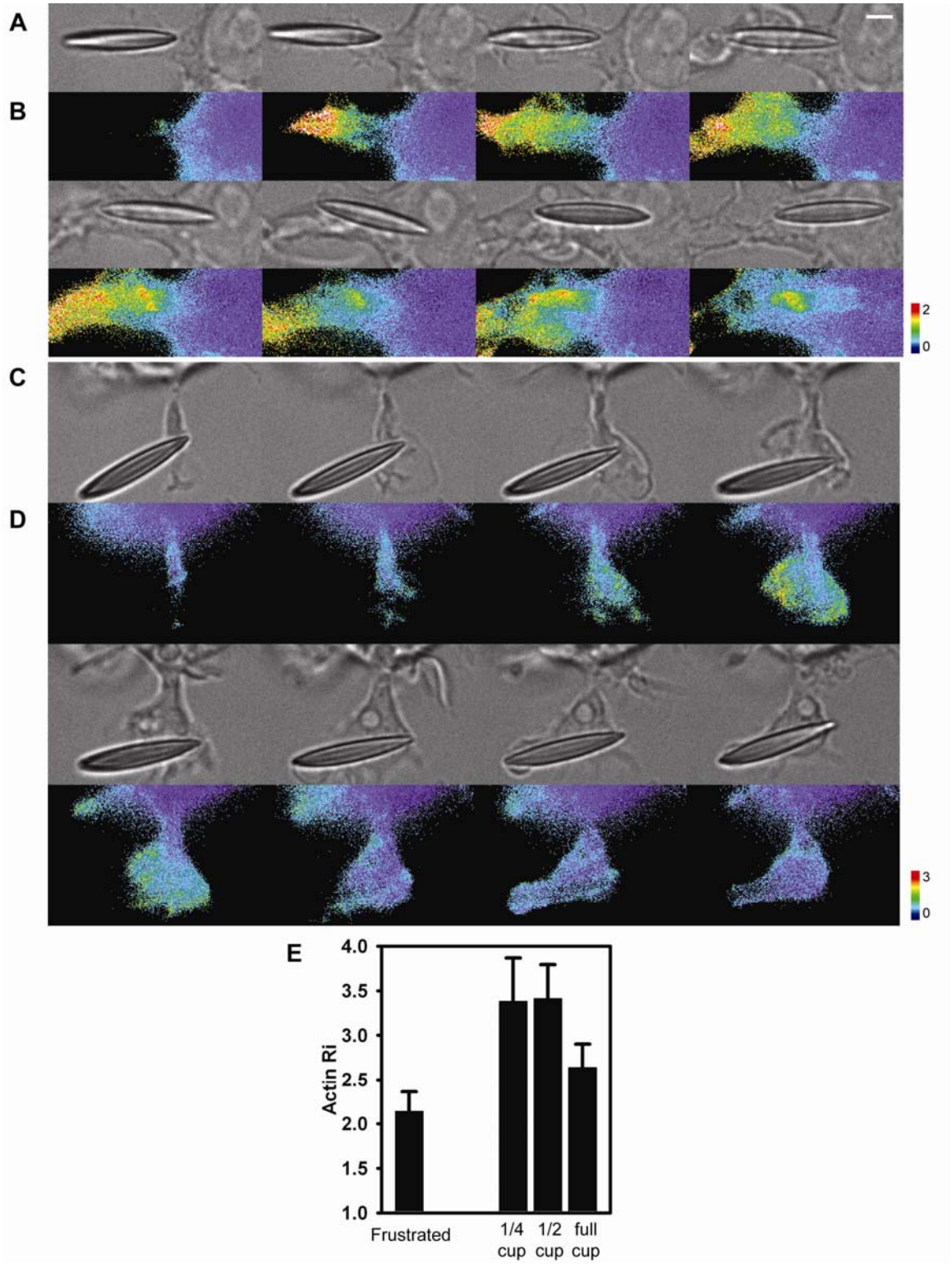
A
B
2
0
C
D
3
0
E
Actin Ri
4.0
3.5
3.0
2.5
2.0
1.5
1.0
Frustrated
1/4 cup
1/2 cup
full cup

Figure 4.3 PKCε-YFP is not recruited to phagocytic cups during frustrated phagocytosis. Time-lapse, phase-contrast (A, D, G), YFP/mCherry Ratio (B, E, H) and CFP images (C, F, I) of RAWs transfected with PKCε-YFP, CFP-actin and mCherry are shown at 80-second intervals. PKCε-YFP was recruited to complete phagocytic cups from rod ends at a later time than CFP-actin recruitment (B, C, E, F), but was undetectable on incomplete cups of frustrated phagocytosis from rod side (H). Scale bar is 3 μm.

Figure 4.3

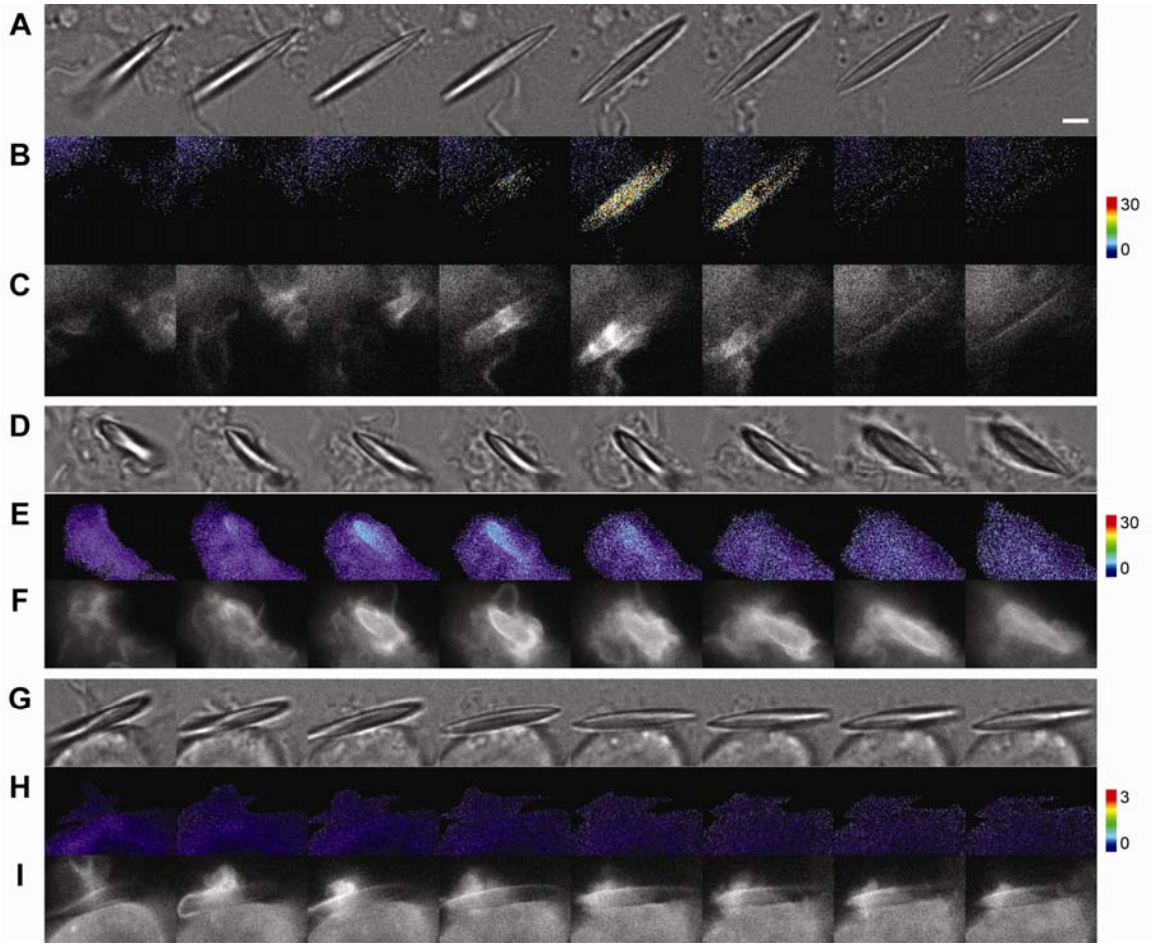

4.6 Bibliography

Beningo, K.A., and Y.-L. Wang. 2002. Fc-receptor-mediated phagocytosis is regulated by mechanical properties of the target. *J. Cell Sci.* 115:849-856.

Brandman, O., and T. Meyer. 2008. Feedback loops shape cellular signals in space and time. *Science*. 322:390-5.

Champion, J.A., and S. Mitragotri. 2006. Role of target geometry in phagocytosis. *Proc Natl Acad Sci U S A*. 103:4930-4.

Corbett-Nelson, E.F., D. Mason, J.G. Marshall, Y. Collette, and S. Grinstein. 2006. Signaling-dependent immobilization of acylated proteins in the inner monolayer of the plasma membrane. *J Cell Biol*. 174:255-65.

Diakonova, M., G. Bokoch, and J.A. Swanson. 2002. Dynamics of cytoskeletal proteins during Fcg receptor-mediated phagocytosis in macrophages. *Mol. Biol. Cell*. 13:402-411.

Gold, E.S., N.S. Morrissette, D.M. Underhill, J. Guo, M. Bassetti, and A. Aderem. 2000. Amphiphysin IIm, a novel amphiphysin II isoform, is required for macrophage phagocytosis. *Immunity*. 12:285-92.

Griffin, F.M., J.A. Griffin, and S.C. Silverstein. 1976. Studies on the mechanism of phagocytosis. II. The interaction of macrophages with anti-immunoglobulin IgG-coated bone marrow-derived lymphocytes. *J. Exp. Med.* 144:788-809.

Gu, H., R.J. Botelho, M. Yu, S. Grinstein, and B.G. Neel. 2003. Critical role for scaffolding adapter Gab2 in FcgR-mediated phagocytosis. *J. Cell Biol.* 161:1151-1161.

Hoppe, A.D., and J.A. Swanson. 2004. Cdc42, Rac1 and Rac2 display distinct patterns of activation during phagocytosis. *Mol. Biol. Cell*. 15:3509-3519.

Larsen, E.C., T. Ueyama, P.M. Brannock, Y. Shirai, N. Saito, C. Larsson, D. Loegering, P.B. Weber, and M.R. Lennartz. 2002. A role for PKC-e in FcgR-mediated phagocytosis by RAW 264.7 cells. *J. Cell Biol.* 159:939-944.

Lee, H.J., E.L. Peterson, R. Phillips, W.S. Klug, and P.A. Wiggins. 2008. Membrane shape as a reporter for applied forces. *Proc Natl Acad Sci U S A*. 105:19253-7.

Swanson, J.A. 2008. Shaping cups into phagosomes and macropinosomes. *Nat Rev Mol Cell Biol*. 9:639-649.

Yoshigaki, T. 2007. Theoretically predicted effects of Gaussian curvature on lateral diffusion of membrane molecules. *Phys Rev E Stat Nonlin Soft Matter Phys*. 75:041901.

Zimmerberg, J., and S. McLaughlin. 2004. Membrane curvature: how BAR domains bend bilayers. *Curr Biol*. 14:R250-2.

Chapter Five

Discussion

5.1 Summary of the thesis findings

5.1.1 Signaling during phagocytosis is coordinated

The first part of this thesis examined how signaling is coordinated during phagocytosis and tried to determine whether signals are proportional to ligand density, as predicted by the zipper model (Griffin and Silverstein, 1974). With the recruitment calculation method, the recruitment magnitudes of YFP chimeras of signaling molecules were measured as a function of IgG densities on particle surfaces during phagocytosis. Higher IgG density on particle surfaces resulted in greater recruitment of early stage signals, such as Syk, the p85 subunit of PI3K, and actin. The difference of recruitment between high and low IgG beads was not strictly proportional to IgG density, indicating the existence of positive and negative feedback regulation. In contrast, PIP_3 generation was uniformly high when phagocytosis could be completed, and the recruitment of the late stage signal PKCε showed an inverse relationship to IgG density on beads. These results suggested that

FcR signaling during phagocytosis was coordinated rather than strictly autonomous.

The mechanism of signal coordination is still unknown, but multiple feedback activities may be involved in phagocytosis, especially for the inverse relationship between PKCε and IgG density. The observation that low IgG densities on particle surfaces, which are unfavorable for phagocytosis, generates higher late stage signals on those phagosomes that can be finished indicates that some forms of negative feedback regulation must be involved. A similar phenomenon was reported earlier (Jongstra-Bilen et al., 2008), in which Bruton's tyrosine kinase (Btk) is activated and recruited to phagosome during phagocytosis. Its inhibitor LFM-A13, which reduced phagocytosis efficiency, increased DAG generation around phagosomes, which is also a late stage signal during phagocytosis (Botelho et al., 2000) and recruits PKCε.

5.1.2 A PIP_3 concentration threshold regulates phagocytosis

YFP-AktPH, which probes PIP_3 concentrations in membranes, was recruited to a similar extent on high and low IgG particles when phagocytosis could be finished, but was recruited much less when phagocytosis stalled. This indicates the existence of a PIP_3 concentration threshold regulating commitment to phagocytosis (Fig. 5.1 B). The PIP_3 threshold was then shown to regulate phagocytosis by the experiment showing that phagocytosis efficiency was decreased by PI3K inhibitors and increased by PTEN

inhibitors, which should modify the cells' ability to synthesize PIP_3. In addition, the PIP_3 concentration threshold regulated PKCε recruitment, which is a late stage signal required for phagocytosis (Fig. 5.1 C). Thus, PIP_3 concentrations regulated the transition to late stages of signaling and cellular commitment to phagocytosis, probably by serving as docking site for multiple signaling molecules and regulating their activities. This indicates more generally that the concentrations of 3'-phosphoinositides generated by activated receptor complexes can integrate signals for receptor-initiated movements of cytoplasm.

These results indicate a revision, rather than exclusion, of the zipper model. As stated by the zipper model, FcR are ligated in an ordered progression during phagocytosis. After ligation, each receptor generates early stage signals. The magnitudes of early stage signals correlate with the ligand densities. However, the independent signaling hypothesis can not be applied to late stage signals. Late stage signals appear only when suprathreshold levels of PIP_3 are generated. Thus, the magnitudes of late stage signals show a binary result rather than correlation with ligand densities.

Feedback loops may explain why the PIP_3 concentrations on phagosomes were similar for high and low IgG particles, which have a 10-fold difference in IgG surface density and induce different overall PI3K recruitment to the phagosome. Grb-associated binder 2 (Gab2), a scaffolding adaptor protein, is recruited to phagosomes by PIP_3 through its

PH domain. Gab2 also interacts with the p85 subunit of PI3K and this interaction is important for optimal PI3K activation (Gu et al., 2003). Thus, a Gab2-dependent positive feedback response may serve as a PIP_3 amplifier during phagocytosis, which may explain the different PIP_3 concentrations on complete and stalled phagocytic cups around particles with similar amount of IgG on their surfaces. On the other hand, PIP_3 and PLCγ form a negative feedback response which may explain how similar concentrations of PIP_3 are generated by particles with a 10-fold difference in IgG surface density. $PI(4,5)P_2$ is phosphorylated by PI3K to generate PIP_3, which contributes to the activation of phosphorylated PLCγ (Sekiya et al., 2004). PLCγ hydrolyzes $PI(4,5)P_2$ almost completely during phagocytosis (Botelho et al., 2000), which limits the $PI(4,5)P_2$ supply for further PIP_3 generation. Thus, although particles with higher IgG densities recruit more PI3K, they generate the same total PIP_3, probably due to $PI(4,5)P_2$ depletion by PLCγ. Although these possible positive and negative feedback responses, which were examined in multiple different systems, can explain the PIP_3 threshold behavior during phagocytosis, experiments monitoring them during phagocytosis at the same time, combined with quantitative modeling, are necessary to determine their exact dynamics in the phagocytic cup.

5.1.3 A PIP_3 concentration threshold regulates GTPase activity transitions

Rho and Arf family GTPases play important roles in phagocytosis. A signal transition of

GTPase activity was identified in both Rho (Hoppe and Swanson, 2004) and Arf GTPase families (Beemiller et al., 2006). Cdc42 and Arf6 are both activated at the initiation of phagocytosis (Fig. 5.1 A) and the activated molecules are mainly located at the leading edge of phagocytic cups. At the base of phagocytic cups, even before phagosome closure, Cdc42 and Arf6 are deactivated and Rac2 and Arf1 are activated. The deactivation of Cdc42 and Arf6 and the activation of Rac2 and Arf1 were inhibited by PI3K inhibitors, indicating that PIP_3 concentrations regulate these GTPase activity transitions (Fig. 5.1 C).

The requirement of a PIP_3 concentration threshold for commitment to phagocytosis is size dependent, since PI3K inhibitors have stronger inhibitory effect on phagocytosis of larger particles (Cox et al., 1999). A similar phenomenon was observed when GTPase activity transitions were inhibited by overexpression of constitutively active Cdc42, indicating that the GTPase activity transition is also necessary for commitment to phagocytosis. Unexpectedly, double inhibition by PI3K inhibitors and overexpression of constitutively active Cdc42 further reduced phagocytosis efficiency for both large and small particles, indicating that PI3K activation and Cdc42 deactivation are parallel and additive activities (Fig. 5.1 C). In addition, activated Cdc42 and some other late stage signals were found to further promote PI3K activity, allowing PIP_3 concentrations to exceed threshold levels (Fig. 5.1 B). Thus, multiple feedback responses exist to generate PIP_3, which is necessary for the GTPase activity transition.

It is still unclear how Cdc42 deactivation regulates phagocytosis. One hypothesis is that Cdc42 activation and deactivation regulate actin polymerization and depolymerization respectively (Fig. 5.1 A, C), which are necessary for generating force for membrane protrusion during phagocytosis. Actin concentrations are highest at the leading edge of phagocytic cups, which correlates spatially with activated Cdc42 (Hoppe and Swanson, 2004). In addition, although neither PI3K inhibition nor overexpression of constitutively active Cdc42 inhibit the initiation of phagocytosis and actin polymerization at phagosomes, the actin does not depolymerize at the base of phagocytic cups and phagocytosis cannot be finished. Further study on the relationship between the Cdc42 activation cycles, actin turnover and membrane protrusion will shed light on how signal transition regulates phagocytosis.

5.1.4 The effect of target geometry on phagocytosis is related to PIP_3 concentration thresholds

Surface curvature of the target particles affects whether they can be phagocytosed successfully by macrophages (Champion and Mitragotri, 2006). We studied signaling molecule recruitment during phagocytosis of rod-shaped particles. When phagocytosis started from the rod end and finished, YFP-AktPH was recruited to high concentrations on the cups and PKCε-YFP was also recruited to the phagosome. When the

macrophage contacted the flat side of a rod, YFP-AktPH was recruited to a lesser extent, PKCε-YFP was not recruited and phagocytosis could not be finished. Actin was recruited in both situations, whether or not phagocytosis could be completed. These results suggest that cell membrane curvature does not affect early stage signals generated by ligation of receptors but affects PIP_3 accumulation in cups, which is necessary for progression to late stage signals and commitment to phagocytosis.

This result is consistent with the requirement to reach a PIP_3 concentration threshold for phagocytosis of particles coated with different amounts of IgG. However, the effect of target geometry on phagocytosis may not be simply explained by feedback responses in signaling pathways, since the IgG density on particles is uniform and should generate similar signaling outcomes regardless of the geometry. There are several possible explanations for the effect of target geometry on phagocytosis. Macrophages may be able to sense the target geometry by molecules such as Amphiphysin (Gold et al., 2000). Amphiphysin, the BAR domain of which can produce and sense membrane curvature (Zimmerberg and McLaughlin, 2004), is recruited to phagosomes in a PI3K-dependent manner and regulates dynamin recruitment and membrane remodeling (Gold et al., 2000). Another possibility is that the target geometry affects the formation of the cup domain, a subregion of plasma membrane in which PIP_3 can reach suprathreshold concentrations required for late stage signaling (Swanson, 2008). If a diffusion barrier exists at the rim of the phagocytic cup, then target geometry may affect whether a

complete barrier can be formed, which can affect the diffusion and concentration of PIP_3 within the cup domain. It is also possible that the PIP_3 diffusion is simply affected by the curvature of membrane (Yoshigaki, 2007).

5.2 Experimental limitations

I developed a method to calculate the magnitude of YFP chimera recruitment to phagosomes, based on ratiometric fluorescence microscopy. Instead of generating a ratio image which shows relative YFP to CFP concentrations (Henry et al., 2004), this method generates a recruitment image whose intensity is proportional to the number of molecules relocated to that pixel. Thus, the average value in a phagosome region of the recruitment image represents the magnitude of YFP chimera recruitment during phagocytosis. However, like all other experimental methods, this method has its own limitations.

First, this method requires that YFP chimeras in resting cells are uniformly distributed in the cytosol, similar to the free CFP molecules. The recruitment of membrane-bound molecules, such as Rab family GTPases, may not be measured accurately by this method since the product of the average ratio and the CFP image does not represent how the YFP would be distributed in resting cells. A membrane marker with CFP or other fluorophores may solve this problem, but the distribution of currently available

membrane markers also depends on the membrane properties, which makes them inappropriate reference markers for YFP chimeras. In addition, some YFP chimeras, such as YFP-actin and YFP-p85, exhibit low concentrations in the nucleus. Thus, when measuring the recruitment of those molecules, the nuclear regions must be excluded before calculating the average ratio. However, it is unavoidable to have some deviation when deciding the nuclear region, which creates deviations in the final result. Fortunately, this deviation was small enough that it did not affect the comparison of recruitment to high and low IgG beads in our experiments.

Second, the overexpression level of YFP chimeras affects the recruitment calculation. During phagocytosis, both endogenous signaling molecules and their YFP chimeras are recruited to phagosomes, but the recruitment calculation only measures the YFP chimeras. Different overexpression levels result in different ratios of endogenous signaling molecules to corresponding YFP chimeras, thereby changing the ratio of YFP chimeras recruited to phagosomes compared with endogenous molecules. To ensure comparable contributions from endogenous signaling molecules, images were acquired from cells with similar YFP-chimera expression levels for each specific probe. In addition, similar overexpression levels can also make the effect of molecule overexpression on phagocytosis comparable for data acquired from different cells.

Third, although the recruitment calculation method corrects for cell thickness changes

during phagocytosis, it is still a 2D image projection of a 3D event. Thus, the orientation of phagocytosis in 3D space will affect the 2D image. For example, phagocytosis starting from the particle side will generate different results with those starting from the particle bottom. To reduce variance among images taken from different cells, only phagocytosis starting from the particle sides were included in the data. A more accurate method would be to measure recruitment in deconvolved 3D images. However, such images would require much more storage space and time-consuming processing. Since the 2D images also provide enough accuracy for our purpose, all of our data were acquired as 2D images.

Lastly, because the recruitment calculation method produces a low signal-to-noise ratio, it can only be used to measure YFP chimeras which are recruited extensively to phagosomes. In our experiment, YFP-actin, YFP-p85, YFP-PH domains, and PKCε-YFP have high levels of recruitment which can be easily detected by the recruitment calculation method. However, Syk-YFP recruitment was relatively low. High IgG beads generated good recruitment signals but low IgG beads and rod-shaped particles, which also have low IgG surface densities, could only generate weak recruitment signals. The low signal-to-noise ratio makes it hard to compare the recruitment of Syk-YFP to low IgG beads with the recruitment to stalled phagosomes.

5.3 Future research directions

This thesis identified the existence of a PIP_3 concentration threshold and indicated the involvement of multiple feedback responses in phagocytosis signaling pathways. However, it is still unclear how the PIP_3 concentration threshold and feedback responses are generated. Quantitative measurement of more fluorescent molecules, with high spatial and temporal resolution, will be necessary to understand the signaling network. In addition, mathematical modeling will contribute to understanding the feedback responses (Brandman and Meyer, 2008). Due to the limited quantitative information on signaling during phagocytosis, quantitative modeling of phagocytosis has not been established. Future experimental data will assist the establishment and calibration of phagocytosis models.

Although this thesis discovered that the PIP_3 concentration threshold is important in generating late stage signals and regulating the GTPase activity transition, it remains unknown how the threshold regulates phagocytosis. Since Cdc42 and Rac play important roles in regulating actin dynamics, I hypothesize that the GTPase activity transition coordinates the polymerization and depolymerization of actin both spatially and temporally. It is also possible that the PIP_3 concentration threshold is required for recruitment of contractile proteins, such as myosins (Diakonova et al., 2002) or fusion of intracellular membrane resources to phagosomes (Huynh et al., 2007), both of which are believed to contribute to the membrane protrusion during phagocytosis. Future

research in these areas will elucidate the mechanism of PIP_3 concentration threshold regulation.

Another question is whether the GTPase activity transition is regulated directly by the PIP_3 concentration threshold or by some other downstream signals, such as PLCγ, DAG or PKCε. Experiments similar to those described in chapter 3 could be performed using PLCγ inhibitors or PKCε inhibitors to confirm which molecules regulate the signal transition directly.

In addition, the study of recruitment of signaling molecules during phagocytosis of rod-shaped particles is only the first step in understanding the effect of target geometry on phagocytosis. Whether different membrane curvatures change the diffusion of membrane-bound molecules, such as PIP_3 or instead recruit different molecules which can sense membrane shape is still unknown. The recruitment of fluorescent chimeras of shape-sensing molecules can elucidate the effect of membrane curvature. Moreover, studying the diffusion of membrane-bound photo-activatable GFP can examine whether molecular diffusion is affected by the shape of phagocytic cups. In cells transfected with membrane-bound photo-activatable GFP, GFP can be activated at phagocytosis sites during the formation of phagocytic cups. The diffusion of photo-activated GFP will shed light on the formation of any diffusion barrier in the phagocytic cup and potential effects of membrane curvature on diffusion.

Many bacteria are rod-shaped. Whether that shape provides a mechanism for bacteria to escape from being phagocytosed by macrophages is an intriguing question to ask. No research has been done about this, but studying the signaling during phagocytosis of rod-shaped bacteria will contribute to our understanding of pathogen invasion and development of novel treatment for infectious diseases.

5.4 Conclusions

In summary, this thesis identified a 3'-phosphoinositide concentration threshold regulating commitment to phagocytosis using a recruitment measurement method based on ratiometric fluorescence microscopy. This threshold is necessary for the signal transition of Cdc42 deactivation, which is required for phagocytosis, to a larger extent for large particles than for small particles. The target geometry can affect the fate of the phagocytic cup, probably by affecting signaling molecule diffusion, and thus 3'-phosphoinositide concentration thresholds, on membranes with different shapes. These three projects studied the role of 3'-phosphoinositide concentration thresholds in signal transduction during phagocytosis from different perspectives with various fluorescence microscopy techniques.

Figure 5.1 The summary of signal coordination by 3' phosphoinositide concentration thresholds during phagocytosis. (A) Early stage signals are generated independent of 3' phosphoinositide concentration thresholds. Ligated FcR mediate the activation of Cdc42 and Rac1. Rac1:GTP and Cdc42:GTP promote the activation of PI4P5K, which in turn generates $PI(4,5)P_2$ at phagosomes. $PI(4,5)P_2$, Rac1:GTP and Cdc42:GTP stimulate actin polymerization, which generates force for phagocytic cup protrusion. Molecules labeled black represent high recruitment or generation around phagosomes while molecules labeled grey represent low levels of activity. (B) PI3K is activated following FcR ligation and its activities are promoted by multiple feedback regulations, including Cdc42:GTP. (C) When PIP_3 in phagocytic cup membrane reaches suprathreshold levels, the cell commits to late stages of phagocytosis. Suprathreshold level of PIP_3 regulates late stage signaling events required for commitment to phagocytosis. These late stage signals include PKCε recruitment (Chapter 2 and 4) and Cdc42 deactivation, which probably regulates actin depolymerization and vesicle fusion at phagosomes (Chapter 3).

Figure 5.1

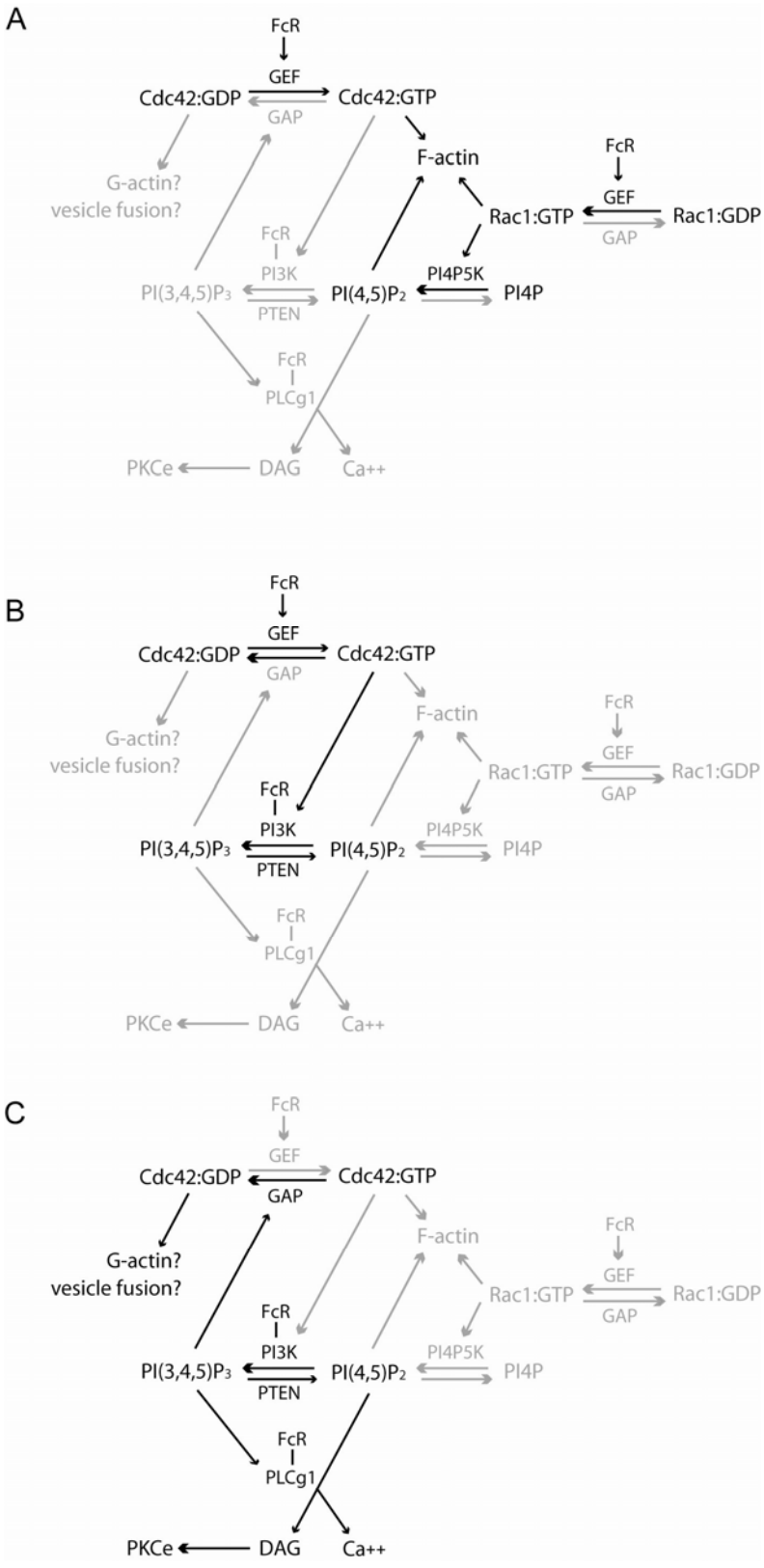
A
FcR
GEF
Cdc42:GDP
Cdc42:GTP
GAP
F-actin
G-actin?
vesicle fusion?
FcR
GEF
Rac1:GTP
Rac1:GDP
GAP
FcR
PI3K
PI4P5K
PI(3,4,5)P3
PI(4,5)P2
PI4P
PTEN
FcR
PLCg1
PKCe
DAG
Ca++
B
FcR
GEF
Cdc42:GDP
Cdc42:GTP
GAP
F-actin
FcR
G-actin?
vesicle fusion?
GEF
Rac1:GTP
Rac1:GDP
GAP
FcR
PI3K
PI4P5K
PI(3,4,5)P3
PI(4,5)P2
PI4P
PTEN
FcR
PLCg1
PKCe
DAG
Ca++
C
FcR
GEF
Cdc42:GDP
Cdc42:GTP
GAP
F-actin
FcR
G-actin?
vesicle fusion?
GEF
Rac1:GTP
Rac1:GDP
GAP
FcR
PI3K
PI4P5K
PI(3,4,5)P3
PI(4,5)P2
PI4P
PTEN
FcR
PLCg1
PKCe
DAG
Ca++

5.5 Bibliography

Beemiller, P., A.D. Hoppe, and J.A. Swanson. 2006. A phosphatidylinositol-3-kinase-dependent signal transition regulates ARF1 and ARF6 during Fcg receptor-mediated phagocytosis. *PLoS Biol*. 4:e162.

Botelho, R.J., M. Teruel, R. Dierckman, R. Anderson, A. Wells, J.D. York, T. Meyer, and S. Grinstein. 2000. Localized biphasic changes in phosphatidylinositol-4,5-bisphosphate at sites of phagocytosis. *J. Cell Biol.* 151:1353-1367.

Brandman, O., and T. Meyer. 2008. Feedback loops shape cellular signals in space and time. *Science*. 322:390-5.

Champion, J.A., and S. Mitragotri. 2006. Role of target geometry in phagocytosis. *Proc Natl Acad Sci U S A*. 103:4930-4.

Cox, D., C.-C. Tseng, G. Bjekic, and S. Greenberg. 1999. A requirement for phosphatidylinositol 3-kinase in pseudopod extension. *J. Biol. Chem.* 274:1240-1247.

Diakonova, M., G. Bokoch, and J.A. Swanson. 2002. Dynamics of cytoskeletal proteins during Fcg receptor-mediated phagocytosis in macrophages. *Mol. Biol. Cell*. 13:402-411.

Gold, E.S., N.S. Morrissette, D.M. Underhill, J. Guo, M. Bassetti, and A. Aderem. 2000. Amphiphysin IIm, a novel amphiphysin II isoform, is required for macrophage phagocytosis. *Immunity*. 12:285-92.

Griffin, F.M., and S.C. Silverstein. 1974. Segmental response of the macrophage plasma membrane to a phagocytic stimulus. *J. Exp. Med.* 139:323-336.

Gu, H., R.J. Botelho, M. Yu, S. Grinstein, and B.G. Neel. 2003. Critical role for scaffolding adapter Gab2 in FcgR-mediated phagocytosis. *J. Cell Biol.* 161:1151-1161.

Henry, R.M., A.D. Hoppe, N. Joshi, and J.A. Swanson. 2004. The uniformity of phagosome maturation in macrophages. *J Cell Biol*. 164:185-94.

Hoppe, A.D., and J.A. Swanson. 2004. Cdc42, Rac1 and Rac2 display distinct patterns of activation during phagocytosis. *Mol. Biol. Cell*. 15:3509-3519.

Huynh, K.K., J.G. Kay, J.L. Stow, and S. Grinstein. 2007. Fusion, fission, and secretion during phagocytosis. *Physiology (Bethesda)*. 22:366-72.

Jongstra-Bilen, J., A. Puig Cano, M. Hasija, H. Xiao, C.I. Smith, and M.I. Cybulsky. 2008. Dual functions of Bruton's tyrosine kinase and Tec kinase during Fcgamma receptor-induced signaling and phagocytosis. *J Immunol*. 181:288-98.

Sekiya, F., B. Poulin, Y.J. Kim, and S.G. Rhee. 2004. Mechanism of tyrosine phosphorylation and activation of phospholipase C-gamma 1. Tyrosine 783 phosphorylation is not sufficient for lipase activation. *J Biol Chem*. 279:32181-90.

Swanson, J.A. 2008. Shaping cups into phagosomes and macropinosomes. *Nat Rev Mol Cell Biol*. 9:639-649.

Yoshigaki, T. 2007. Theoretically predicted effects of Gaussian curvature on lateral diffusion of membrane molecules. *Phys Rev E Stat Nonlin Soft Matter Phys*. 75:041901.

Zimmerberg, J., and S. McLaughlin. 2004. Membrane curvature: how BAR domains bend bilayers. *Curr Biol*. 14:R250-2.